# EFFECT OF PRETREATMENT FOR SYNTHESIS OF OIL PALM FROND BASED CATALYST FOR BIODIESEL PRODUCTION

**HENG ZENG WEI**

**A project report submitted in partial fulfilment of the requirements for the award of Bachelor of Engineering (Honours) Chemical Engineering**

**Lee Kong Chian Faculty of Engineering and Science**
**Universiti Tunku Abdul Rahman**

**May 2019**

# DECLARATION

I hereby declare that this project report is based on my original work except for citations and quotations which have been duly acknowledged. I also declare that it has not been previously and concurrently submitted for any other degree or award at UTAR or other institutions.

Signature : _____

Name : HENG ZENG WEI

ID No. : 1402740

Date : 15th APRIL 2019

**APPROVAL FOR SUBMISSION**

I certify that this project report entitled **"EFFECT OF PRETREATMENT FOR SYNTHESIS OF OIL PALM FROND BASED CATALYST FOR BIODIESEL PRODUCTION"** was prepared by **HENG ZENG WEI** has met the required standard for submission in partial fulfilment of the requirements for the award of Bachelor of Engineering (Honours) Chemical Engineering at Universiti Tunku Abdul Rahman

Approved by,

Signature : _____

Supervisor : Dr. Steven Lim

Date : 15th APRIL 2019

## ACKNOWLEDGEMENTS

The completion of this research project would not have been a success if it was not for the participation, assistance and support of many individuals. First and foremost, I would like to convey my heartiest thanks to my research supervisor, Dr. Steven Lim for giving me the opportunity to undertake my final year project under his supervision. Throughout the research project, Dr. Steven Lim gave me very in-time valuable advice and extensive guidance with enormous patience.

Next, my deepest thanks to Universiti Tunku Abdul Rahman (UTAR) for providing me a great platform and learning ground to complete my final year project. Throughout the project, I was very fortunate to be blessed with the technical supports from all Assistant Laboratory Managers of Department of Chemical Engineering in Lee Kong Chian Faculty of Engineering and Science.

Last but not least, I would also like to express my greatest gratitude to my loving parents who gave me unconditional support and encouragement during my venture. Their help allowed me to complete my research and thesis successfully. A special thanks to my helpful seniors, Ms. Tang Zo Ee, Mr. Danny Chin, Ms. Wong Wan Ying and Mr. Chon Wen Xian who had offered invaluable suggestions and assistance unconditionally.

## ABSTRACT

In this study, cost-effective carbon-based solid catalyst was synthesised by preparation of activated carbon derived from agricultural waste materials. The performances of synthesised catalysts were tested in esterification of high free fatty acid feedstock (Palm Fatty Acid Distillate) to produce biodiesel. The main focus in this research was to study the effects of pretreatment parameters on the effectiveness of carbon based catalyst produced by varying the types of biomass precursor and activating agent used, particle sizes, impregnation ratio (1:0.1, 1:0.5, 1:1), impregnation temperature (50˚C, 70˚C, 90˚C) and carbonisation temperature (400˚C, 600˚C, 800˚C). The resulting activated carbon was then sulfonated by direct sulfonation, thermal decomposition of ammonium persulfate and arylation of 4-benzenediazonium sulfonate (4-BDS) and its catalytic activity was investigated in the esterification of PFAD and methanol. SEM micrographs showed that the activated carbon (AC) carbonised at 600 ℃ had porous structure and exhibited highest surface area. Besides that, EDX and FT-IR had confirmed the successful attachment of $–SO_3H$ groups onto the activated carbon. TGA result showed that the catalyst was thermally stable up to the temperature of 225 ˚C. Moreover, it was determined in TPR analysis that 890 ℃ was the most ideal reduction temperature with 1052 μmol/g of hydrogen gas was consumed. The optimum pretreatment condition obtained was at 600 ˚C carbonisation temperature, 1:0.5 impregnation ratio and at 90 ˚C of impregnation temperature. The optimum catalyst, Cat_0.5 possessed the total acid density of 7.36 mmol/g and had achieved maximum FAME yield of 82.71% and conversion of 93.54% in the esterification reaction.

# TABLE OF CONTENTS

# LIST OF TABLES

# LIST OF FIGURES

# LIST OF SYMBOLS/ ABBREVIATIONS

| | |
|---|---|
| $a_i$ | initial acid value of feedstock, mg KOH/g |
| $a_f$ | final acid value of mixture after reaction, mg KOH/g |
| $M$ | molarity of KOH solution, mol/L |
| $MW$ | molecular weight of KOH, g/mol |
| $V$ | volume of solution used, L |
| $W$ | weight of PFAD, g |

| | |
|---|---|
| 4-BDS | 4-benzenediazoniumsulfonate |
| AC | activated carbon |
| BET | Brunauer-Emmett-Teller |
| BP | British Petroleum |
| CI | compression ignition |
| EFB | empty fruit bunch |
| FAME | fatty acid methyl ester |
| FFA | free fatty acid |
| FID | flame ionisation detector |
| FTIR | Fourier Transform Infrared Spectroscopy |
| GC | Gas Chromatography |
| GDP | gross domestic product |
| GHG | green house gases |
| IEA | International Energy Agency |
| mtoe | million tons of oil equivalent |
| MWCNT | multi-walled carbon nanotubes |
| OPF | oil palm frond |
| OPT | oil palm trunk |
| PFAD | palm fatty acid distillate |
| SCB | sugarcane bagasse |
| SEM-EDX | Scanning Electron Microscopy with Energy Dispersive X-Ray |
| TGA | Thermogravimetric Analysis |
| TPR | Temperature Programmed Reduction |

# LIST OF APPENDICES

# CHAPTER 1

# INTRODUCTION

## 1.1 Global Energy Scenario

Presently, natural gas, coal and crude oil are the main energy sources in the world, which are the lifeblood of modern era. Due to the new discoveries in science and technology, world energy consumption is skyrocketing and is increasing at a faster pace than the population growth. In the near future, this non-renewable energy source will eventually run out and result in serious shortage. This alarming problem has attracted the awareness of all nations to search for alternative energy in order to ensure sustainable development.

According to BP Statistical Review of World Energy (2018), there was an increase in fuel consumption from 11,588.4 million tons of oil equivalent (Mtoe) to 13,511.2 Mtoe in ten years' time from 2007 to 2017 as shown in Table 1.1. The total energy consumption was primarily contributed by fossil fuels which accounted for 85.2%, while hydroelectricity and nuclear energy contributed only a little with 6.8% and 4.4%, respectively. Astonishingly, the share for renewables still remains small which reflected that the populations are still strongly relied on traditional fossil fuel as a primary energy source. World primary energy consumption grew by 2.2% in 2017, which was the fastest growth since 2013. This rapid expansion was mostly driven by the developing countries in Asia, particularly China which contributed over one-third of that growth. According to the energy forecast done by International Energy Agency (IEA), this projected consumption will continue to expand by 30% until 2040, with a global economy growing at an average rate of 3.4% per year and a population that expands from 7.4 billion to above 9 billion in 2040 (Iea.org, 2018). The main driver of this demand growth comes from developing countries in Asia, especially in India which accounts for almost one-third of global energy growth as shown in Figure 1.1.

Table 1.1: Global Primary Energy Consumption by Fuel (Worldcat.org, 2018)

| Source | 2007 | | 2017 | |
|---|---|---|---|---|
| | Mtoe | Share (%) | Mtoe | Share (%) |
| **Petroleum** | 4167.8 | 35.97 | 4621.9 | 34.21 |
| **Coal** | 3451.8 | 29.79 | 3731.5 | 27.62 |
| **Natural Gas** | 2543.4 | 21.95 | 3156.0 | 23.36 |
| **Nuclear** | 621.5 | 5.36 | 596.4 | 4.41 |
| **Hydropower** | 696.9 | 6.01 | 918.6 | 6.80 |
| **Renewables** | 107.0 | 0.92 | 486.8 | 3.60 |
| **Total** | 11588.4 | 100 | 13511.2 | 100 |

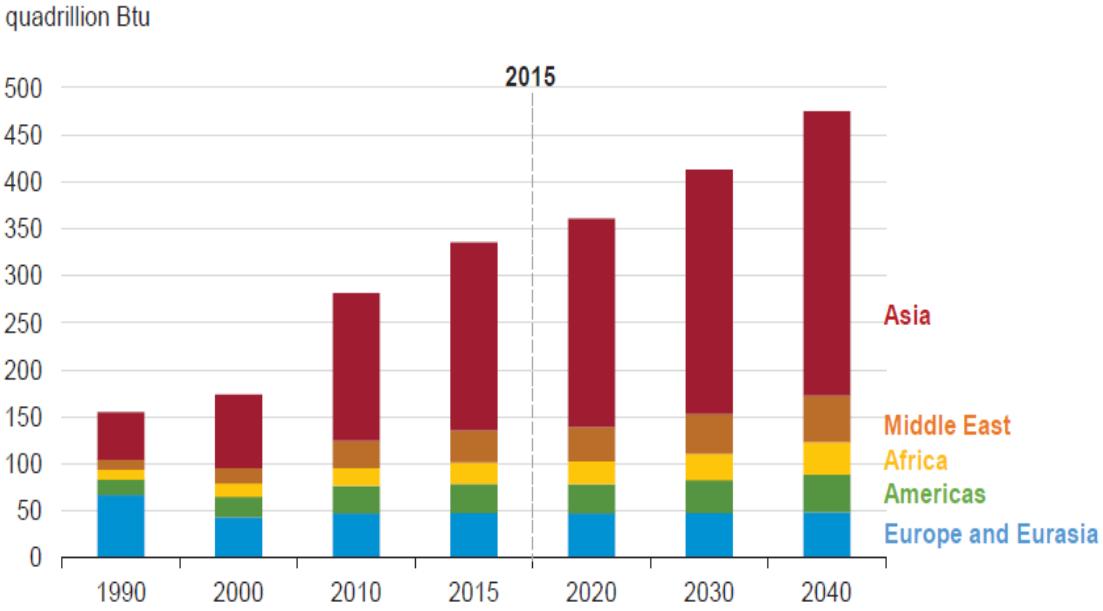


Figure 1.1: Energy Consumption by Regions (Eia.gov, 2018)

At current production rate, the world oil production is reaching its peak and is expected to decrease at a constant rate in the future. According to BP statistics, the global proven oil and natural gas reserves of 1696.6 thousand million barrels and 193.5 trillion cubic meters are only sufficient for 50.2 and 52.6 years respectively. Conversely, world established coal reserves of 1.04 trillion tonnes at end of 2017 is estimated to last for 112 years. However, the combustion of fossil fuels to generate electricity emitted harmful greenhouse gases (GHG) which raised the climate change issue. It was reported that 19,380 million tons of carbon dioxide was emitted in 1980

and the amount continue to rise rapidly to 33,444 million tons in 2017. The continuous use of fossil fuels will continue to increase the carbon dioxide emission and aggravate the situation. Due to the short life expectancy of fossil fuels and the pressing environmental issues, tremendous efforts are needed to develop renewable energy as an alternative and reliable energy source. Currently, renewable energy only contributes 10.4% of the total global energy used.

## 1.2 Malaysia energy scenario

According to Department of Statistics, Malaysia (2017), Malaysia had a population of 32 million in 2017 and is expected to reach 41.5 million by 2040. Malaysia is a fast developing country that recorded a 5.9% GDP in 2017 (The Edge Markets, 2018). As such, it is expected that Malaysia's energy consumption will increase at the same pace with GDP growth. Due to the rapid urbanisation and industrialisation, Malaysia's primary energy supply had increased almost tenfold from 10.9 Mtoe in 1980 to 93.4 Mtoe in 2016, which was the third highest consumption among the Southeast Asia countries as shown in Figure 1.2. Figure 1.3 shows the total energy consumption by sectors in Malaysia from 1980 to 2016. The increasing trend indicated that transportation sector had the highest energy consumption, followed by the industrial sector, the residential and commercial sector, and lastly the agriculture sector in the year of 2016. Although advancement in transportation is one of the drivers for economic growth, this sector also contributes to a substantial amount of greenhouse gases emissions as it is mostly powered by petroleum products.

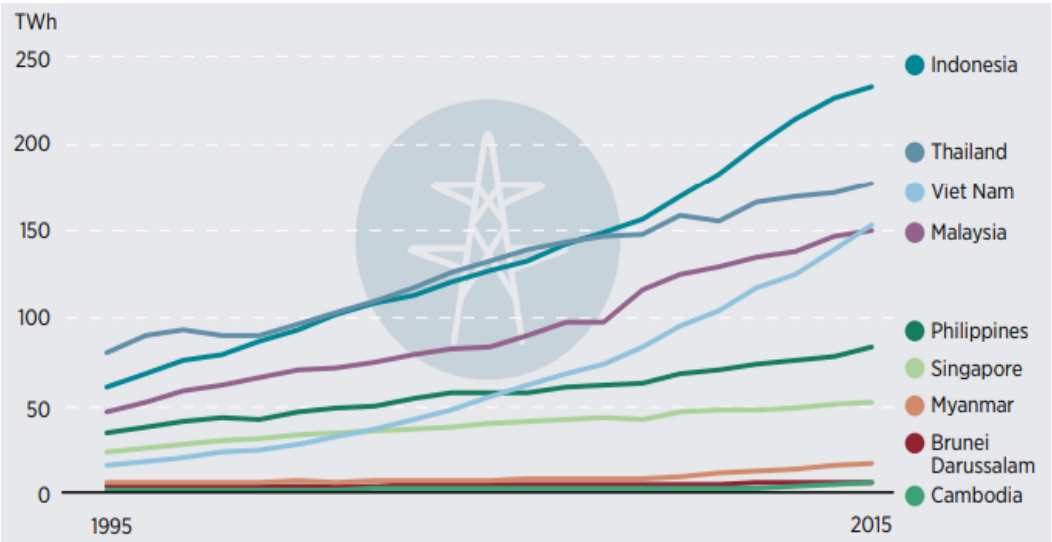


Figure 1.2: Electricity Generation by Southeast Asia Country from 1995 to 2015 (Renewable Energy Market Analysis: Southeast Asia, 2018)

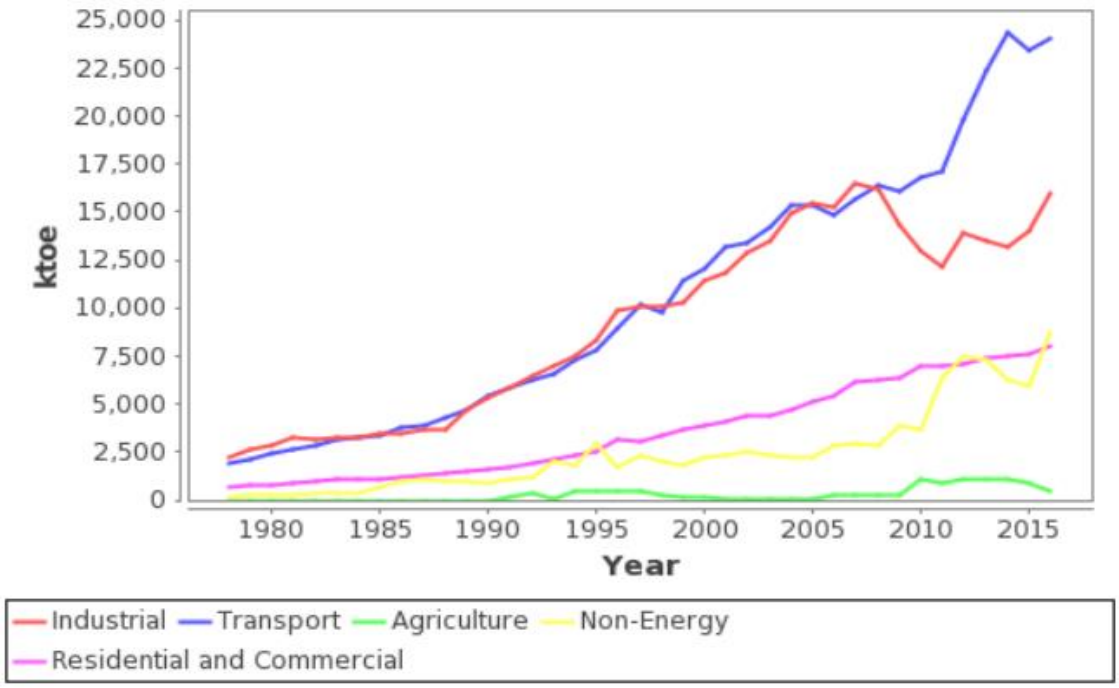


Figure 1.3: Total Energy Consumption by Sectors in Malaysia from 1980 to 2016 (Meih.st.gov.my, 2018)

Even though Malaysia has abundant fossil fuel resources, it is not sustainable since it will deplete eventually someday. Considering the depletion of fossil fuel reserves and adverse environmental impact, energy security and sustainability have become a challenging issue faced by Malaysia's power sector currently. In 2000, Malaysia government had announced renewable energy as the 5th fuel in the Five-Fuel Diversification Policy which included hydro energy, solar energy, wind energy and biomass. Malaysia is a potential contributor in biodiesel production since our country is blessed with abundant amount of palm oil residues such as oil palm shell, palm oil mill effluent, mesocarp fiber and empty fruit bunch (EFB).

## 1.3 Biodiesel in Malaysia

As one of the world's largest palm oil producer and exporter, Malaysia has great potential in the development of biomass renewable energy thanks to the large amount of biomass feedstock available. Each year, Malaysia will process approximately 71.3 million tons of fresh fruit bunch and release about 19 million tons of palm oil leftover waste in the form of, mesocarp fibre, empty fruit bunch (EFB), palm oil mill effluent and oil palm shell which have a very low economic values (Sumathi, Chai

and Mohamed, 2008). However, the energy contained in these solid wastes can be extracted and recovered into more valuable and usable forms, such as biodiesel which serves as a substitute to petroleum-based diesel. In Malaysia, palm oil is mainly utilised as feedstock in biodiesel production due to its huge availability, low price and good oil properties. The abundance of raw materials allows biodiesel developers to cut down the production cost, making it more feasible for commercial production.

Biodiesel, also known as methyl ester, is mainly derived from triglycerides in vegetable oils through transesterification process with methanol. Apart from vegetable oils, microalgae, waste cooking oils and animal fats can also be used as feedstocks in biodiesel production. However, animal fats such as chicken fat, tallow and yellow grease are seldom used since they contain high amount saturated fatty acids that tend to solidify at room temperature, rendering the production process difficult. Besides, waste cooking oil that contains high amount of undesired impurities, such as free fatty acids and water encounters problems in meeting the specific fuel quality standards. According to Rincón, Jaramillo and Cardona (2014), European Union countries mostly utilised rapeseed oil, Argentina and United States used soybean oil, and tropical countries such as Malaysia, Nigeria, Colombia and Indonesia preferred palm oil. Although the yield and fuel properties of biodiesel may differ by using different feedstock, all the fuel grade biodiesel produced in the world must conform to the strict specifications such as ASTM D 6751 to ensure the performance and quality.

Vegetable oils can be divided into non-edible and edible oils in which edible oils accounted for 95% of biodiesel feedstocks due to its low free fatty acid content. Common edible oils used in industry include soybean, rapeseed, sunflower, corn, Linseed and palm oil while non-edible oils include Mahua, Neem, rubber seed, sea mango, Castor, Karanja and Jatropha. Although edible oils predominate the biodiesel raw material market, the extensive usage has cause several feedstock issues such as deforestation, limited plantation land and food versus fuel debate. As such, many researches divert their attention to non-edible oils which are toxic and unsafe for consumption. Besides, non-edible oils can be produced in high yield from degraded and low productive lands without intensive care, preserving arable lands for food crop production. The only shortcoming is that the high free fatty acids contained in non-edible oils will cause saponification, hence it requires additional steps in

pretreatment and separation process. This may add burden to the production cost and lower the biodiesel quality to below the standards.

The oil yield from the crop itself is always the key factor in deciding the suitability of a feedstock for biodiesel production. Among the various vegetable oils, palm oil with the highest oil yield only requires small land area to cultivate 5000 kg/hectare of oil. Besides, palm oil has the lowest unit production cost which is 20% lower than soybean, followed by rapeseed with the highest unit production cost (Gui, Lee and Bhatia, 2008). Table 1.2 shows that palm oil biodiesel was sold at the lowest price as the feedstocks cost accounted for about 70-80% of the total production cost. Palm oil biodiesel has been proven to possess higher fuel quality as compared to biodiesel produced from soybean and rapeseed oil. This is because palm oil is more saturated, which means less double bonds is present to give better oxidative stability. As such, palm oil biodiesel has a better ignition quality in CI engine but it is more difficult to be used in cold climate due to the high cloud and pour point. In addition, oxidative stability is important to ensure a good engine performance as oxidation by-products will cause problems such as filter plugging, deposits and corrosion.

Table 1.2: Oil Yields for Major Non-edible and Edible Oil Sources (Gui, Lee and Bhatia, 2008)

| **Types of oil** | **Oil yield (kg oil/ha)** | **Oil yield (wt.%)** | **Price (USD/Ton)** |
|---|---|---|---|
| **Non-edible oil** | | | |
| **Jatropha** | 1590 | Seed: 35-40<br>Kernel: 50-60 | N/A |
| **Rubber seed** | 80-120 | 40-50 | N/A |
| **Castor** | 1188 | 53 | N/A |
| **Karanja** | 225-2250 | 30-40 | N/A |
| **Sea mongo** | N/A | 54 | N/A |
| **Edible oil** | | | |
| **Soybean** | 375 | 20 | 684 |
| **Palm** | 5000 | 20 | 478 |
| **Rapeseed** | 1000 | 37-50 | 683 |

As a clean-burning fuel, biodiesel is non-toxic, biodegradable and environmental friendly. As compared to conventional diesel, biodiesel with high cetane number provides high brake power and better combustion due to its auto ignition characteristic which reduces ignition delays. Besides, biodiesel with low sulfur and aromatic content has successfully reduced the emissions of exhaust gases such as sulfur dioxide, carbon monoxide, particulate matter and unburned hydrocarbons to large extent. Moreover, the high flash point of biodiesel allows safe handling and storing of biodiesel. The high clarity and purity of biodiesel allow it to be used without adding additional lubricant which can extend engine life and reduce the maintenance frequency. Similar to conventional diesel fuel, biodiesel blend fuel does not require engine modification up to B20 and can be used directly in compression ignition (CI) engine due to its similar physical properties.

Despite the aforementioned advantages, biodiesel still cannot fully replace fossil fuel due to numerous practical issues that yet to be solved. Biodiesel with high pour and cloud point is not suitable for usage in cold climate country as it tends to gel and freeze, resulting in clogged filters and plugged pipelines. Although biodiesel has a lower emission profile for most of the exhaust gases, it emits more NOx gases which can result in the formation of smog and acid rain. Besides, the viscosity of biodiesel which is about 11–17 times greater than diesel fuel leads to problems in direct-injection engines (Hassan and Kalam, 2013). High viscosity of biodiesel will form deposits which plug the orifices of injector systems, resulting in poor atomisation and fuel pumping. In addition, it will cause problems such as coking deposits of carbon, gelling and thickening of lubricating oil. Moreover, polyunsaturated fatty acids contained in biodiesel are prone to oxidative polymerisation. Hence, biodiesel will degrade easily and cannot be stored for long periods. In addition, calorific value of biodiesel is 9% lower than conventional diesel, which gives a lower energy output, resulting in higher biodiesel consumption in order to produce the same amount of energy (Aransiola, et al., 2014).

## 1.4 Biodiesel Processing Technology

### 1.4.1 Direct use and Blending

In the past couple of decades, various researchers found that blending of diesel with vegetable oil up to 20% had successfully improved the viscosity of pure vegetable oils so that it can be easily used in diesel engines. However, in terms of long term

durability, the performance is unsatisfactory since it has problems with high viscosity, free fatty-acid content, acid composition, carbon deposits, gum formation and thickening of lubricating-oil. However, it is possible to use pure vegetable oil after modification of engine such as changing of injector and piping construction materials. Or else, it will speed up the engine wear and increase the maintenance costs. It was reported that other processing methods such as micro-emulsification, pyrolysis and transesterification could reduce the viscosity of vegetable oils.

### 1.4.2 Micro-emulsification

Micro-emulsification is described as a transparent, colloidal dispersion of fluid microstructure with dimension of 1-150 nm in a methanol solvent, forming two immiscible phases. Micro-emulsions will lower the viscosity of vegetable oils and ease the atomisation process, thus improve the spray characteristics of biodiesel. Besides, the methanol solvent used has high latent heats of vaporisation which can help to cool the combustion chamber and reduces nozzle coking problems. However, micro-emulsions generate lesser energy than diesel fuel due to its lower volumetric heating value.

### 1.4.3 Thermal Cracking/ Pyrolysis

Pyrolysis is defined as the thermal degradation of long chain fatty acids in the absence of oxygen by using catalyst. (Abbaszaadeh, et al., 2012). Thermal decomposition of vegetable oils which compose mainly of triglycerides is said to be a promising pathway for biodiesel production since the fuel properties are likely to approach diesel fuels. In pyrolysis method, different intermediates and products can be formed due to the complex mechanism and multiple reaction pathways that makes pyrolytic chemistry difficult to be characterised. This method, however, is not widely implemented because cracking process produces low-quality fuel oil that is highly unstable, corrosive, tarry, and will release foul odour (Balat, 2008). Besides, high cost of thermal cracking equipment used is not suitable for modest production.

### 1.4.4 Transesterification

Transesterification is the most widely used method to produce biodiesel by converting triglycerides with an alcohol to form fatty acid methyl esters (FAME) and glycerol. According to the overall equation illustrated in Figure 1.4, 1 mole of

triglyceride is reacted with 3 moles of alcohol to form 3 moles of FAME as main product and 1 mole of glycerol as by-product. Excess alcohol is added to shift the equilibrium towards the production of more biodiesel.

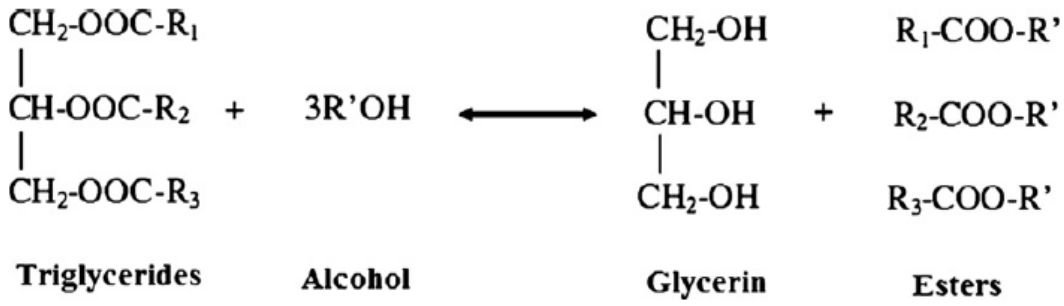


Figure 1.4: Overall Transesterification Reaction of Triglyceride with Alcohol (Ma and Hanna, 1999)

#### 1.4.4.1 Catalyst and alcohol used

Among all alcohols, methanol and ethanol are the most commonly employed alcohol in commercial transesterification process because they can react rapidly with triglyceride molecules and dissolve easily in alkaline catalyst. Methanol is of great interest because it is very much cheaper and is more abundant than ethanol which makes the biodiesel production more economical. The usage of methanol allows an easier downstream recovery of unreacted alcohol since it does not form any azeotrope with water like ethanol. However, methanol vapour is highly flammable and is more likely to explode, thus it needs to be handled with care. Although ethanol is more environmental friendly and is less toxic, it is not a preferred option because it is more expensive and less reactive than methanol.

Generally, alcohol and triglycerides with different density and polarity are immiscible, resulting in poor surfaces contact between methanol and vegetable oils which will impede the reaction. To address this problem, catalysts are used to improve the surface contact and consequently speed up the reaction rate, giving a higher yield and conversion. Catalysts used in biodiesel production can be either homogeneous or heterogeneous types. Homogeneous catalyst is normally in liquid phase which is the same as the liquid reactants, thus handling becomes much easier. On the contrary, heterogeneous solid catalyst is immiscible with liquid or gaseous phase. However, it can be easily recovered after used. Besides that, catalyst can be

further divided into acid and base catalyst where the selection generally determined by the free fatty acid (FFA) content in the feedstock oil.

#### 1.4.4.2 Homogeneous and Heterogeneous Catalyst

Conventionally, homogeneous catalysts such as sodium hydroxide (NaOH), potassium hydroxide (KOH), sulfuric acid ($H_2SO_4$) and phosphoric acid ($H_3PO_4$) are commonly used in industrial biodiesel production as they are cheap and easily available. They are more preferable due to their high catalytic performance and their ability to perform under mild operating conditions within short duration time. According to a report from Bobbili and Mosali (2011), since the catalyst is working out in same phase as the reactants, handling becomes much easier whereby handling all materials in liquid state is more convenient than handling liquid and solid together. However, homogeneous catalysts are very sensitive to FFA, hence high-quality feedstocks with low FFA (<3 wt%) is needed to prevent undesirable saponification. Major problems associated with the usage of homogeneous catalysts include the difficult catalyst recovery, low catalyst reusability, corrosion of equipment, low purity of glycerin, complicated product purification, high water consumption and waste stream pollution. Due to the various setback encountered in homogeneous catalyst, recently, heterogeneous catalysts such as solid catalysts and enzyme catalysts are highly researched to simplify and economise the transesterification process.

Presently, the application of heterogeneous catalyst had gain popularity in biodiesel production due to the numerous advantages that able to solve the technical problems encountered in homogeneous catalyst. The advantages include heterogeneous catalyst can produce high yield of biodiesel without the formation of fatty acid and soap, which results in easier product separation. Next, heterogeneous process directly produces pharmaceutical grade glycerin with high purity and low water content, reducing the number of distillation column and refining process. Meanwhile, no salt contaminants are formed, hence cost associated with waste treatment is greatly reduced. Even the amount of glycerin generated is 20% less than that of homogeneous process. However, pharmaceutical grade glycerin is a versatile and valuable chemical that has high economic profit. Heterogeneous solid catalyst also reduces the usage of corrosive chemicals such as sulfuric acid and sodium methoxide, thus less potential contaminants are disposed to waste stream.

. Besides, the usage of solid catalyst reduces equipment corrosion and lower the maintenance and insurance cost as well. Moreover, heterogeneous catalyst like activated carbon derived from biomass is cheap and thermally stable, and it can be recovered and reused. The long durability of catalyst makes the operation and maintenance become easier because it does not need to be replaced regularly. (Kiss, Jovanović and Bošković, 2010). Furthermore, heterogeneous catalyst does not need additional storage and careful handling like corrosive chemicals used in homogeneous process, making the process safer and reliable. In addition, heterogeneous catalyst has higher tolerance on free fatty acid present in feedstock. This allows the use of cheaper low-grade oil which can save substantial amount of biodiesel production cost. Lastly, the usage of solid catalyst increases the number of reactor options, such as fixed-bed or slurry reactor. The pores of solid catalyst can be modified to enhance the selectivity towards the desired product. (Kiss, Jovanović and Bošković, 2010).

On the other hand, there are some limitations of using heterogeneous catalyst. Due to lower catalyst activity, heterogeneous reaction that requires extreme reaction condition is carried out at higher pressure and temperature. This increases energy consumption, therefore, higher utility cost is needed to operate. Besides, the use of heterogeneous catalyst will contribute to depletion of fossil energy resources and higher emission of greenhouse gases due to higher energy and methanol consumption. Lastly, there are some possible issues related to the use of solid catalyst such as poisoning and leaching of catalyst active site, which will result in contamination of product.

#### 1.4.4.3 Alkaline-catalysed transesterification

Base-catalysed transesterification is commonly used in commercial production since it requires only mild operating condition to produce over 98 % conversion yield in relatively short period (< 1hr); and the conversion rate is high with no intermediate compounds formed (Refaat, 2009). However, base catalyst which is sensitive to FFA content needs high-quality feedstock with low FFA content (< 1 % w/w). In addition, moisture content is crucial in base-catalysed transesterification, hence all reactants used must be substantially anhydrous (0.06 % w/w). The water present in it will promote saponification to form soap and hydrolyse the produced ester into FFA. Subsequently, the FFA will irreversibly consume and deactivate by base catalyst to

form alkaline salt. This will reduce catalyst efficiency and lead to lower ester yield. Meanwhile, the soap formed will increase the viscosity of ester formed, leads to gel formation and complicates the biodiesel purification process. Saponification can be avoided by using high-quality refined feedstocks which is much more expensive, and renders the biodiesel production not profitable.

The most commonly used homogeneous base catalyst includes potassium hydroxide (KOH), sodium hydroxide (NaOH), potassium methoxide ($KOCH_3$) and sodium methoxide ($NaOCH_3$). Among these homogeneous alkaline catalysts, alkaline metal alkoxides such as $CH_3ONa$ are believed to perform better since they can reach high yield (>98 wt%) in short reaction time (30 min) and no water is formed during the reaction. However due to their toxicity, disposal problem and lower price of metal hydroxide, NaOH and KOH are mostly employed in large-scale production. For heterogeneous base catalyst, the most widely used catalysts are alkaline earth metal oxides (CaO, MgO), zeolites, supported alkali metal and hydrotalcite. These metal oxides, particularly CaO and MgO are cheap and readily available. Therefore, they are more to be active and stable, which will be desirable catalysts for industrial biodiesel production (Abbaszaadeh, et al., 2012). Similar to their homogeneous counterparts, solid-base catalyst is more active than solid-acid catalyst due to their higher activity. Heterogeneous base catalyst is better than homogeneous catalyst in terms of separation and purification. However, the reaction rate for solid catalyst is relatively slow due to the mass transfer limitation in two-phase system.

#### 1.4.4.4 Acid-catalysed transesterification

For raw material with high FFA content, a strong acid catalyst such as hydrochloric, sulfuric, phosphoric acid or organic sulfonic acid is usually more favorable since it gives a better conversion with no soap formation. Thus, acid catalyst has the advantage of esterifying low-value feedstock such as waste cooking oil in biodiesel production. A two-step transesterification is carried out with acid-catalysed esterification followed by transesterification to convert FFA into methyl ester. Besides, it is important to maintain the moisture content of raw material below 0.5 wt% as acid catalyst is very sensitive to the presence of water. According to Dalai and Baroi (2012), the increase in water content by 5% reduced ester yield significantly

from 95% to 5.6%, showing that acid catalyst will be deactivated by the presence of small amount of water.

Acid-catalysed reactions are less effective as compared to base-catalysed reactions due to the extreme operating conditions needed to operate. Moreover, excess methanol is used to increase the conversion of triglyceride molecules. In practice, in order to reduce the reaction time, acid catalyst is only used to convert FFA to esters during esterification step while base catalyst is used to catalyse the transesterification of triglycerides to esters. In general, acid-catalyst transesterification is usually performed at the following conditions: a high molar ratio of methanol to oil of 12:1; high temperatures of 80-100 $^{o}$C; and a strong acid namely sulfuric acid (Thanh, et al., 2012). Other disadvantages of using acid catalyst are corrosive effluent, low catalyst regeneration and high equipment cost.

Compared to homogeneous acid catalyst, solid-acid catalyst has better performance since it contains various strong and weak acid sites such as Bronsted and Lewis acid. Solid acid catalysts with high acid density such as sulfated zirconia, Nafion-NR50 and tungstated zirconia are favourable for biodiesel production (Aransiola, et al., 2014). Besides, heterogeneous acid catalyst is popular in industrial processes since it eliminates the need for biodiesel purification as the catalyst can be separated easily. Unlike homogeneous acid catalyst, heterogeneous solid acid catalyst is insensitive to FFA content and will not cause corrosion problem (Abbaszaadeh, et al., 2012).

## 1.5 Problem Statement

Due to the energy security issues and the growing environmental awareness brought by the extensive usage of fossil fuel, the search for alternatives energy becomes a worldwide effort. For now, biodiesel is hailed as a potential saviour for the environment which can substitute diesel fuel in energy generation. Although biodiesel production is widely studied in industry and research, none of them come out with a perfect solution to solve the practical issues faces currently. The major obstacle encountered in commercial biodiesel production is the high production cost which is about threefold of the conventional diesel. In order to lower the production cost, low-cost feedstocks with high FFA content such as palm fatty acid distillate (PFAD) can be used. Yet, current industry practice fails to process low-grade feedstock with high FFA and moisture content.

Besides, design of effective catalyst is also an important element to achieve more economic production. Currently, homogeneous alkaline catalyst employed in commercial production has the largest limitation dealing with the high FFA content although it shows higher reaction rate than acid catalyst. On the contrary, heterogeneous acid catalyst is a preferable option to deal with high FFA raw materials as it does not form soap and easy to be separated after reaction. In this case, heterogeneous catalyst seems to be a potential catalyst to be used in the biodiesel process due to its high yield of biodiesel formed and simple purification procedure.

In this study, various chemical pretreatment parameters were studied to obtain the optimum conditions to synthesise a highly porous and reactive biomass catalyst. The usage of different biomass material as activated carbon precursor need to be studied as different biomass has its own carbon content.

## 1.6 Aims and Objectives

This research project aims to study the effect of different pretreatment parameters on the solid acid and alkaline catalyst derived from three different biomass using three different sulfonation methods. The objectives of this study include:

i. To investigate the optimum pretreatment conditions for oil palm frond precursor.

ii. To compare the optimum sulfonation method from 4-BDS, ammonium persulfate and direct sulfonation.

iii. To characterise the chemical and physical properties of synthesised catalyst using SEM-EDX, TGA, FTIR, TPR and GC.

## 1.7 Scope and Limitation of the study

This research project focuses on the pretreatment parameters used to synthesis solid catalyst from the biomass. The first part of the project focus on the selection of optimum biomass among 3 different biomass precursors which are banana peel, palm oil frond and empty fruit bunch. Part 2 of the research focuses on the determination of optimum pretreatment condition to synthesise a thermally stable and high activity activated carbon. After the biomass is activated, three different sulfonation methods that include 4-BDS, direct sulfonation and sulfonation with ammonium persulfate are investigated to obtain the sulfonated activated carbon with the best outcome. Part 4 of the research is carried out to study the production of biodiesel by using the catalyst

synthesised from previous parts. The efficiency of sulfonated solid catalyst will be tested in esterification of palm fatty acid distillate (PFAD) and various parameters of the process are manipulated to obtain the optimum conditions with best performance.

However, there are several limitations which need to be considered and can be improved in the near future. The scope of this study only covers the pretreatment parameter of the catalyst. Other parameters regarding the sulfonation process and biodiesel production such as sulfonation duration, concentration of sulfuric acid, catalyst loading, reaction duration, reaction temperature and methanol to PFAD molar ratio are not being investigated.

## 1.8 Contribution of the Study

Most of the researchers had discussed about the biomass-derived heterogeneous catalyst for biodiesel production. Chemical activation of biomass using phosphoric acid and zinc chloride are the typical acid activating agents used. However, alkaline activating agent, NaOH is going to be implemented in this research study. Besides, the impregnation process will be conducted with mild heating, which is not implemented in the previous research studies. Other than that, activated carbon is commonly sulfonated via arylation using 4-benzenediazoniumsulfonate (4-BDS). Nevertheless, in this study, direct sulfonation using concentrated sulfuric acid will be conducted to synthesise catalyst.

## 1.9 Outline of the Report

Chapter 1 outlines the brief overview of the current energy scenario and the common biodiesel production technology used. Problem statement, aims and objectives, scope and contribution of the study are discussed. Chapter 2 reports the results obtained from related research journals on heterogeneous catalyst production. This includes prior empirical study of the types of biomass precursors and activating agent used, pretreatment conditions such as carbonization temperature and impregnation ratio, catalyst sulfonation method and reaction mechanisms of biodiesel production. Next, Chapter 3 describes the research methodology and planning of synthesising the solid acid catalysts and subsequent biodiesel production. Chapter 4 discuss on the data obtained through analysis and interpretation on the performance of catalysts. Lastly, Chapter 5 concludes the study and suggests the possible recommendations.

# CHAPTER 2

# LITERATURE REVIEW

## 2.1 Transesterification mechanism

Biodiesel can be produced by transesterification process which consists of a number of reversible and consecutive reactions in which alcohol is added in excess to shift the equilibrium towards the desired fatty acid methyl esters (FAME). Figure 2.1 shows the stepwise conversion of triglyceride to diglyceride and monoglyceride intermediates, and eventually generates 3 moles of FAME and 1 mole of glycerol. Commonly, the use of acid or base catalyst is highly dependent on the FFA content present in the feedstock. Acid-catalyst transesterification is preferable for oils with high FFA and moisture content while base-catalyst is recommended for oil with FFA content less than 1wt%.

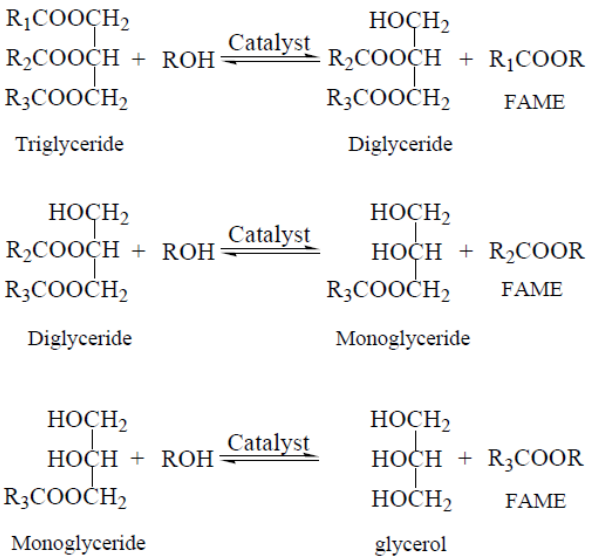


Figure 2.1: Transesterification Reactions of Triglyceride with Alcohol (Ma and Hanna, 1999)

### 2.1.1 Mechanism for base-catalysed transesterification

Figure 2.2 summarises the stepwise mechanism of triglyceride breakdown in base-catalysed transesterification. Firstly, protonated catalyst and nucleophilic alkoxide (methoxide ion) are generated in the reaction of alcohol with the base catalyst. The second step is the formation of tetrahedral intermediate due to the nucleophilic attack of alkoxide at the electrophilic part of the carbonyl carbon atom on the triglyceride.

The third step involves the breakdown of the unstable intermediate tetrahedral into fatty acid methyl ester and the corresponding diglyceride anion. Lastly, the catalyst is deprotonated through proton transfer, thus active species are recovered for the use in subsequent catalytic cycle. The same mechanisms steps are repeated for cleavage of each fatty acid methyl ester and conversion of diglycerides and monoglycerides to a mixture of three fatty acid methyl esters and one glycerol.

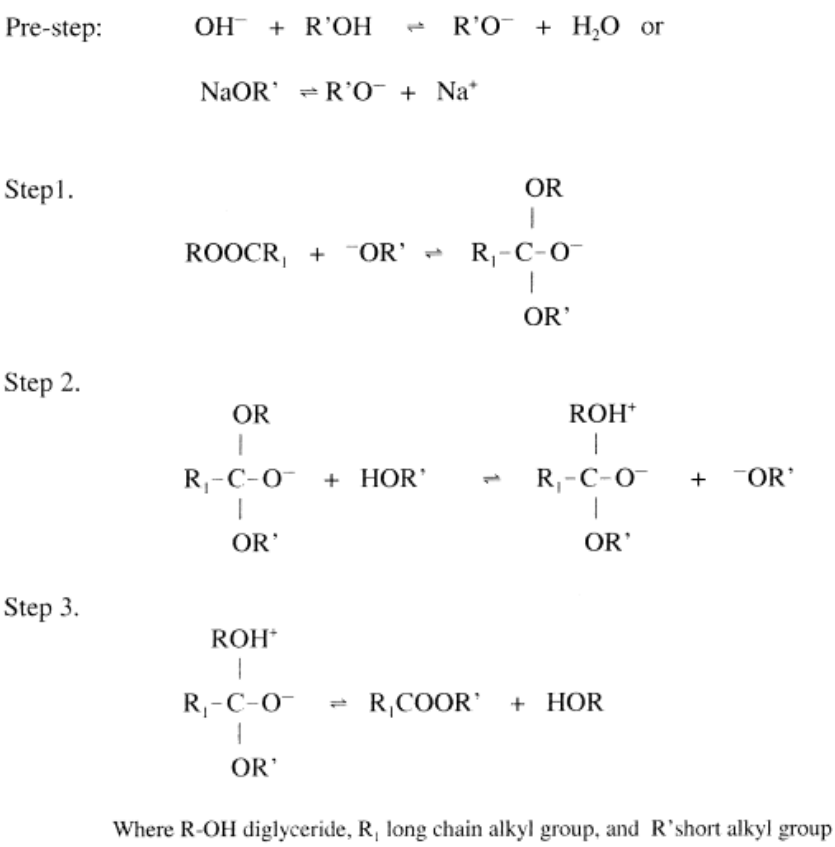


Figure 2.2: Mechanism for Base-catalysed Transesterification (Ma and Hanna, 1999)

For an alkali-catalysed transesterification, the reaction of hydroxide with alcohol will form water which will hydrolyse some of the produced esters and cause saponification. The undesirable soap produced reduces the FAME yield and results in difficult separation of the separation of ester from by-product due to the formation of emulsions which increase the viscosity of product mixture. Therefore, feedstock with low FFA content is needed for alkali-catalysed transesterification. Or else, a two-step transesterification is employed to esterify the FFA content in triglyceride before transesterification process can be conducted.

### 2.1.2 Mechanism for acid-catalysed transesterification

Figure 2.3 shows the mechanism of acid-catalysed transesterification of triglycerides. Firstly, the hydrogen ions generated from the acid catalyst will protonate the carbonyl group on the triglycerides. Then, a tetrahedral intermediate forms after nucleophilic attack of the alcohol on the carbonium ion. Lastly, unstable tetrahedral intermediate will be broken down and leads to proton migration. After repeating twice, three new fatty acid methyl esters and one glycerol were produced as products and the catalyst was regenerated. During the catalytic process, protonation of carbonyl group boosts the catalytic effect of acid catalyst by increasing the electrophilicity of the adjacent carbonyl carbon atom. However, FAME yield will be affected due to the competitive formation of carboxylic acids by reaction of water with carbonium ions generated. This phenomenon can be avoided by conducting the acid-catalysed transesterification in the absence of water.

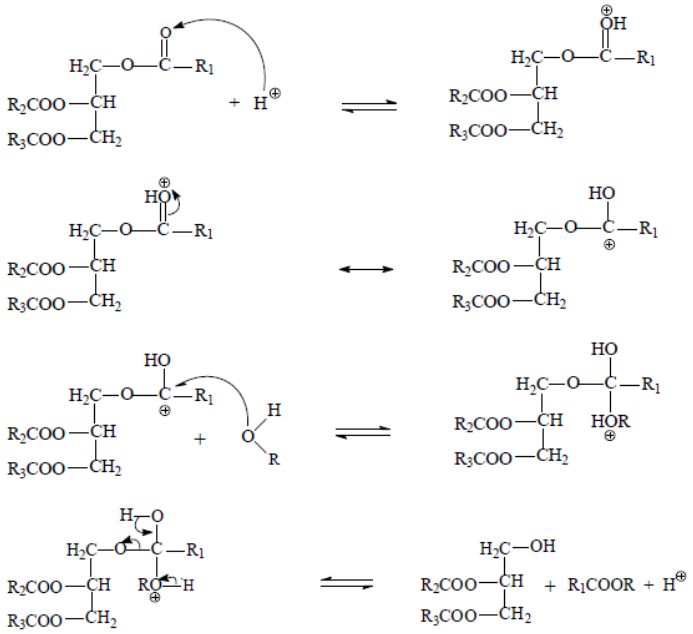

Figure 2.3: Mechanism for Acid-catalysed Transesterification (Ma and Hanna, 1999)

### 2.2 Esterification mechanism

This method is useful when dealing with low-value feedstocks which need to be pretreated (esterification) to reduce FFA content before base-catalysed transesterification reaction can be carried out at an FFA mass fraction lower than 0.5% (Aransiola, et al., 2014). A two-step transesterification process involves the first step which is the acid catalysed esterification of the FFA to FAME, followed by a second step which is the common alkali catalysed transesterification.

In homogeneous acid-catalysed esterification, FFA will release hydroxide ions while methanol will release proton without intermediate process. On the contrary, heterogeneous acid-catalysed esterification will supply carbonium ion which involves intermediate process. Figure 2.4 shows the mechanism of solid acid-catalysed esterification. Firstly, carbonyl carbon of triglycerides is protonated by protons from solid acid catalyst to form a carbonium ion. Next, a tetrahedral intermediate is formed after attack of alcohol on the carbonium ion. Finally, proton migration and breakdown of unstable intermediate takes place which generates FAME and water. The proton is then reformed and ready to be used for next catalytic reaction.

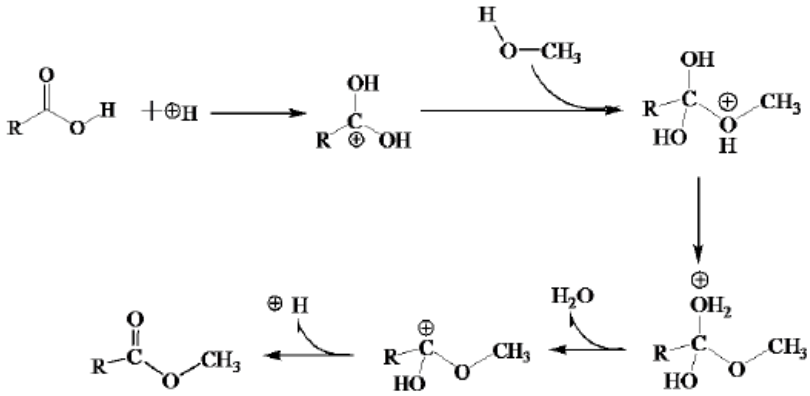

Figure 2.4: Solid Acid-catalysed Reaction Mechanism of Esterification (Ma and Hanna, 1999)

## 2.3 Carbon-based Solid Catalyst

Owing to the mass transfer diffusional resistance brings up by heterogeneous catalysis, catalyst support which can provide large surface area ranging from about 500 to 1500 m2/g with a highly developed internal pore structure for active species to anchor and react was utilised to increase the reaction rate to a large extent. In recent years, activated carbon has been widely used as it has a distinctive structure with high porosity, large surface area, high adsorption capacity, high chemical and mechanical resistance and the presence of various surface functional groups.

### 2.3.1 Activated Carbon Precursors

Recently, agricultural wastes with high carbon and low ash content have been widely used as activated carbon precursors because they are cheap, renewable and easily available, resulting in low-cost and environmentally benign biodiesel production.

The agricultural wastes used for activated carbon synthesis also offers an environmental friendly and cost-effective way to overcome the waste disposal problems. Basically, the choice of precursor to synthesise activated carbon depends on its availability, purity, price, potential to be activated, possibility of degradation by aging and inherent porosity and filterability (Yahya, Al-Qodah and Ngah, 2015). Table 2.1 present the lignocellulosic composition of a variety of agricultural residues, which will directly affect the properties, quality and performance of the activated carbon produced.

Table 2.1: Lignocellulosic Composition of Agricultural Residues (Yahya, Al-Qodah and Ngah, 2015)

| Agricultural waste | Cellulose | Hemicellulose | Lignin |
|---|---|---|---|
| **Palm shell** | 29.0 | 47.7 | 53.43 |
| **Coconut shell** | 19.8 | 68.7 | 30.1 |
| **Almond shell** | 32.5 | 25.5 | 24.8 |
| **Walnut shell** | 40.1 | 20.7 | 18.2 |
| **Almond tree pruning** | 33.7 | 20.1 | 25.0 |
| **Olive stone** | 30.8 | 17.1 | 32.6 |
| **Banana empty fruit bunch** | 8.30 | 21.23 | 19.06 |
| ***Delonix regia* fruit pod** | 13.90 | 24.13 | 23.36 |
| **Pomegranate seed** | 26.98 | 25.52 | 39.67 |
| **Coconut husk** | 0.52 | 23.70 | 3.54 |
| **Cocoa pods** | 41.92 | 35.26 | 0.95 |
| **Kola nut pod** | 38.72 | 40.41 | 21.29 |
| **Plantain peel (ripe)** | 13.87 | 15.07 | 1.75 |
| **Plantain peel (unripe)** | 10.15 | 11.38 | 1.75 |
| **Coconut shell** | 15.0 | 35.0 | 50.0 |
| **Apple pulp** | 16.0 | 16.0 | 21.0 |
| **Plum pulp** | 6.5 | 14.5 | 39.0 |

Table 2.1 (Continued)

| Agricultural waste | Cellulose | Hemicellulose | Lignin |
|---|---|---|---|
| **Plum stone** | 23.0 | 20.0 | 49.0 |
| **Olive stone** | 14.0 | 15.0 | 42.0 |
| **Soft wood** | 36.0 | 18.5 | 30.5 |
| **Coconut shell** | 14.0 | 32.0 | 46.0 |
| **Sugarcane bagasse** | 42.16 | 36.0 | 19.30 |
| **Cocoa pod husk** | 41.92 | 35.26 | 0.95 |

## 2.4 Activated Carbon Preparation

In general, physical and chemical treatment are the two common methods employed in activated carbon preparation to change the physical properties of the support. In physical treatment, the biomass precursor is first carbonised followed by activation under a flow of carbon dioxide or steam. High degree of burning will burn off large amount of internal carbon mass, which eventually form activated carbon with high porosity.

In chemical treatment, activating reagent ($ZnCl_2$, $H_3PO_4$, NaOH and KOH) is used to impregnate carbon precursors prior to carbonisation under an inert atmosphere. The dehydrogenation effect of chemical reagents will form cross-links and develop a rigid matrix which is less susceptible to volatile loss and is less likely to shrink when used (Islam, et al., 2018). Nevertheless, chemical activation is now widely implemented owing to its simplicity, lower activation temperature, lower volatile matter content, higher product yield, higher surface area and good development of micropores. However, the impregnated carbon material need to be washed thoroughly in order to remove the remaining activating agent which is corrosive. The choice of activation technique will determine the adsorption performance and pore characteristics of activated carbon.

### 2.4.1 Physical Activation

As aforementioned, physical treatment consists of two steps which are carbonisation and activation. It is a dry oxidation process since the sample is reacted under gas mixture ($CO_2$ and air) or steam at carbonisation and activation temperature ranges between 400-850$^oC$ and 600–900$^oC$ respectively (IOANNIDOU and ZABANIOTOU, 2007). It is more preferable to use $CO_2$ gas since it is clean, easy to operate and its

slow reaction rate allows the temperature to be maintained at around 800 $^{o}$C. (Yahya, Al-Qodah and Ngah, 2015) In addition, activation using $CO_2$ can develop pores with high uniformity as compared to steam.

According to Prahas, et al. (2008), polymeric cellulose or lignin undergoes pyrolytic decomposition and eliminates gases and tars which consists of light volatile elements and aromatic compounds. This process will initiate the formation of pores in the carbonaceous char with high content of fixed carbon. Then, this carbonaceous char will be activated to form high porosity activated carbon through further gasification.

During activation, the pores initially formed in the char is further developed when organic matter that is more volatile is eliminated selectively, hence generating highly porous activated carbon. Pores and channels are formed when oxidising gases entering into the carbon bulk bring away the volatile matters through particles, creating more pores which result in ordered carbon structure with high porosity. The pores developed during physical activation can be summarised into three phases; creation of new pores, widening of old pores, and porosity development by selective removal of cellulose material (Li, et al., 2008). Physical and chemical properties of the synthesised activated carbon are highly dependent on the type and degree of thermal activation.

### 2.4.2 Chemical Activation

Chemical activation, also known as wet oxidation involves the impregnation of carbon precursor in activating reagent before it is heat-treated under inert atmosphere. According to Yahya, Al-Qodah and Ngah, (2015), chemical activation is conducted at a relatively low temperature range between 450 to 600 $^{o}$C, depending on the dehydration action of the activating agent on cellulose component in the starting material. The chemical catalysts that usually used can be divided into basic reagent (KOH, NaOH) and acidic reagent ($ZnCl_2$, $H_3PO_4$, $H_2SO_4$, HCl, $HNO_3$). Of the many chemical reagents proposed, $ZnCl_2$, $H_3PO_4$ and KOH are the most commonly used. The use of chemical agent restricted the formation of the tar or ash, this not only increases the carbon yield in the carbonised product but also changes the pyrolysis decomposition of the precursors, resulting in enhanced porosity. Besides, activating agents can introduce oxygen functional groups to the surface of the carbon precursor. After activated by chemical, acid or alkali was used to wash the activated carbon

followed by water to wash away the activating agents occupied in the pores of activated carbon so that porosity can be developed.

## 2.5 Effect of Chemical Activation Parameters

### 2.5.1 Effect of activating agents

In chemical activation method, carbon precursors can be impregnated by a wide range of acid and base chemical agents such as $ZnCl_2$, $H_3PO_4$, $H_2SO_4$, $K_2CO_3$, KOH and NaOH. Both acid and alkali activating agents could improve the pore properties of carbonised carbon and introduce different functional groups onto the surface of biochar, increasing the availability of binding sites. The chemical attack of acid and alkali agent removes volatile matter which corresponds to the decomposition of lignin and cellulose component. This develops porosity (micropores and mesopores) and increases specific surface area of carbon.

Various literatures reported that $ZnCl_2$ and $H_3PO_4$ are commonly used among the acid chemical activating agents for lignocellulosic materials. Chemical treatment with $ZnCl_2$ mainly produces microporous structure with significant surface area as compared to $H_3PO_4$. $ZnCl_2$ which acts as dehydrating agent induces the charring by breaking the lateral bond in lignocellulosic structures into fragments. This allows reorganisation of the fragments into a new matrix, causing the particles to swell and develop voids between carbon layers. The voids created will eventually develop microporous structure upon activation. (Kalderis, et al., 2008) Fragmentation also inhibited the tar formation which avoided the blocking of pores and fissures, resulting in enhanced carbon yield. Besides, $ZnCl_2$ has the ability to increase the combustion energy during pyrolysis process could enhance the porosity development of the activated carbon. (Yahya, Al-Qodah and Ngah, 2015)

It was reported that $H_3PO_4$ was effective in producing the mesopores with high pore volumes and diameter, resulting in wide pore size distribution. The surface area obtained from the chemical treatment of $H_3PO_4$ was far lower than the one treated by $ZnCl_2$ (350 – 700 $m^2$ /g by $H_3PO_4$ activation and 500 –2000 $m^2$ /g by $ZnCl_2$ activation) (Ismail, Taha and Ramli, 2016). The lower surface area of the carbon obtained may be due to the strong bonding of phosphates within the lignocellulosic structure, leading to the formation of cross-link structures which will shrink and reduce the porosity at activated carbon at high temperature. The usage of $H_3PO_4$ activator only required low activation temperature at around 400 $^oC$ and still

produce activated carbon with good chemical and thermal stability. Although $ZnCl_2$ activation results in significant surface area, nevertheless $H_3PO_4$ is more favourable than $ZnCl_2$ since it is eco-friendlier.

An example of the usage of $ZnCl_2$ and $H_3PO_4$ for activation is the work of Hayashi, et al. (2000) who prepared activated carbon from Kraft lignin pulping. It was observed that the surface area obtained for $ZnCl_2$ is higher than that of $H_3PO_4$, which were 1000 $m^2/g$ and 700 $m^2/g$ at 500 $^oC$, respectively. Similar results were obtained by Liou and Wu (2009) in his studies on chemical activation of rice husk using $H_3PO_4$ and $ZnCl_2$ as activating agents. The result showed that $ZnCl_2$ activated carbon had a more remarkable BET surface area (2434 $m^2/g$) as compared to $H_3PO_4$ activated carbon (1741 $m^2/g$) at the same activation condition. Unlike Zn salts, the strong bonding of phosphorus compounds with carbon makes it hard to be recovered during washing steps after activation, hence restricting the pores development and resulted in reduced surface area. Pua, et al. (2011) studied the optimum BET surface area of activated carbon supported catalyst and the optimal reaction conditions of biodiesel production. It was reported that the phosphoric treated Kraft lignin activated carbon yielded a high contact area of 654.4 $m^2/g$, indicated that phosphoric pretreatment developed well-defined pores on the carbon surface. The solid catalyst produced able to give a high biodiesel yield of 96.3% via esterification of non-pretreated Jatropha oil. Various researches done by using different carbon precursors such as coconut shell and *Jatropha curcas* fruit shell treated with $H_3PO_4$ and their respective reaction conditions were summarised in Table 2.2.

For alkaline activator, KOH and NaOH are the most commonly used activating agents due to their ability to produce activated carbon with well-developed porosity and narrow pore size distribution. It has been proposed that the activation mechanisms of alkaline activators were different from those of acid activators like $ZnCl_2$ and $H_3PO_4$. This is proved in a research work done by Hayashi, et al (2000) that the alkali treated carbon had a maximum surface area at the temperature of 800$^o$C while $ZnCl_2$ and $H_3PO_4$ had the best results at the temperature of 600$^o$C, but do not work well at temperature beyond that. Although activation with $ZnCl_2$ only required a low temperature, however, the use of KOH was preferred because it is eco-friendlier as compared to $ZnCl_2$.

In previous literatures, it has been always concluded that KOH was more effective than NaOH. However, this statement was proved wrong after a few recent

researchers found that the effectiveness of NaOH depends on the structural organisation of the carbon precursors, which was not previously considered. There were clear evidences that NaOH was better for carbons with poorly organised materials (e.g., almond shell), whereas KOH was found effective for carbon with any structural order (e.g., anthracite), especially more efficient with increasing crystallinity. The difference in effectiveness is attributed to the ability of K and Na metal to intercalate into the carbon structure. According to Raymundo-Piñero, et al. (2005), the intercalation ability of KOH and NaOH was studied using nanotube materials with different crystallinity including highly ordered graphite walls and nanotubes with amorphous layers. It was reported that K metal intercalates well into the well-organised nanotubes walls while Na metal can intercalate better in poorly organised or defective structure. K metal that intercalates better than Na metal able to develop microporosity with more binding sites. In conclusion, the degree of crystallinity of carbon precursor is an important parameter which must be taken into consideration when dealing with alkali agents.

Muniandy, et al. (2014) had carried out the activation of rice husk by adding 3g of rice husk carbon into 40% (w/w) of KOH and NaOH solution. From the result, it was observed that KOH activation gave a higher surface area (682.6 $m^2/g$) compared to NaOH (594.9 $m^2/g$) at the same temperature of 750$^oC$. The larger surface area was owing to the fact that K metal is more reactive than Na metal, the effective activation generates highly porous carbon with micropores. Table 2.2 summarises the use of KOH and NaOH to activate various agricultural residues and their respective reaction conditions for esterification process.

Table 2.2: Various Activating Agent Used and the Corresponding Performance of the Activated Carbon Catalyst

| **Biomass** | **Activating agent** | **BET Surface Area ($m^2/g$)** | **Reaction Conditions** | | | | | **Yield (%)** | **Reference** |
|---|---|---|---|---|---|---|---|---|---|
| | | | **Feed Stock** | **Temperature (°C)** | **Alcohol to Oil molar ratio** | **Reaction time (h)** | **Catalyst Loading (wt%)** | | |
| **Kraft Lignin** | $H_3PO_4$ | 654.4 | Jatropha Oil | 80 | 12:1 | 5 | 5 | 96.3 | Pua, et al. (2011) |
| **Coconut Shell** | $H_3PO_4$ | 898.6 | WFO | 60 | 25:1 | 2 | Catalyst bed height: 250mm | 86 | Buasri, et al.(2012) |
| ***Jatropha curcas* Fruit Shell** | $H_3PO_4$ | 927.85 | WFO | 60 | 16:1 | 2 | Catalyst bed height: 250mm | 87 | Buasri, et al. (2012) |
| ***Albizia Lebbeck* Pods** | $H_2SO_4$ | 1827.23 | Rubber Seed Oil | 55 | 7:1 | 1.5 | 1.5 | 97.2 | Subramonia Pillai, et al.(2017) |

Table 2.2 (Continued)

| Biomass | Activating agent | BET Surface Area ($m^2/g$) | Reaction Conditions | | | | | Yield (%) | Reference |
|---|---|---|---|---|---|---|---|---|---|
| | | | Feed Stock | Temperature (°C) | Alcohol to Oil molar ratio | Reaction time (h) | Catalyst Loading (wt%) | | |
| **Pomelo Peel** | KOH | 278.2 | Palm Oil | 65 | 8 | 2.5 | 6 | 98 | Zhao, et al. (2018) |
| **Meat and bone meal** | KOH | 430.52 | Palm Oil | 65 | 7:1 | 2.5 | 5 | 98.2 | Wang, et al. (2017) |
| **Flamboyant Pods** | KOH | 820 | Rubber Seed Oil | 55 | 15 | 1 | 3.5 | 89.81 | Dhawane, Kumar and Halder (2016) |
| **Palm Shell** | KOH | 1015 | Palm Oil | 64.1 | 24 | 1 | 30.3 | 97.72 | Baroutian, et al.(2010) |
| **Green Mussels Shell** | NaOH | N/A | Palm Oil | 65 | 2:1 weight ratio | 3 | 7.5 | 95.12 | (Hadiyanto, et al., 2017) |

### 2.5.2 Effect of Impregnation Ratio

Impregnation ratio is defined as the ratio of the weight of the carbon precursor to the activating agent, which are typically in the range of 1:0.5 to 1:3 based on dry matter. The degree of impregnation ratio is one of the key factors which will affect the chemical activation process and is seen as an analogue to the magnitude of burn-off in physical activation. Generally, at higher chemical concentration, better porosity development in activated carbon is observed since the effect of the activation agent increases with increasing dose. According to Ismail, Taha and Ramli (2016), he found out that by varying impregnation ratio of rice husk to $ZnCl_2$ from 1:1 to 1:4, the carbon yield and BET surface area increased proportionally with the impregnation ratio. The yield and BET surface area increased from 37.85% to 40.9% and from 412.686 $m^2/g$ to 922.319 $m^2/g$, respectively. This is because by increasing the impregnation ratio, the formation of tar was inhibited, hence carbon yield was enhanced.

Similar result was obtained by Md Arshad, et al. (2016) in which three different concentrations of KOH activating agent (0.5M, 1.0M and 2.0M) were used in the impregnation of 4g of activated carbon, which was empty fruit bunch in this case. BET result indicated that the samples surface area increased from 305 $m^2/g$ to 687 $m^2/g$ when KOH concentration increased from 0.5M to 2.0M. The increase in surface area also accompanied by an increase in pore diameter and micropore volume. At greater amount of KOH impregnation concentration, the dehydration effect becomes more significant which led to the opening of pores, leading to formation of porous structure and increased sample surface area.

However, in the study of Kalderis, et al. (2008), the effect of impregnation ratio to two different carbon precursors, bagasse and rice husk was slightly different from the previous studies. In this study, both bagasse and rice husk were impregnated with $ZnCl_2$ at a ratio of 0.25, 0.5, 0.75 and 1. With the increased ratio from 0.75 to 1 for bagasse, a turning point was observed where surface area started to decrease. The decrease in surface area may due to the collapsing and widening of micropores, leading to the development of mesopores. Whereas for rice husk, the carbon with the highest surface area (750 $m^2/g$) was obtained at a ratio of 1:1 (w/w), no turning point was observed as in bagasse.

In a work by Budi, et al. (2016), coconut shell charcoal carbon was activated using varied concentration of KOH solution at 30, 40, 50 and 60%. It was reported

that the pore number increased and pore size distribution became narrow as KOH concentration was increased. However, at higher KOH concentration, the number of pores decreased and pore size distribution was widened due to the aggressive attack of chemical that weakened and progressively collapsed the incipient carbon structure. Thus, optimisation of impregnation ratio is important to achieve a balance between the two competing mechanism phenomenons during activation process, namely micropore formation and pore widening.

### 2.5.3 Effect of Carbonisation Temperature

In general, the increase in carbonisation temperature usually accompanied by an increase in number of pores and surface area because volatile matter tends to escape from carbon precursor at high temperature, leaving vacancies for new pores formation. However, the further increase in temperature will destroy the micropore structure by collapsing or closing of pores and ultimately lowering the surface area and carbons yields.

Kalderis, et al. (2008) studied the effect of temperature on the pores properties of activated carbon prepared from bagasse and rice husk by $ZnCl_2$ activation performed at temperatures of 400, 600, 700 and 800 $^oC$. The results indicated that the highest surface area for both materials, which were 674$m^2/g$ and 750 $m^2/g$ respectively, was obtained at the optimum activation temperature of 700 $^oC$. The higher temperature released more tars and gasses which eventually generated new micro- and mesopores. However, at a temperature beyond 800 $^oC$, the surface area of activated carbon for both bagasse and rice husk will decrease significantly due to the violent gasification reaction. This will widen and collapse the existing pores, hence reducing the surface area available for binding sites attachment.

Zhao, et al. (2018) investigated the effect of the carbonisation temperature on the surface area and pore structure of activated carbon produced from pomelo peel. They found that as calcination temperature increased from 500 to 600 $^oC$, the yield rose from 97.1% to 98%, reaching the maximum. However, further increase of temperature to 800 $^oC$ was not favorable since the elevated temperature might be too high and cause sintering of catalyst surface to occur. The sharp decreased in surface area might reduce the availability of active sites on the carbon surface.

Another study showed that when carbonisation temperature varied from 400-700 $^oC$ , both $ZnCl_2$ and $H_3PO_4$ activated rice husks samples had the highest BET

surface area at 500 $^{o}$C as shown in Table 2.3 and Figure 2.5. Liou and Wu (2009) stated that at temperature below 500 $^{o}$C, biomass precursors was not fully carbonised, pores may not fully develop and therefore resulted in a low surface area. However, at a temperature greater than 500 $^{o}$C, the violent gasification reactions might inhibit the micropores formation and collapse or destroy part of the developed micropores, resulting in mesopores formation. As a result, increased carbonisation temperature widen the micropores and led to an increase in mesopore volume.

Table 2.3: Surface Area and Pore Characteristics for Carbonation and Activation of Sample (Liou and Wu, 2009)

| **Activation Temperature ($^{o}$C)** | **$S_{BET}$ ($m^2/g$)** | **$V_T$ ($cm^3/g$)** | **$V_{mic}$ ($cm^3/g$)** | **$V_{meso}$ ($cm^3/g$)** | **$V_{mac}$ ($cm^3/g$)** | **$D_p$ (nm)** |
|---|---|---|---|---|---|---|
| **$H_3PO_4$ activation** | | | | | | |
| **400** | 1278 | 0.722 | 0.366 | 0.308 | 0.048 | 2.26 |
| **500** | 1741 | 1.315 | 0.286 | 0.672 | 0.357 | 3.02 |
| **600** | 1425 | 1.004 | 0.286 | 0.486 | 0.232 | 2.82 |
| **700** | 1380 | 0.912 | 0.293 | 0.405 | 0.214 | 2.75 |
| **$ZnCl_2$ activation** | | | | | | |
| **400** | 1545 | 0.798 | 0.463 | 0.285 | 0.050 | 2.06 |
| **500** | 2434 | 1.344 | 0.590 | 0.682 | 0.072 | 2.21 |
| **600** | 2062 | 1.090 | 0.473 | 0.593 | 0.024 | 2.11 |
| **700** | 1798 | 1.008 | 0.415 | 0.552 | 0.041 | 2.24 |

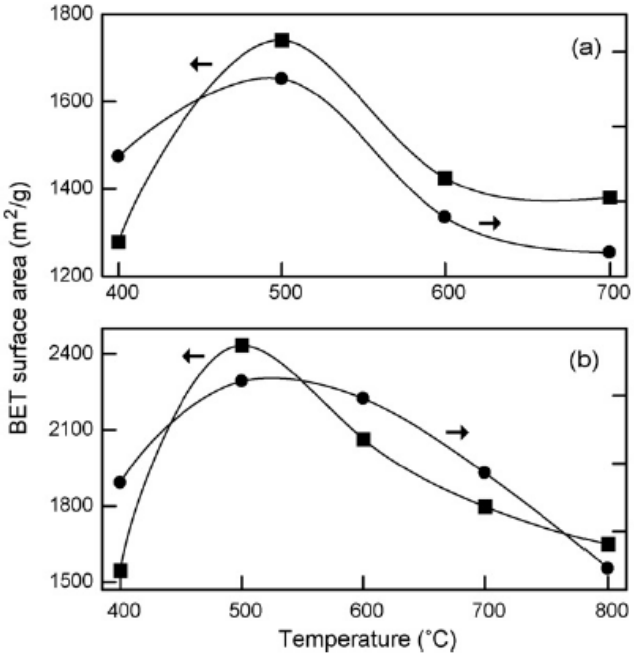


Figure 2.5: Effect of Carbonisation Temperature on the Surface Area of Samples: (a) $H_3PO_4$ Activation and (b) $ZnCl_2$ Activation (Liou and Wu, 2009)

## 2.6 Sulfonation of activated carbon

After carbonisation and activation steps, acid functional groups were attached to the activated carbon surface through different sulfonation methods such as direct sulfonation, arylation of 4-benzenediazonium sulfonate (4-BDS) and sulfonation by thermal decomposition of ammonium persulfate to form heterogeneous acid catalyst. Table 2.4 summarises a number of literatures that reported the application of sulfonated activated carbon as an effective catalyst for biodiesel production

According to Konwar, et al. (2015), different carbon precursors such as J. *curcas*, P. *pinnata* and M. *ferra* L were sulfonated to prepare mesoporous solid catalyst. Direct sulfonation and sulfonation by arylation of 4-BDS methods were studied to investigate the effects of preparation method on the $-SO_3H$ density and pores characteristics. It was reported that 4-BDS (4-benzenediazoniumsulfoante) was a better sulfonating agent as compared to the conventional $H_2SO_4$ in the sulfonation of rigid and highly ordered carbon structures such as activated carbon and graphene. Sulfonated carbon catalyst prepared by 4-BDS method exhibited well-developed pores and high $-SO_3H$ density. 4-BDS sulfonation method was claimed to be more effective than direct sulfonation method due to the ability to preserve the morphological structure of catalyst support under a mild temperature. This method is

mostly employed for carbon precursors with rigid and highly ordered structures. In this method, reduction of 4-BDS in the presence of $H_3PO_2$ generated aryl radicals which attached covalently on the carbon surface.

FTIR spectra with emergence band of S=O and -$SO_3H$ stretching proved successful incorporation of -$SO_3H$ and $PhSO_3H$ groups on the carbon surface. The attachment of acid groups was consistent with the reduction in pore volume (28–40%), pore diameters (0.4–1.9 nm) and surface areas (300–400 $m^2/g$) of the sulfonated materials. It was reported that the $SO_3H$ density obtained by 4-BDS was higher than that of direct sulfonation. The high $SO_3H$ density in 4-BDS was due to the increase in C content where more sites were available for 4-BDS radicals to attach on it. On the contrary, direct sulfonation exhibited relatively low $SO_3H$ density since $H_2SO_4$ sulfonation was difficult to sulfonate activated carbon with rigid and ordered frameworks even at higher temperature. Furthermore, it was demonstrated that the weight ratio of 4-BDS to sulfanilic acid barely affect the $SO_3H$ density, instead, the $SO_3H$ density depends on the amount of carbon content ($Sp_2C$ sites) for $PhSO_3H$ attachment. Besides, Konwar, et al. (2015) also found that the highest acid conversion in esterification by 4-BDS sulfonated catalyst was attributed to its highly porous carbon structure with relatively high $SO_3H$ density. Further, the stability of 4-BDS sulfonated catalyst also outperformed the conventional $H_2SO_4$ sulfonation method which had poor reusability owing to the easy leaching of $SO_3H$ groups from the sulfonated catalyst.

According to Ezebor, et al. (2014), activated carbon prepared from oil palm trunk (OPT) and sugarcane bagasse (SCB) were sulfonated using concentrated $H_2SO_4$ through direct sulfonation method in catalyst production. The study aimed to investigate the effect of sulfonation method on surface acidity, surface properties and catalytic activity of catalyst prepared. Results of FT-IR vibration band of –$SO_3H$ functional group indicated that appreciable sulfonation had taken place and the FT-IR spectra of catalysts prepared at varied sulfonation duration from 4h to 10h showed no large difference in the intensity of –$SO_3H$ peak. This proved that sulfonation duration had a negligible effect on the total acid density of catalyst surface. Sulfonic acid density was the highest at the beginning of sulfonation but it started to decrease and reached a plateau as the available sites for sulfonation decreased with time. Besides, the decrease in void volume after sulfonation proved that the Bronsted acid sites were successfully anchored on the carbon surface, resulting in less pore opening.

The oil palm trunk and sugarcane bagasse catalyst showed a high FAME yield of 80.60% and 83.32%, respectively in the esterification of palmitic acid conducted at 130 ℃. SCB derived catalyst had a slightly better result than OPT due to its higher $SO_3H$ density which allowed more reactants to access the Bronsted acid sites. In addition, both catalysts able to reduce high FFA content oil rapidly from 42wt% to <1 wt% in 15min of esterification. In catalyst reusability test, it was reported that both catalysts able to maintain the 98% of catalytic activity after four cycles, this indicated that no leaching of sulfonic acid occurred.

Next, the feasibility of sulfonation by thermal decomposition of ammonium persulfate was examined by Shuit and Tan (2014). The FAME yield of 88% was achieved by the sulfonated multi-walled carbon nanotubes (MWCNT) catalysed esterification at 170 ℃ for 3 hours. This high yield can be explained by the high sulfonic acid density in the catalyst (0.029 mmol/g) which can contribute more active sites for esterification. In catalyst reusability test, the sulfonated MWCNTs can be reused for at least 5 cycles with the biodiesel yield maintained at above 70%. The thermal stability of catalyst was tested and the TPD results showed that the sulfonated catalysts were stable at the temperature of 170 $^oC$, beyond that leaching of $SO_3H$ will occur which reduced the effectiveness of catalyst. This method was highly recommended since it was easy to operate and was acid-free which does not cause corrosion problem.

Table 2.4: Different Sulfonation Method of Carbon Catalyst

| Sulfonation Method | Carbon Source | Characterisation | Esterification | | | Reference |
|---|---|---|---|---|---|---|
| | | | Operating Conditions | Conversion (C)/ Yield (Y) | Catalyst reusability | |
| **Sulfonation by arylation of 4-BDS** | *J. curcas* deoiled seed waste cake | $V_{pore}$= 0.23$cm^3$/g; $S_{BET}$ = 96$m^2$/g; $SO_3H$ density= 0.7mmol/g | Feedstock= Oleic acid; Methanol/Oil ratio= 20:1; Reaction time= 10h; Reaction temperature= 64$^oC$; Catalyst Loading= 3wt% | C = 68% | C = 50% after 3 cycles | Konwar, et al.(2015) |
| **Sulfonation by arylation of 4-BDS** | *P. pinnata* deoiled seed waste cake | $V_{pore}$= 0.46 $cm^3$/g; $S_{BET}$ = 483$m^2$/g; $SO_3H$ density= 0.84mmol/g | | C = 96% | C = 60% after 3 cycles | |
| **Sulfonation by arylation of 4-BDS** | *M. ferrea L.* deoiled seed waste cake | $V_{pore}$= 0.41 $cm^3$/g; $S_{BET}$ = 468$m^2$/g; $SO_3H$ density= 0.75mmol/g | | C = 95% | C = 62% after 3 cycles | |

Table 2.4 (Continued)

| Sulfonation Method | Carbon Source | Characterisation | Esterification | | | Reference |
|---|---|---|---|---|---|---|
| | | | Operating Conditions | Conversion (C)/ Yield (Y) | Catalyst reusability | |
| **Sulfonation by thermal decomposition of ammonium sulfate** | Multi-walled carbon nanotubes (MWCNT) | Acid density= 0.029mmol/g | Feedstock= PFAD; Methanol/Oil ratio= 20:1; Reaction time= 3h; Reaction temperature= 170$^{o}$C; Catalyst Loading= 2wt% | Y = 88% | Yield = 77% after 5 cycles | Shuit and Tan (2014) |
| **Direct Sulfonation** | Oil palm trunk | $SO_3H$ density= 0.57mmol/g | Feedstock= Palmitic acid; Methanol/Oil ratio= 1.17mL/min; Reaction time= 4h; Reaction temperature= 130$^{o}$C; Catalyst Loading= 12wt% | Y = 80.6% | Yield = 98% of the catalytic activity after 4 cycles | Ezebor, et al.(2014) |
| **Direct Sulfonation** | Sugarcane bagasse | $SO_3H$ density= 0.53mmol/g | | Y = 83.2% | | |

# CHAPTER 3

# METHODOLOGY AND WORK PLAN

## 3.1 List of materials and apparatus

### 3.1.1 Materials and Chemicals

In this study, various types of chemicals and materials need to be prepared prior to the experiment. In this research, palm empty fruit bunch, palm frond and banana peel were selected as the biomass precursor to synthesis the solid catalyst for biodiesel production. Activation of carbon materials was done by using both sodium hydroxide and phosphoric acid activating agent. Sulfonation was carried out using 3 different methods which include direct sulfonation, thermal decomposition of ammonium sulfate and arylation by 4-BDS. The complete list of chemicals and materials needed in activation of biomass, sulfonation of carbonised char and esterification to produce FAME are listed in Table 3.1.

Table 3.1: List of Chemicals and Materials Required for Experiment

| Chemicals/ Materials | Source | Purity | Usage |
|---|---|---|---|
| **Palm Empty Fruit Bunch** | Oil Palm Estate at Tanjung Tualang | - | Carbon precursor to synthesise activated carbon |
| **Oil Palm Frond** | Oil Palm Estate at Tanjung Tualang | - | Carbon precursor to synthesise activated carbon |
| **Banana Peel** | Pasar Pagi at Sungai Long | - | Carbon precursor to synthesise activated carbon |
| **Sodium Hydroxide** | Merck | ≥85% | Activating agent of carbon precursor |
| **Palm Fatty Acid Distillate (PFAD)** | UTAR | - | Feedstock to produce biodiesel by esterification |

Table 3.1 (Continued)

| Chemicals/ Materials | Source | Estimated Quantity | Usage |
|---|---|---|---|
| **Methanol** | Merck | ≥ 99.8% | Reactant to produce biodiesel by esterification |
| **Hydrochloric acid** | Merck | 37% | To synthesise 4-BDS and determine acid density of catalyst |
| **Sulfanilic Acid** | Merck | 99% | To synthesise the sulfonating agent 4-BDS |
| **Sodium Nitrite** | ACROS Organic | 98% | To synthesise the sulfonating agent 4-BDS |
| **Ethanol** | Synerlab | 99.9% | To synthesise the sulfonating agent 4-BDS |
| **Ortho-Phosphoric Acid** | Merck | 85% | To activate biomass and sulfonate activated carbon by 4-BDS method. |
| **Ammonium Persulfate** | Merck | 98% | To sulfonate activated carbon by thermal decomposition of ammonium sulfate |
| **Sulfuric Acid** | Merck | 98% | To sulfonate activated carbon by direct sulfonation method, |
| **Potassium Hydroxide** | Merck | ≥ 99% | To determine the acid value of ester |
| **Phenolphthalein** | UTAR | 1g/L | pH indicator |
| **n-Hexane** | Merck | ≥ 99% | To dissolve biodiesel ester |
| **Deionised Water** | UTAR | - | To wash off excess reactant from solid catalyst |
| **Distilled Water** | UTAR | - | To wash off excess reactant from solid catalyst |

### 3.1.2 Apparatus, Equipment and Instrument

Table 3.2 shows the apparatus and equipment required to conduct the whole experiment. The respective specification and usage for each apparatus and equipment are listed as well. Table 3.3 shows the instruments required in feedstock, catalyst and biodiesel characterisation.

Table 3.2: List of Apparatus and Equipment Required for Experiment

| Apparatus/Equipment | Specification | Usage |
|---|---|---|
| **Oven** | Memmert | To dry the carbon precursor and carbonised carbon. |
| **Furnace** | Carbolite | To carbonise carbon precursors. |
| **Grinder** | Deer | To grind the raw material into powder. |
| **Sieve Tray** | 300μm, 1mm, 2mm | To separate the grounded powder into 3 different sizes. |
| **Mortar and Pestle** | 3 oz | To crush the carbonised material into smaller form |
| **Hot Plate** | IKA RH basic 2 | To heat up reaction mixture to desired temperature. |
| **Magnetic Stirrer** | - | To mix the carbon material with activating agent. |
| **Vacuum Pump** | - | To filter 4-BDS precipitate and solid catalyst. |
| **Filter Funnel** | 90mm diameter | To filter 4-BDS precipitate and solid catalyst. |
| **Reflux Condenser** | Coil type | To reflux methanol during esterification. |
| **Round Bottom Flask** | Three-necked | To carry out esterification of PFAD |
| **Ice Water Bath** | 2L | To maintain the temperature during synthesis of 4-BDS and solid catalyst |

Table 3.2 (Continued)

| Apparatus/ Equipment | Specification | Usage |
|---|---|---|
| **Oil Bath** | 1L | To maintain the reaction temperature of esterification. |

Table 3.3: List of Instruments Required for Characterisation of Feedstock, Catalyst and FAME

| Instrument | Specification | Usage |
|---|---|---|
| **Scanning Electron Microscopy (SEM)** | Hitachi Model S-3400N | To determine surface morphology, chemical composition and crystalline structure of catalyst. |
| **Energy Dispersive X-ray Spectroscopy (EDX)** | Ametek | To identify the elemental composition of catalyst. |
| **Thermogravimetric Analysis (TGA)** | NETZSCH model STA 2500 Regulus | To determine the thermal stability of catalyst. |
| **Temperature Programmed Reduction (TPR)** | Thermo Scientific (TPDRO 1100) | To determine the reducibility of the catalyst. |
| **Fourier Transform Infrared Spectrometer (FTIR)** | Nicholet IS10 | To determine the functional groups and the chemisorption of molecules on the catalyst |
| **Gas Chromatography (GC)** | GC-FID Perkin Elmer Clarus 500 | To determine compound present in oil feedstock and biodiesel sample. |

## 3.2 Research Methodology

The whole experiment involves a series of methodology steps with pretreatment of biomass precursors as the main focus of the research. Figure 3.1 summarises the overall research methodology that can be separated into several sections which include raw material preparation, synthesis of solid catalyst, characterisation of catalyst and process study.

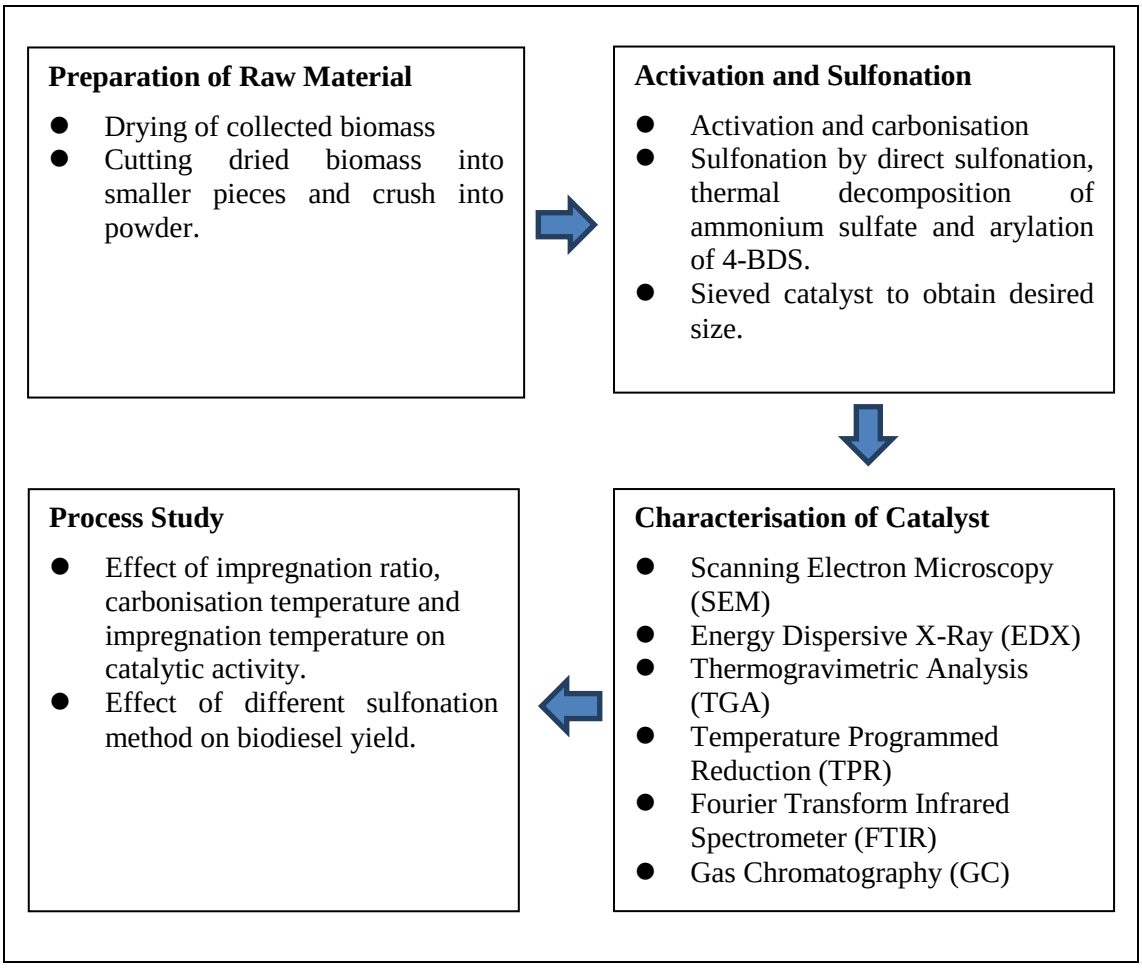


Figure 3.1: Schematic Flow of Research Methodology

## 3.3 Experiment Procedures

### 3.3.1 Activation and Carbonisation of Biomass

The raw biomass collected (EFB, palm frond and banana peel) was cut into pieces and washed thoroughly with tap water to remove impurities. The rinsed biomass was then dried overnight in oven at a temperature of 80 $^{o}$C to remove moisture. It was then ground into powder form with a grinder and sieved to three particle sizes (300μm, 1mm, 2mm) prior to activation. After drying, the biomass was activated by chemical reagent (NaOH or $H_3PO_4$) through impregnation method. A sample of 50 g of biomass was immersed in activating solution with variables of biomass to reagent ratio of 0.1, 0.5 and 1 (w/w). The mixture was then homogenised by magnetic stirring and was heated using hotplate at a mild temperature (50, 70, 90 $^{o}$C) and stored for overnight until a thick uniform paste was obtained. Subsequently, the activated sample was filtered and washed several times with distilled water until the washing effluent reached pH 7 to remove any traces of sodium hydroxide or phosphoric acid, followed by drying in the oven at 80 $^{o}$C for 24h. After dried, the activated sample was subsequently carbonised for 2 hours in furnace at 3 different temperatures (400, 600, 800 $^{o}$C) with a heating rate of 5 $^{o}$C/min. The resulted biochar was cooled and grounded into fine powder using pestle and mortar and was kept in air-tight container (Konwar, et al., 2014). An illustration of the steps mentioned above is shown in Figure 3.2.

In part 1 of the experiment, the effect of choice of biomass precursors, impregnating agents and biomass particle size was investigated and the optimum results were determined prior to part 2 study. In part 2 of the experiment, the effect of pretreatment parameters which included impregnation ratio, impregnation temperature and carbonisation temperature were studied.

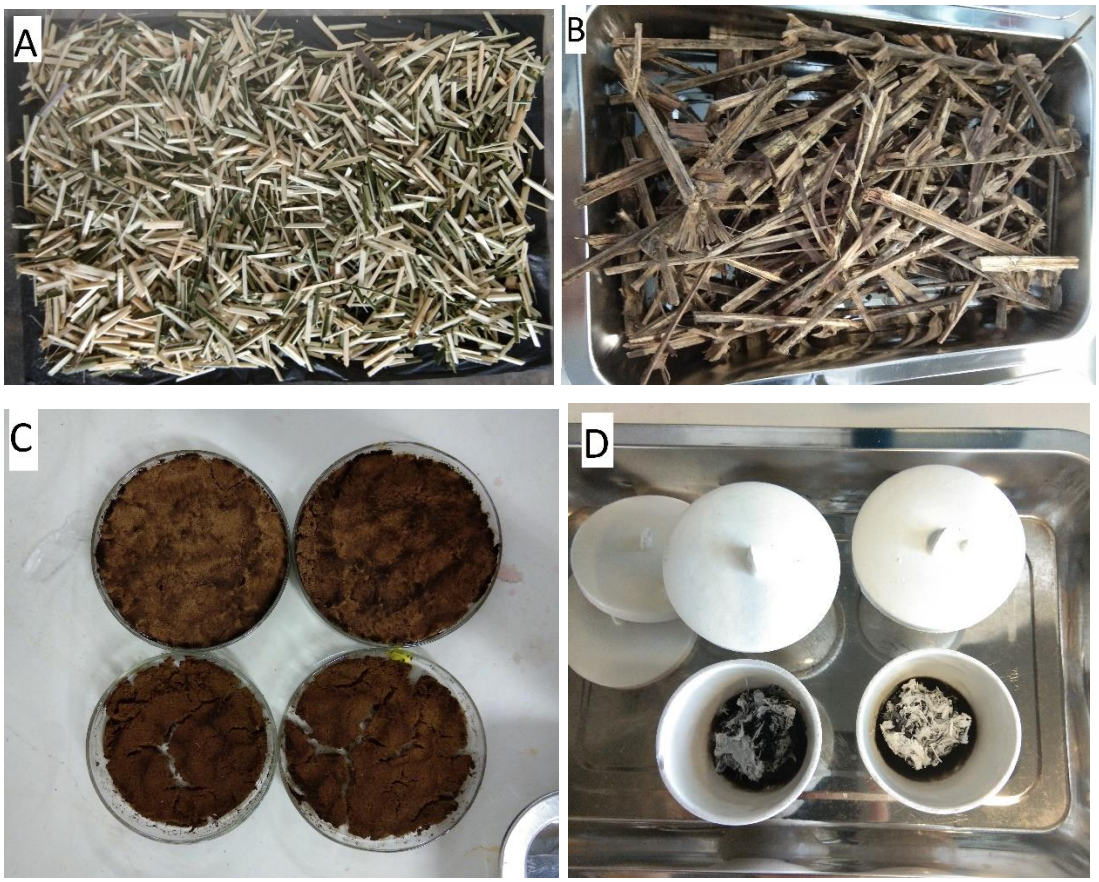


Figure 3.2:(A) Raw Oil Palm Frond (B) Dried Palm Frond (C) Impregnated Palm Frond (D) Carbonised Palm Frond

### 3.3.2 Sulfonation of Activated Carbon

#### 3.3.2.1 Direct Sulfonation

In direct sulfonation method, 5g of activated carbon sample was mixed with 250ml of concentrated $H_2SO_4$ (98%) in a quick-fit round-bottomed flask. It was refluxed at 150$^oC$ under continuous stirring for 6h to introduce $SO_3H$ groups onto the catalyst surface. After sulfonation, the mixture was cooled to room temperature and diluted with distilled water for catalyst to sediment. The precipitate was filtered and washed thoroughly until a neutral filtrate was obtained to remove impurities such as sulfate ions. The resulted black catalyst was dried overnight in oven at 80$^oC$ to remove moisture adsorbed on the catalyst. Figure 3.3 shows the experimental set up for direct sulfonation of activated carbon.


Figure 3.3: Experimental Set Up of Direct Sulfonation

### 3.3.2.2 Sulfonation by Arylation of 4-BDS

First, 4-BDS was synthesised by dissolving 33g of sulfanilic acid in 300ml of 1M hydrochloric acid in a round bottom flask immersed in ice water bath. The temperature of ice bath need to be maintained at below 5$^{o}$C and the mixture was stirred continuously. Next, 90 ml of 1M sodium nitrite solution was added dropwise into the mixture until a clear solution was obtained, followed by 1 hour of continuous stirring. The resulted white precipitate of 4-BDS was filtered and washed with deionised water.

To functionalise activated carbon, the 4-BDS produced was mixed with 200 mL of deionised water, 60 mL of ethanol and 3g of activated carbon. Then, 100 ml of 30% (v/v) phosphoric acid was added and stirred under a controlled temperature of below 5 $^{o}$C. After 30 min of stirring, another portion of 50ml of 30% (v/v) phosphoric acid was added and stirred for another 1.5 hours. The sulfonated catalyst was filtered and washed several times with distilled water, followed by drying overnight in the oven at 80 $^{o}$C. Figure 3.4 shows the experimental set up for 4-BDS sulfonation method.


Figure 3.4: Experimental Set Up of 4-BDS

#### 3.3.2.3 Sulfonation by Ammonium Persulfate

To sulfonate the activated carbon, thermal decomposition of ammonium persulfate, $(NH_4)_2S_2O_8$ was done by impregnation of activated carbon with 0.5 mol/l $(NH_4)_2S_2O_8$ solution at a solution to solid ratio of 15 ml/g. The mixture was heated at 90℃ and stirred at 500 rpm for 1 h. Next, the precipitated solid catalyst was filtered, washed and subsequently dried at 80 ℃ to remove excess $(NH_4)_2S_2O_8$ solution prior to carbonisation at 650℃ for 3 h in air. The calcined catalyst was then cooled, washed and dried overnight.

### 3.3.3 Biodiesel Production by Esterification

Esterification process was conducted to test the catalytic activity of the solid catalyst synthesised. 10g of PFAD was mixed with methanol at a methanol/oil molar ratio of 20:1 and 5 wt% of catalyst loading in a round bottom flask immersed in oil bath equipped together with a reflux condenser. The mixture was stirred and refluxed at temperature 100 $^{o}$C for 4h. The biodiesel formed was separated from the solid catalyst and was collected for product analysis. Figure 3.5 shows experimental set up for esterification of PFAD to FAME.

Figure 3.5: Experimental Set Up of Esterification Process

## 3.4 Biodiesel Characterisation

### 3.4.1 Gas Chromatography (GC)

The biodiesel samples collected were analysed with gas chromatography equipped with a capillary inlet (on column mode) and a Flame Ionization detector (FID). The biodiesel sample injected into the GC column was instantly vaporised and the gas mixture travels through the column by the help of inert gas. As the mixture travels through the column, the constituent gases that travel at different speed were separated and detected by FID. The GC setting used to analyse the biodiesel sample was listed in Table 3.4. The methyl ester peaks were identified by comparing the retention time with the external standard calibration curves while the yield of methyl ester was quantified by comparing the peak area. The external calibration curves for methyl palmitate, methyl stearate, methyl oleate and methyl linoleate are shown in Figure 3.6, Figure 3.7, Figure 3.8, and Figure 3.9, respectively. Biodiesel yield can be calculated using Equation 3.1.

$$Biodiesel\ Yield\ (\%) = \frac{(\sum Concentration\ of\ each\ methyl\ esters) \times (Volume\ of\ oil\ layer)}{10g\ of\ PFAD} \times 10 \quad (3.1)$$

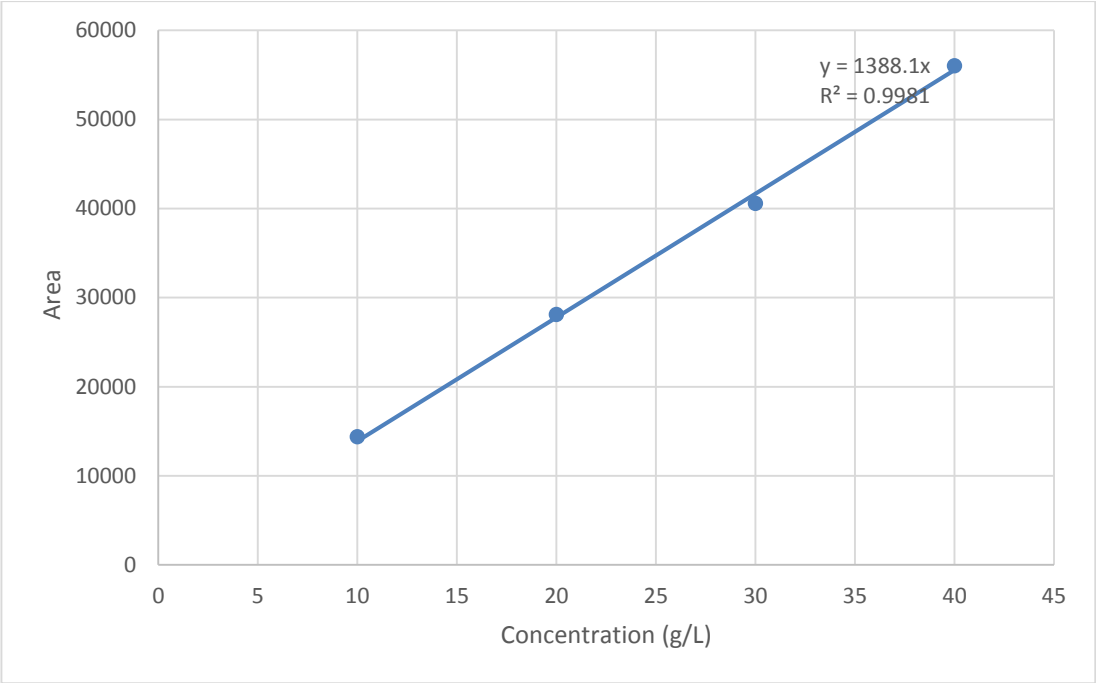


Figure 3.6: External Calibration Curve of Methyl Palmitate

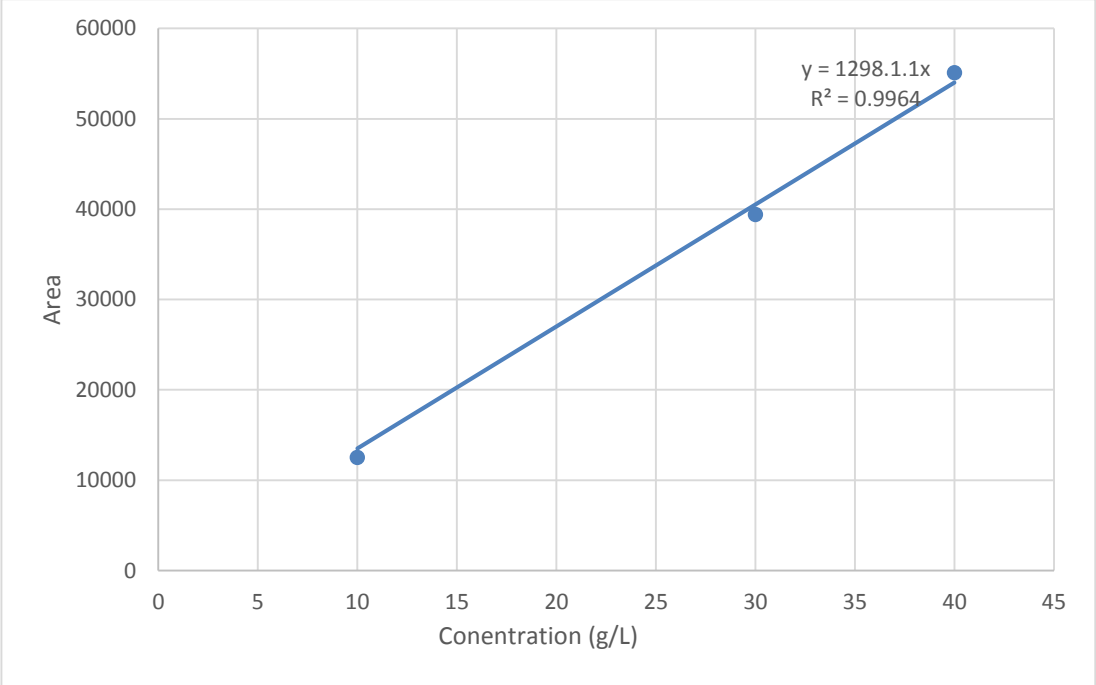


Figure 3.7: External Calibration Curve of Methyl Stearate

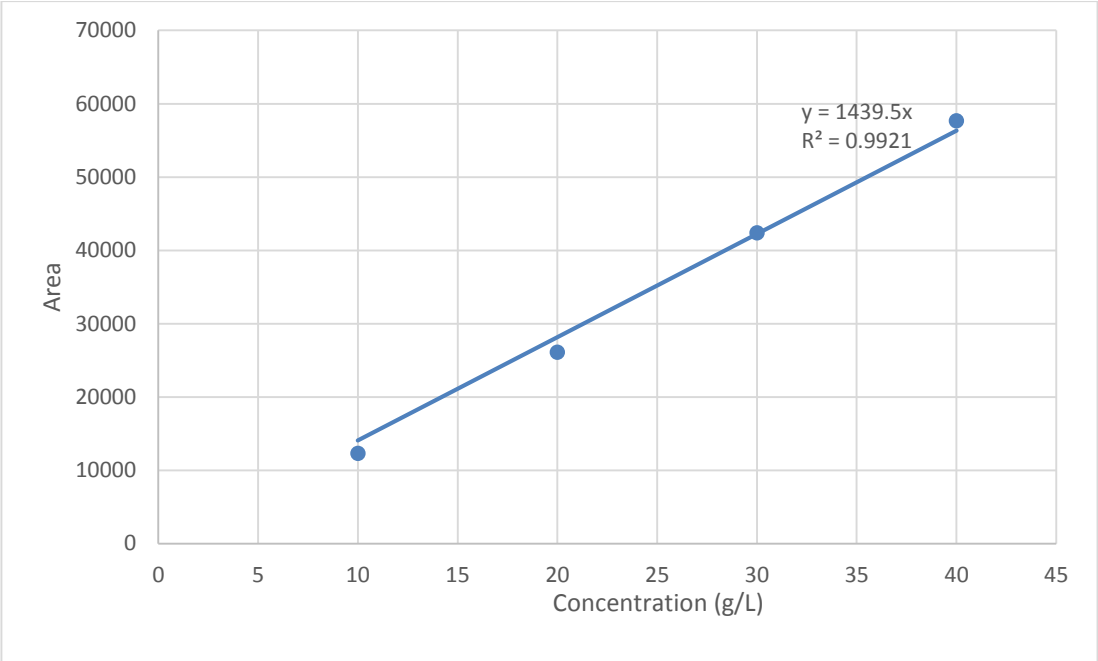


Figure 3.8: External Calibration Curve of Methyl Oleate

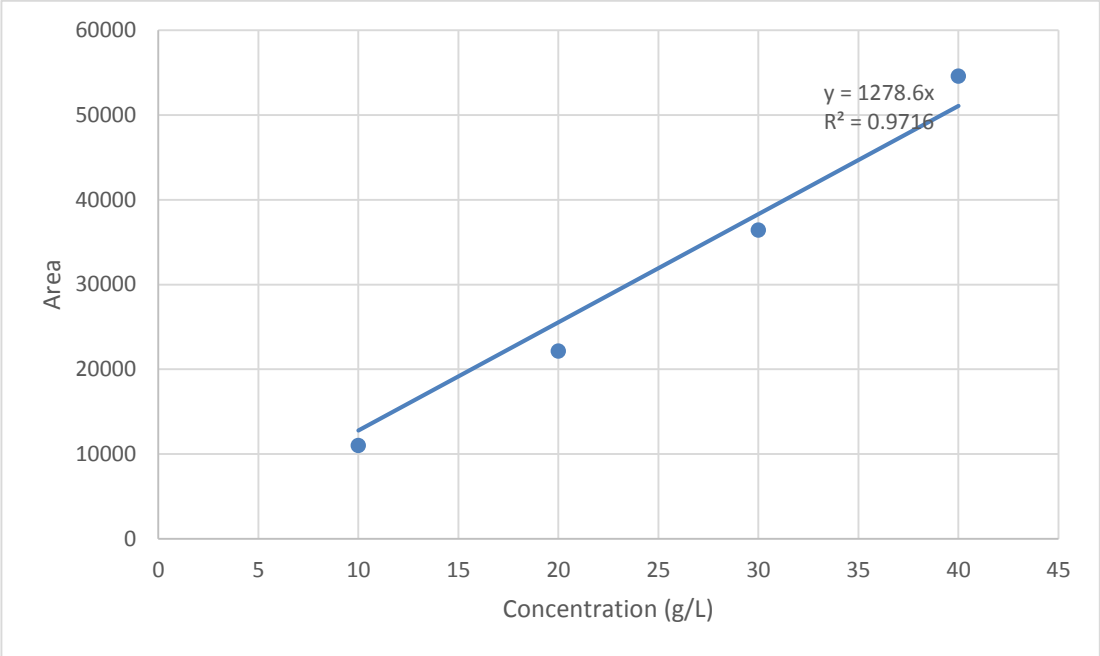


Figure 3.9: External Calibration Curve of Methyl Linoleate

Table 3.4: Gas Chromatography Setting for Biodiesel Sample

| GC Setting | Specification |
|---|---|
| **Carrier Gas** | Helium Gas |
| **Carrier Gas Flowrate (mL/min)** | 2 |
| **Carrier Gas Pressure (psi)** | 24.7 |
| **Injector Temperature (°C)** | 250 |
| **Flame Ionization Temperature (°C)** | 270 |

### 3.4.2 Acid Value

Acid values for feedstock PFAD and biodiesel produced were determined by using titration method. In this experiment, 1g of biodiesel was added with 5 ml of propanol solvent and 3 drops of phenolphthalein indicator. The mixture in conical flask was titrated with 0.1N KOH solution until a clear pink colour solution was formed. The volume of KOH solution used in the titration was recorded. FAME conversion was calculated using Equation 3.2 and Equation 3.3.

$$Acid\ Value, AV\ (mgKOH/g) = \frac{V \times N \times MW}{W_S} \tag{3.2}$$

where

$V = Volume\ of\ KOH\ solution\ used$

$N = Normality\ of\ KOH\ solution; 0.1N$

$MW = Molecular\ Weight\ of\ KOH; 56.11 g/mol$

$$Acid\ Value\ Conversion\ (\%) = \frac{a_i - a_f}{a_i} \times 100 \tag{3.3}$$

where

$a_i$= Acid value of PFAD ($\frac{mg\ KOH}{g}$)

$a_f$ =Acid value of FAME produced ($\frac{mg\ KOH}{g}$)

## 3.5 Catalyst Characterisation

Throughout the study, various characterisation techniques were used to study the effect of various synthesis parameters on the chemical and physical properties of the catalyst produced. The characterisation instrument used includes Scanning Electron Microscope (SEM), Energy Dispersive X-ray (EDX), Temperature Programmed Reduction (TPR), Fourier Transform Infra-Red (FTIR) and Thermogravimetric Analysis (TGA).

### 3.5.1 Scanning Electron Microscopy (SEM-EDX)

The Scanning Electron Microscopy (SEM) was conducted simultaneously with the Energy-Dispersive X-ray (EDX) to determine the surface texture morphology and elemental composition of the catalyst using SEM/EDX system. The sulfonated carbon catalysts were scanned under magnification of 2000x and 3000x. The SEM images gave information on grain size, pore diameter and the pore development of catalyst. Elemental analysis of the catalyst surface was done by EDX which identified the elements attached on the surface and their respective percentage.

### 3.5.2 Temperature Programmed Reduction (TPR)

TPR was carried out to determine the reduction temperature of solid catalysts. The oxidised solid catalysts were subjected to a mixture of reducing gas, hydrogen and inert gases, nitrogen as the analysis proceeded. The reduction rate on the catalysts was determined based on the amount of hydrogen gas consumed which indicated the removal of oxygen throughout the analysis. Before running TPR analysis, the solid catalysts were pre-treated to remove any impurities attached on it. The conditions for pre-treatment as well as the reduction process were shown in Table 3.5.

Table 3.5: Conditions for Pretreatment and TPR Analysis

| | **Type of Gas** | **Flow rate ($cm^3$/min)** | **Temperature ($^oC$)** | **Ramp Rate ($^oC$/min)** |
|---|---|---|---|---|
| **Pre-treatment** | Nitrogen | 20 | 250 | 10 |
| **TPR** | 5.47% Hydrogen and 94.53% Nitrogen | 25 | 1000 | 5 |

### 3.5.3 Fourier Transform - Infrared Spectroscopy (FTIR)

FTIR analysis was used to determine the $SO_3H$ functional groups or active sites attached on the carbon-based solid catalyst by observing the vibration of FTIR spectrum ranging from 400 to 4000 wave number. The amount of functional groups was also quantified by looking at the size of the peaks in the spectrum.

### 3.5.4 Thermogravimetric Analysis (TGA)

The thermal stability of the sulfonated catalysts was investigated by thermogravimetric analysis from room temperature to 1000 $^oC$ at a ramping rate of 5$^oC$/min under atmosphere of air or nitrogen. The temperature at which the functional group detached from the carbon support indicated the thermal stability of the activated carbon. The settings and specifications of TGA analyser were shown in Table 3.6.

Table 3.6: TGA Setting and Specification

| Setting | Specification |
|---|---|
| **Furnace** | Pt-Rh Furnace |
| **Sample Carrier** | Platinised slip-on plates |
| **Crucible** | $Al_2O_3$ crucible with pierced lid |
| **Temperature Program** | 25 $^oC$ -1000$^oC$ with 5 $^oC$/min |
| | 1000 $^oC$-25 $^oC$ with 5 $^oC$ /min |
| **Atmosphere** | 25 $^oC$ -900 $^oC$ under nitrogen (70mL/min) |
| | 900 $^oC$ -1000 $^oC$ under synthetic air (70mL/min) |

### 3.5.5 Total Acid Density

After sulfonation, the total acid density of the catalyst was determined using the titration method, whereby 0.1 g of sample catalyst was added into 60 ml of 0.01M sodium hydroxide solution and stirred for 30 minutes at room temperature. Next, the mixture was filtered and the filtrate was titrated using 0.02M hydrochloric acid with phenolphthalein as pH indicator. Once the solution turns from pink to colourless, the amount of HCl used for neutralisation was recorded and the acid density of the catalyst was calculated by using Equation 3.4 and Equation 3.5.

Moles of HCl used (mol)

$$= Volume\ of\ HCl\ used(mL) \times \frac{1L}{1000mL} \times 0.02\frac{mol}{L} \quad (3.4)$$

$$Mole\ of\ NaOH\ used\ to\ neutralize\ the\ acid\ sites\ on\ catalyst$$
$$= Initial\ mole\ of\ NaOH - Mole\ of\ NaOH\ neutralized\ by\ HCl$$

$$Total\ Acid\ Density\ \left(\frac{mmol}{g}NaOH\right)$$
$$= \frac{Mole\ of\ NaOH\ used\ to\ neutralize\ acid\ sites\ on\ catalyst}{0.1g} \quad (3.5)$$

# CHAPTER 4

# RESULTS AND DISCUSSION

## 4.1 Preliminary Studies

A preliminary study was carried out prior to the pretreatment parameters study which focused on the selection of optimum biomass, activating agent and particle size. In this study, six catalysts were synthesised from 3 different biomass sources and 2 types of chemical activating agent. The biomass precursors included banana peel, oil palm frond and empty fruit bunch while the activating agents used included phosphoric acid and sodium hydroxide. After the optimum precursor and activating agent were decided, catalyst synthesised from 3 different particle sizes which included 300$\mu m$, 1mm and 2mm was compared. In this section, the efficiency of catalyst produced was evaluated in terms of their acid density.

Among the six catalysts synthesised, catalyst produced from oil palm frond activated by NaOH possessed the highest acid density value. The acid density value for the rest of the catalysts is summarised in Table 4.1. The result shows that catalyst prepared from oil palm frond activated with $H_3PO_4$ and NaOH was the top two in the list due to the carbon-rich nature of the raw material. According to Salman and Hameed (2010), oil palm frond had high potential for activation, high possibility of degradation of lignocellulosic material and inherent good porosity and filterability. As compared, banana peel and empty fruit bunch showed lower catalytic performance.

For the activating agent, NaOH was slightly better than $H_3PO_4$ as the total acid density value obtained was near to each other. Various literatures reported that acid and alkali activating agents work well at a certain carbonisation temperature, yielding carbon support with maximum surface area for functionalisation purpose. It was reported that $H_3PO_4$ was more effective at lower activation temperature at around 400℃, which can yield activated carbon with good thermal and chemical stability. (Ismail, Taha and Ramli, 2016) This was due to the fact that when activation temperature was high, phosphates in $H_3PO_4$ bonded strongly to the lignocellulosic structure, leading to the formation of cross-link structures which shrunk and inhibited the pore development of activated carbon. According to Hayashi, et al. (2000), the research work done proved that alkali treated carbon had a

maximum surface area at the temperature of 600℃ but did not work well at temperature beyond that. Since the carbonisation process in this preliminary study was conducted at 600℃, thus alkali activating agent yield activated carbon with better surface morphology as compared to acid activating agent which needed a lower carbonisation temperature.

Biomass powder with particle size of $300\mu m$, 1mm and 2mm were then prepared and compared using oil palm frond and NaOH as activating agent. According to the acid density results in Table 4.2, catalyst prepared at the smallest particle size, $300\,\mu m$ exhibited an abundance amount of binding sites. Various literatures reported that decreasing the particle size significantly improved surface area, adsorption capacity and mechanical strength of the catalyst. Smaller particle size provided a larger contact surface area which promoted collisions between the reactant molecules with the active sites of the catalyst, thus accelerated the rate of esterification. Besides, small particle size also improved the diffusion of reactants and products in the catalyst particle by minimising the pore diffusion effects.

The optimum catalyst was then tested in esterification reaction carried out at 100℃ for 4 hours using 1: 20 methanol to PFAD molar ratio and 5 wt% of catalyst loading. The biodiesel produced was subjected to GC and acid value analysis in order to obtain the FAME conversion and yield as shown in Table 4.3. In conclusion, oil palm frond derived catalyst activated using NaOH with a particle size of $300\mu m$ showed a remarkable FAME yield and conversion. Thus, it was selected in the following research to investigate the effect of pretreatment parameters on the catalytic performance in biodiesel production.

Table 4.1: Total Acid Density of Different Precursors Activated by Acid and Alkali

| Biomass Precursors | Activating Agent | Total Acid Density (mmol/g) |
|---|---|---|
| **Banana Peel** | NaOH | 3.92 |
| | $H_3PO_4$ | 1.94 |
| **Oil Palm Frond** | NaOH | 9.86 |
| | $H_3PO_4$ | 7.56 |
| **Empty Fruit Bunch** | NaOH | 1.56 |
| | $H_3PO_4$ | 4.42 |

Table 4.2: Total Acid Density of Oil Palm Frond with Different Particle Sizes

| Particle Size | Total Acid Density (mmol/g) |
|---|---|
| **300$\mu m$** | 9.86 |
| **1mm** | 4.76 |
| **2mm** | 3.04 |

Table 4.3: FAME Yield and Conversion of Oil Palm Frond Derived Catalyst

| Catalyst | FAME Yield (%) | FAME Conversion (%) |
|---|---|---|
| **Oil palm frond** | 43.25 | 89.61 |

## 4.2 Characterisation of Activated Carbon and Catalyst

In this study, characterisation of catalyst was conducted to study their differences between the catalysts produced from different pretreatment conditions. Table 4.4 depicts the catalyst annotation and the corresponding preparation conditions for the carbon samples prepared.

Table 4.4: Carbon Samples and the Preparation Conditions

| Carbon Samples | Pretreatment Conditions | | |
|---|---|---|---|
| | Carbonisation Temperature | Impregnation Ratio | Impregnation Temperature |
| **Cat_400** | 400 | 1:1 | 90 |
| **Cat_600** | 600 | 1:1 | 90 |
| **Cat_800** | 800 | 1:1 | 90 |
| **Cat_0.1** | 600 | 1:0.1 | 90 |
| **Cat_0.5** | 600 | 1:0.5 | 90 |
| **Cat_50** | 600 | 1:0.5 | 50 |
| **Cat_70** | 600 | 1:0.5 | 70 |

### 4.2.1 Scanning Electron Microscopy

The surface morphology of the optimum catalyst, Cat_0.5 prepared at different stages from raw biomass precursor, chemically activated palm frond, palm frond derived activated carbon to synthesise catalyst was studied using scanning electron microscope at the magnification of 2000x and 3000x. As shown in Figure 4.1, the

SEM micrographs obviously indicated that there were significant differences between the surface topography of untreated and treated oil palm frond (OPF). It can be seen that in Figure 4.1(a), the surface of the raw OPF was completely smooth and dense with little porosity available for the sulfonic group to anchor. A naturally rigid and well-organised ladder-like internal structure was identified, which is similar to the structures reported by Lai and Idris (2013). After chemical activation using NaOH, an irregular internal structure with tiny cavities formed on the rugged surface was observed. The partial disruption of lignocellulosic material proved that chemical activation was able to induce and promote pores development on OPF biomass which allowed more volatile material to be exposed and released during carbonisation.

After undergoing carbonisation, a well-developed porous surface with many open holes and channels arranged in a honeycombed-like manner was clearly visible inside a cylinder-like tube fibres. This was identical to the morphological features reported by Md Arshad, et al. (2016). The formation of pores was attributed to the decomposition and volatilisation of the non-carbon elements at high temperature, eventually leaving irregular cavities over the carbon surface. As compared to the raw palm frond, the abundance of pores on the activated carbon provided higher surface area for the adsorption of active sites on the carbon support. This made the catalyst hydrophilic, allowing more methanol molecules access to the active sites during chemical reaction. Figure 4.1(d) shows an SEM micrograph of the sulfonated catalyst with sulfonic group grafted in the pores of the carbon support. Another notable feature was that the porous structure of the sulfonated catalyst retained the same as the activated carbon. This proved the statement claimed by Salman (2014) that the carbon surface structure was preserved with no noticeable difference after sulfonation.

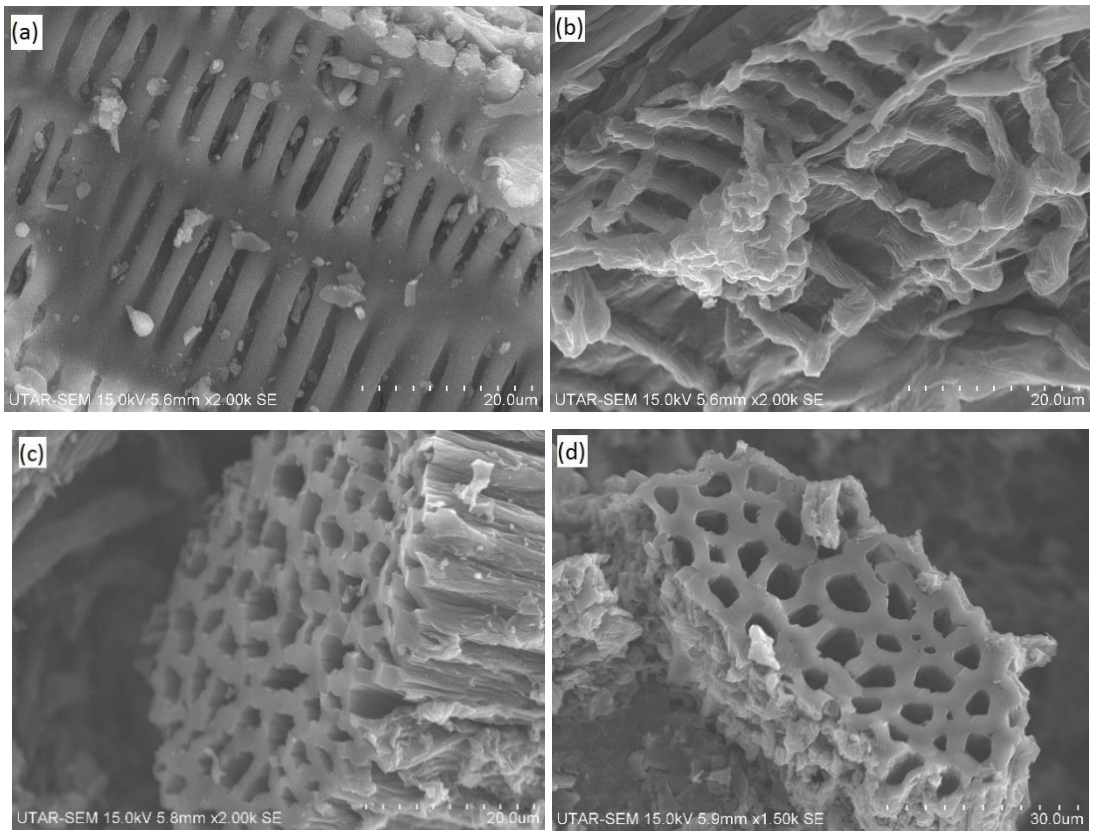


Figure 4.1: SEM Image of (a) Raw Oil Palm Frond 2000x (b) Chemically Activated Palm Frond 2000x (c) Activated Carbon 2000x and (d) Palm Frond Derived Catalyst 2000x

Figure 4.2 illustrates the changes in the surface pore structure of the activated carbon carbonised at increased temperature from 400℃ to 800℃. The SEM images depicted that all samples exhibited the same uniform rough surface, but with different pores size and distribution at different temperatures. It can be found that pore development improved with the increased temperature from 400℃ to 600℃, but it started to decrease from 600℃ onwards. This was due to the fact that 400℃ was not sufficient to provide high activation burn-off which eventually produced irregular shaped pores with random pore distribution. As the temperature raised to 600℃, the current pores were enlarged to a large extent and new pores were formed as well. Thus, this transforms the irregular carbon support to a honeycomb-like structure with well-defined pore distribution (Salman, 2014). The enhancement in pore size was proven by the significant increase of pore diameter from approximately 2.67 μm to 8.33 μm. Larger pore size allowed more molecules to enter the carbon bulk and react, eliminating the mass transfer problem which decreased the catalytic activity.

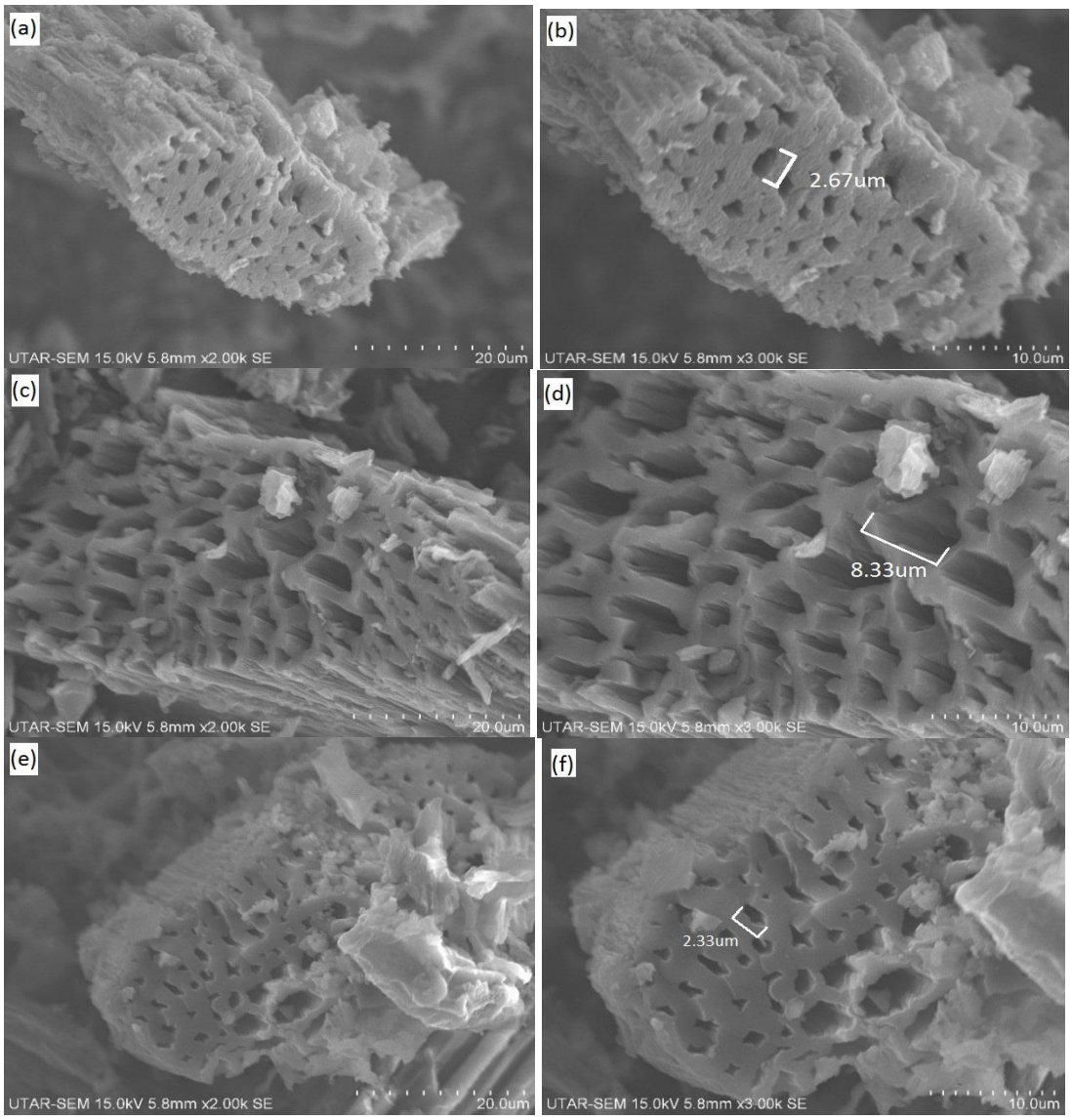


Figure 4.2: SEM Image of Activated Carbon Carbonised at (a) 400 ˚C at 2000x (b) 400 ˚C at 3000x (c) 600 ˚C at 2000x and (d) 600 ˚C 3000x (e) 800 ˚C at 2000x (f) 800 ˚C 3000x

On the other hand, Figure 4.2(f) shows that the pore diameter of catalyst carbonised at 800℃ had significantly decreased from 8.33 μm to 2.33 μm. This was not in accordance with the results reported by Yahya, Al-Qodah and Ngah (2015) that higher carbonisation temperature provided better activation and pore development. Yet, the decrease in pore diameter was possible due to the violent gasification reaction that could cause collapsing or contraction of pores wall, eventually causing blockage of the pores.

### 4.2.2 Energy Dispersive X-Ray

Energy Dispersive X-ray (EDX) analysis was carried out to identify the elemental composition present on the surface of raw biomass, chemically activated palm frond, activated carbon and palm frond derived catalyst. A summary of the atomic percentage of the elements present (C, O, Na and S) in untreated and treated palm frond was tabulated in Table 4.5.

Table 4.5: Elemental Composition of Samples

| Samples | Elemental Composition (Wt %) | | | | Elemental Composition (At %) | | | |
|---|---|---|---|---|---|---|---|---|
| | C | O | Na | S | C | O | Na | S |
| **Raw OPF** | 56.06 | 43.16 | 0.56 | 0.22 | 63.11 | 36.47 | 0.33 | 0.09 |
| **Chemically activated OPF** | 58.00 | 41.22 | 0.59 | 0.19 | 64.93 | 34.64 | 00.35 | 0.08 |
| **Activated carbon** | 87.69 | 11.69 | 00.62 | 0.00 | 90.60 | 9.06 | 0.34 | 0.00 |
| **OPF derived catalyst (Cat_0.5)** | 64.82 | 25.01 | 0.20 | 9.97 | 74.13 | 21.48 | 0.12 | 4.27 |

As shown in Table 4.5, raw palm frond mainly composed of carbon and oxygen element which was 63.11 at% and 36.47 at%, respectively. Carbon content was the highest among all elements since biomass was carbon-rich in nature. It could be seen that the atomic percentage of carbon increased significantly from 63.11 at% to 90.60 at% after carbonised at 600℃ for 2 hours. This was attributed to the released of volatile materials which leave behind the rigid carbon structure. On the other hand, the increase in carbon content in activated carbon was accompanied by the decrease in oxygen content from 36.47 at% to 9.06 at%. The significant reduction in oxygen was contributed by the decomposition of organic matters at high temperature.

Besides, all of the samples consisted of negligible amount of sodium, which was all less than 1 at %. There was no noticeable difference between the sodium content in raw palm frond and the chemically activated sample. This might due to the sufficient washing of sample using mild acetic acid that removed almost all traces of

sodium present after alkaline treatment. From Table 4.5, it could be seen that all samples prior to sulfonation consisted of traces or zero amount of sulfur. Figure 4.3 shows the EDX spectra of the sulfonated catalyst, Cat_0.5. The S peak showed that sulfur content had increased apparently from 0 at% to 4.27 at% after undergone sulfonation process, which revealed the successful attachment of sulfonic groups on the carbon support. The acidic nature of catalyst associated with the presence of $SO_3H$ functional group encouraged a high catalytic activity during biodiesel production.

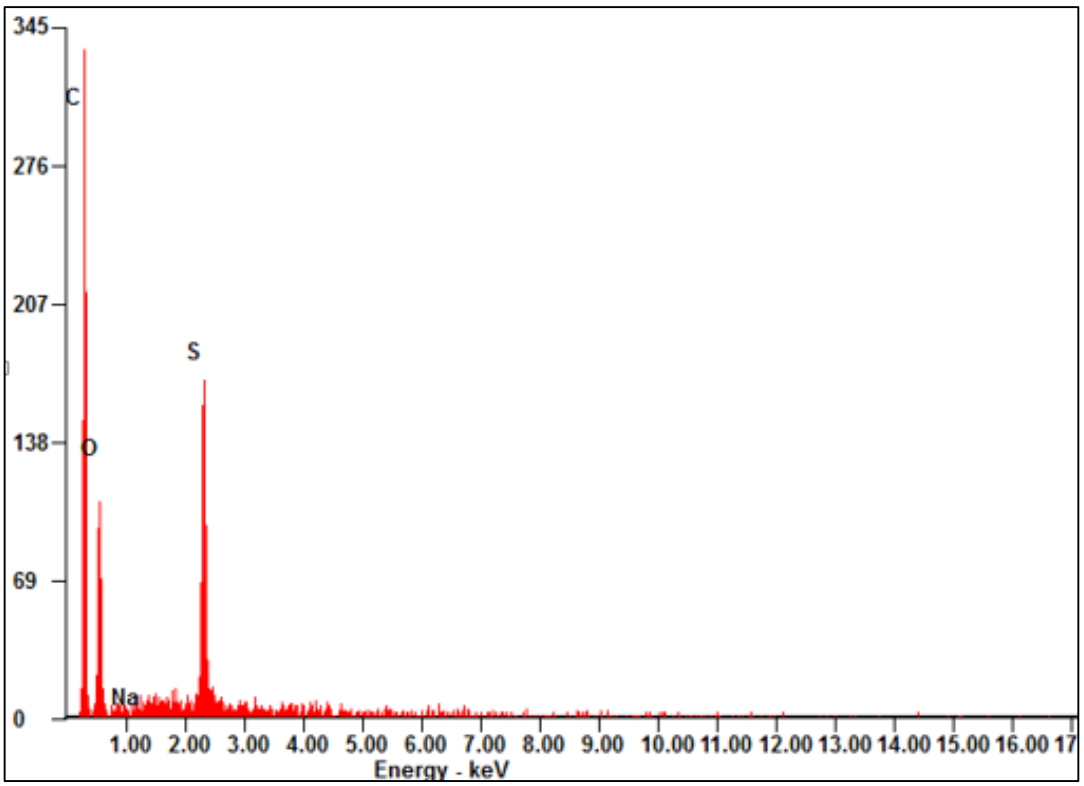


Figure 4.3: EDX Spectrum of Cat_0.5

### 4.2.3 Thermogravimetric Analysis

In order to evaluate the thermal stability and decomposition characteristics of the synthesised catalyst, the catalyst was subjected to TGA analysis where it was heated from 30℃ to 1000℃ in nitrogen atmosphere. As shown in Figure 4.4, the TGA profile could be studied to determine the stages with significant weight loss at a certain temperature range. From Figure 4.4, it could be seen that the weight loss of catalyst Cat_0.5 could be divided into three main stages.

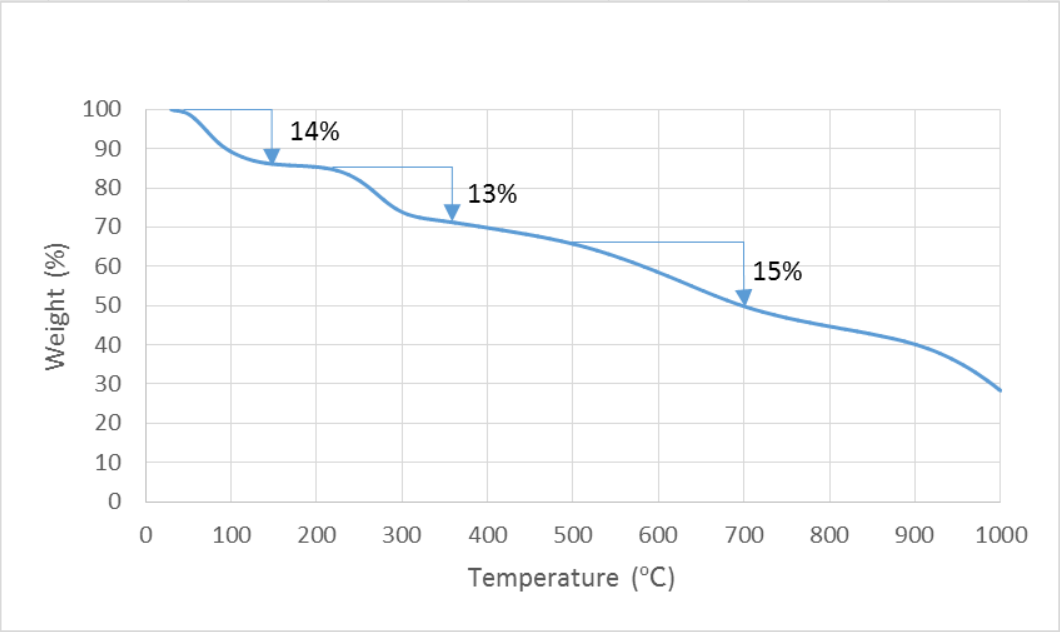


Figure 4.4: Temperature Dependant Weight Loss Curve for Cat_0.5

The first stage of weight loss occurred at the temperature range of 50℃-150℃. This phenomenon happened due to the evaporation of moisture that was physically adsorbed on the catalyst surface. The significant weight loss was approximately 14% of the total catalyst weight due to the large surface area of catalyst available for moisture adsorption. The second weight loss region was observed at the temperature of 225℃ where the catalyst weight was no longer stable and began to decrease significantly by 13%. The reduction in weight was mostly related to the decomposition of $SO_3H$ functional group anchored on the carbon support. This finding revealed that palm frond derived catalyst showed excellent thermal stability up to 225℃. This, in turn, meant that the $SO_3H$ groups were stable and the catalyst could perform well if the reaction temperature did not go beyond the catalyst decomposition temperature. Similar findings were also made by Konwar, et al. (2015) who claimed that activated carbon that prepared using direct sulfonation method was physically stable and could maintain its structure up to 250℃.

Apart from the weight loss occurred in the first two stages, the TGA profile showed a further weight loss of about 15% at temperature between 500℃ to 700℃. The weight reduction at this stage was associated with the rapid breakdown and removal of hemicellulose, cellulose and lignin material present in the carbon-based catalyst. This thermal decomposition zone corresponded to the SEM results whereby the catalyst carbonised at 400℃ was only partially carbonised whereas the catalyst

carbonised at 800 ℃ had collapsed pore structure. Therefore, carbonisation temperature in the range of 500℃-700℃ is recommended to provide sufficient burned off of volatile and organic matter, at the same time prevent the excessive breakdown of carbon structure at elevated temperature. At temperature above 700℃, weight loss continued but at a much slower rate, which became constant eventually.

### 4.2.4 Fourier Transform Infrared Spectroscopy

FT-IR was conducted to identify the functional groups, mainly $SO_3H$ that present on the surface of catalyst before and after sulfonation. The specific peaks or stretching found on the FT-IR spectra with spectrum of 400 $cm^{-1}$ to 4000 $cm^{-1}$ could verify the anchoring of active sites on the catalyst. As shown in Figure 4.5, the FT-IR spectra for activated carbon and catalyst were mostly similar to the same band found at specific frequencies. Several typical functional groups that exhibited on a carbon-based catalyst included C=C and C=O stretching, O-H stretching, $–SO_3H$ and O=S=O stretching. Table 4.6 summarises the vibration regions for the determination of functional groups on catalyst samples.

Table 4.6: Infrared Stretching Frequencies (Konwar, et al., 2014)

| Vibration | Wave Number Range ($cm^{-1}$) |
|---|---|
| **C=O** | 1700 |
| **C=C** | 1580 |
| **$-SO_3H$** | 1176 |
| **O=S=O** | 1008 |

Figure 4.5 compares the FT-IR spectra of activated carbon with Cat_0.5, revealing the effect of direct sulfonation on the catalyst support. Both spectra exhibited similar peaks and bands except for the $–SO_3H$ and O=S=O stretching that only found on the catalyst surface. The FT-IR spectra for both activated carbon and catalyst had a peak at about 1550 $cm^{-1}$ and a peak at around 1700 $cm^{-1}$. The peak at 1550 $cm^{-1}$ corresponded to the C=C stretching of the aromatic rings while the peak at 1700 $cm^{-1}$ was associated with the C=O bond of phenol groups such as weak carbonyl C-O-C or carboxylic acid –COOH on the catalyst surface. These findings were in agreement with those reported by Cheenmatchaya and Kungwankunakorn (2014) who claimed that the conjugated C=C bond formed was attributed to the

incomplete decomposition of carbonaceous materials during carbonisation process.

As aforementioned, asymmetric $–SO_3H$ and symmetric O=S=O stretching can only be found in the FT-IR spectra of sulfonated catalyst at around 1120 $cm^{-1}$ and 1020 $cm^{-1}$, respectively. The presence of these characteristic peaks were more significant compared to others as it proved the active sites were successfully incorporated on the carbon framework which was in accordance with those reported by several literatures (Konwar, et al., 2014, Md Arshad, et al., 2016, Muniandy, et al., 2014).

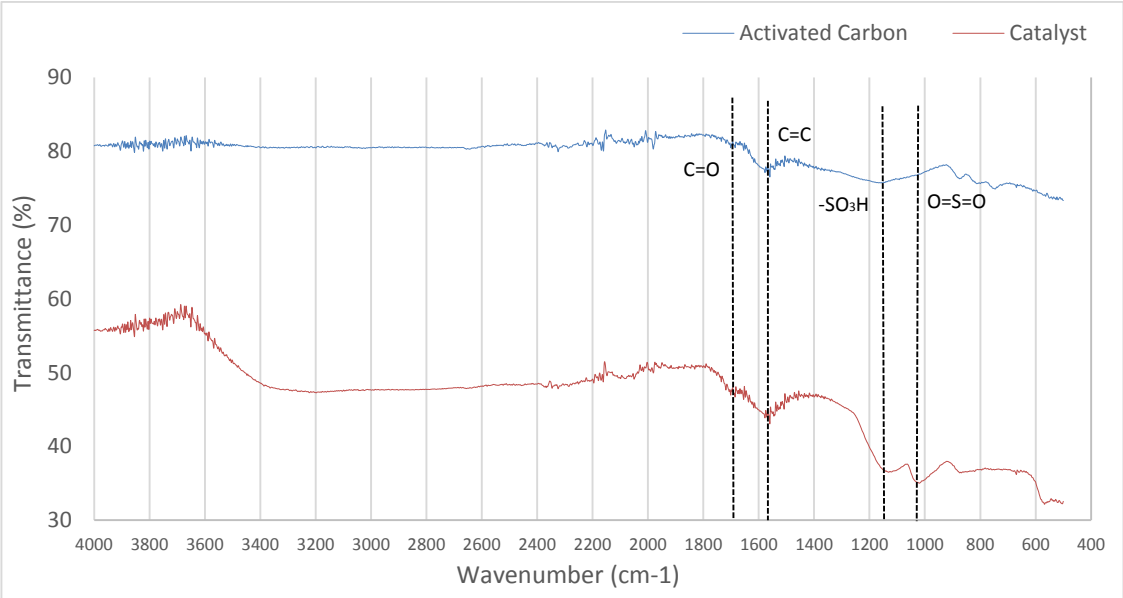


Figure 4.5: Comparison of FTIR Spectra of Activated Carbon and Cat_0.5

Figure 4.6 compares the FT-IR spectra of various catalyst carbonised at varied temperature of 400℃, 600℃ and 800℃. All the catalysts displayed the typical characteristic peaks of C=C and C=O that signified the presence of aromatic ring and weak carboxylic acid on catalyst surface, respectively. Most importantly, the $–SO_3H$ and O=S=O stretching were clearly visible in the FT-IR spectra of all catalyst which was consistent with the good incorporation of active sites on the carbon framework. It was observed that the $–SO_3H$ and O=S=O peaks intensities of Cat_600 were higher than the others as the well-developed pores in Cat_600 allowed high concentration of sulfonic acid group to anchor on the support.

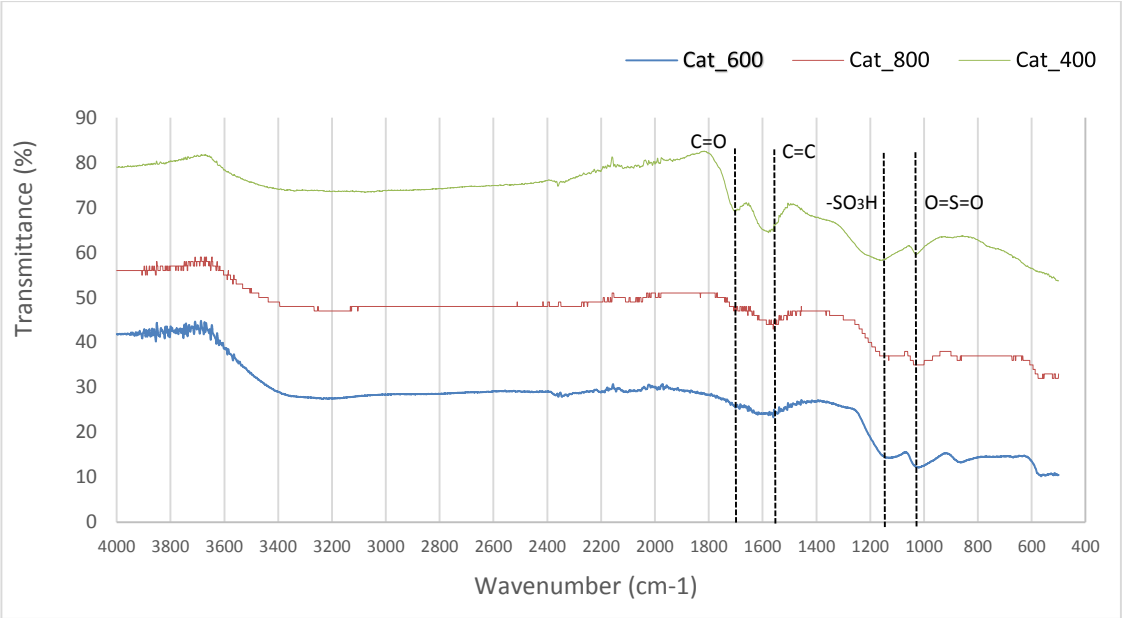


Figure 4.6: Comparison of FTIR Spectra of Catalyst Synthesised at Different Carbonisation Temperatures

### 4.2.5 Temperature Programmed Reduction

Temperature programmed reduction (TPR) was conducted to study the reduction process of oxygen-bearing functional groups attached on the activated carbon. The reducing gas, hydrogen was being consumed as the catalyst was reduced at increasing temperature. The oxygen-bearing groups could be categorised into strong and weak acid site whereby the strong acid site was contributed by the active sulfonic group (–$SO_3H$) while the weak acid site was due to the presence of carboxylic acid (-COOH) and hydroxyl (-OH) groups on the carbon surface.

The TPR plot of sulfonated and unsulfonated activated carbon in Figure 4.7 shows the respective peaks at 740℃ and 890℃. The reduction temperatures at 740℃ and 890℃ corresponded to the maximum rate of reduction for activated carbon and catalyst, respectively. It was also worth pointing that the amount of hydrogen gas adsorbed was 338.443$\mu mol/g$ for activated carbon and 1051.876 $\mu mol/g$ for palm frond derived catalyst. The amount of hydrogen adsorbed was assigned to the removal of oxygen from the oxidised catalyst. It could be observed that the amount of oxygen removed from sulfonated catalyst was higher than activated carbon. This was attributed to the removal of additional sulfonic groups (–$SO_3H$) from the catalyst which confirmed that sulfonated activated carbon exhibited higher acid. Thus, it could be concluded that the addition of sulfonic group might lead to enhancement of

the reduction temperature as compared to unsulfonated activated carbon.

Besides, the reduction temperature provided useful information of the reusability of the catalyst surface, as well as its high sensitivity to chemical changes resulting from any modification on the catalyst surface. Therefore, TPR result could act as a benchmark to control the quality of catalyst during manufacturing process. The high reduction temperature of the catalyst also allowed it to be used in other applications such as hydrogenation.

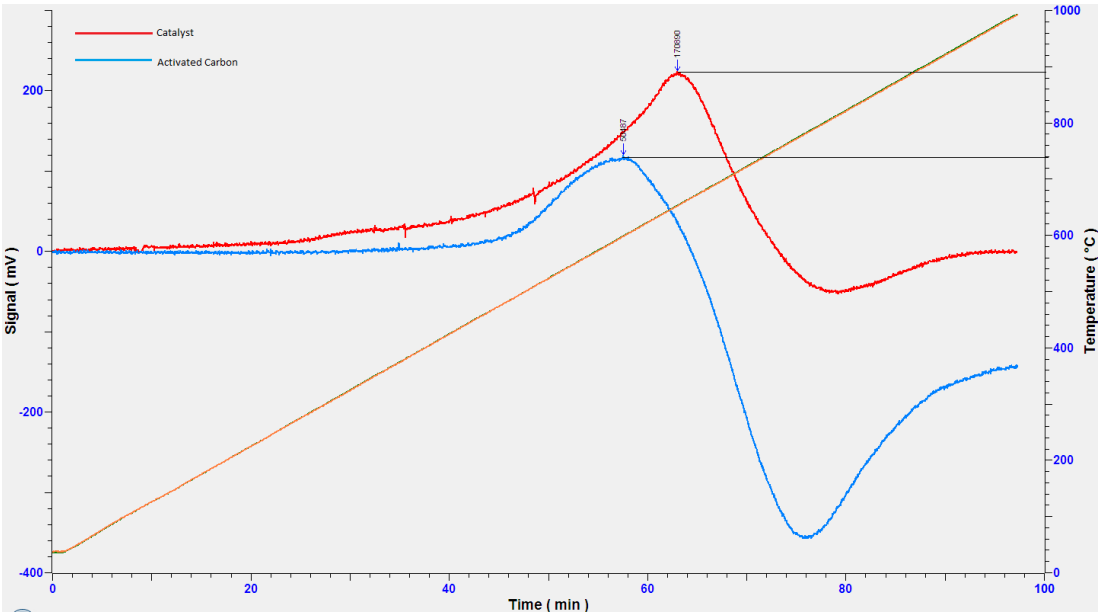


Figure 4.7: TPR Spectra of Activated Carbon and Palm Frond Derived Catalyst

### 4.2.6 Total Acid Density Test

Total acid density test is a measurement of acidic sites using back titration method by determining the amount of sodium hydroxide used to neutralise the acid functional group present in the carbon-based catalysts. The acid functional groups not only contributed by $–SO_3H$ group but also include weak carboxylic acid –COOH and hydroxyl –OH groups which help to enhance the hydrophilicity of the catalyst. The efficiency of catalyst is determined by measuring the amount of acidic sites present. The higher the concentration, the better is the catalyst performance since FAME yield is dependent on the total acid density of catalyst. Besides, carbon catalyst with high acid density had no mass transfer limitation as it was able to disperse easily in the reactant mixture as presented by Konwar, et al. (2014). The total acid densities evaluated for catalyst carbonised under different temperatures were calculated and

the corresponding trend is clearly depicted in Figure 4.8.

As depicted in Figure 4.8, Cat_600 was evaluated to be the most efficient catalyst owing to its high acid density 4.46 mmol/g. The total acid density of the synthesised catalyst increased when the carbonisation temperature increased from 400℃ to 600℃. However, when the temperature further increased to 800℃, a turning point was observed with the acid density value decreased significantly to 3.26 mmol/g. This was because as the carbonisation temperature increased from 400℃ to 600℃, more volatiles matter escaped which eventually generated new pores and widen the existing one. Such a well-developed pore structure provided additional surface area for more acidic site to be grafted on the catalyst surface and thus resulting in higher distribution of acidity. However, when beyond a certain temperature, the violent gasification might destroyed the pore by collapsing or contraction of pores wall and ultimately lowering the surface area and yielded fewer acid sites. This trend was in good agreement with the SEM results for activated carbon synthesised under different carbonisation temperatures.

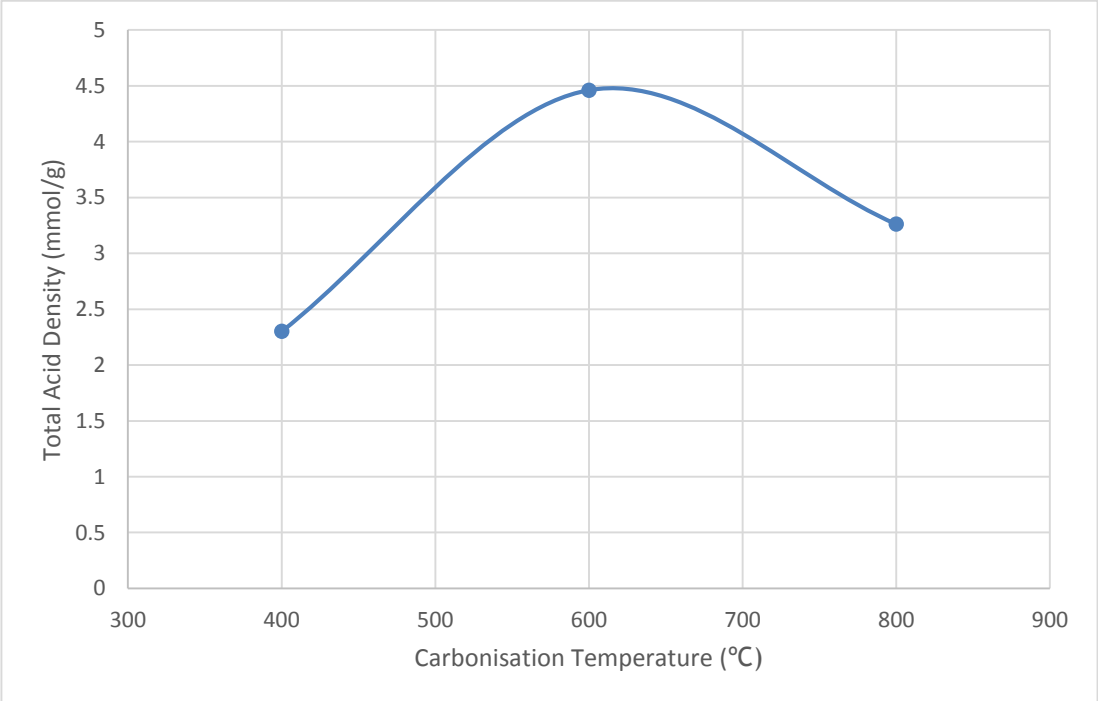


Figure 4.8: Total Acid Density of Catalyst Carbonised at Different Temperatures

Next, the effect of impregnation ratio on the total acid density of catalyst is illustrated in Figure 4.9. At the impregnation ratio of 1:0.1, the acid density value obtained was 6.35 mmol/g. The total acid density was then increased gradually and

achieve the maximum value of 7.36 mmol/g when the impregnation ratio was 1:0.5. However, when the impregnation ratio increased above 1:0.5, the total acid density of the catalyst showed an opposite trend which decreased drastically to 4.46 mmol/g. As aforementioned, impregnation ratio was the key factors in chemical activation which determine initial porosity development of carbon prior to carbonisation. Generally, at higher activating agent concentration, better pores structure in activated carbon was obtained since the effect of the activation agent increased with increasing dose. (Ismail, Taha and Ramli, 2016). However, concentrated solution might give opposite effect to the catalyst due to the excessive chemical attack that weakened and progressively collapsed the incipient carbon structure. Thus, optimisation of impregnation ratio was important to achieve a balance between the pore formation and pore widening (Budi, et al., 2016).

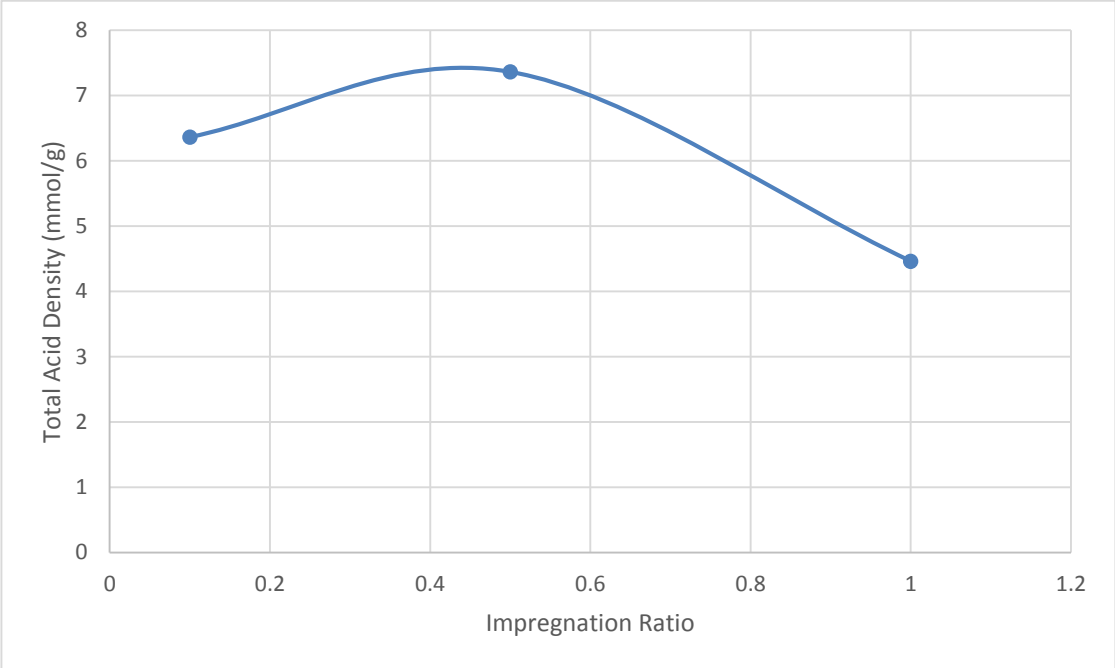


Figure 4.9: Total Acid Density of Catalyst Synthesised at Different Impregnation Ratios

In the case of chemical activation at different temperatures, Figure 4.10 shows the total acid density of catalysts increased as the impregnation temperature increased. For Cat_50, the acid density value obtained was the lowest due to the low temperature. As the temperature increased further, an upward trend was observed and the total acid density value started to become stable when the temperature reached 90℃, which was 7.36 mmol/g. At very low temperatures, in this case was 50℃, the

activating agent lack of sufficient energy to attack the carbon precursors and created defects and crevices, allowing less oxidising gases into the char during carbonisation. This ultimately resulted in narrow pores and poor acid distribution.

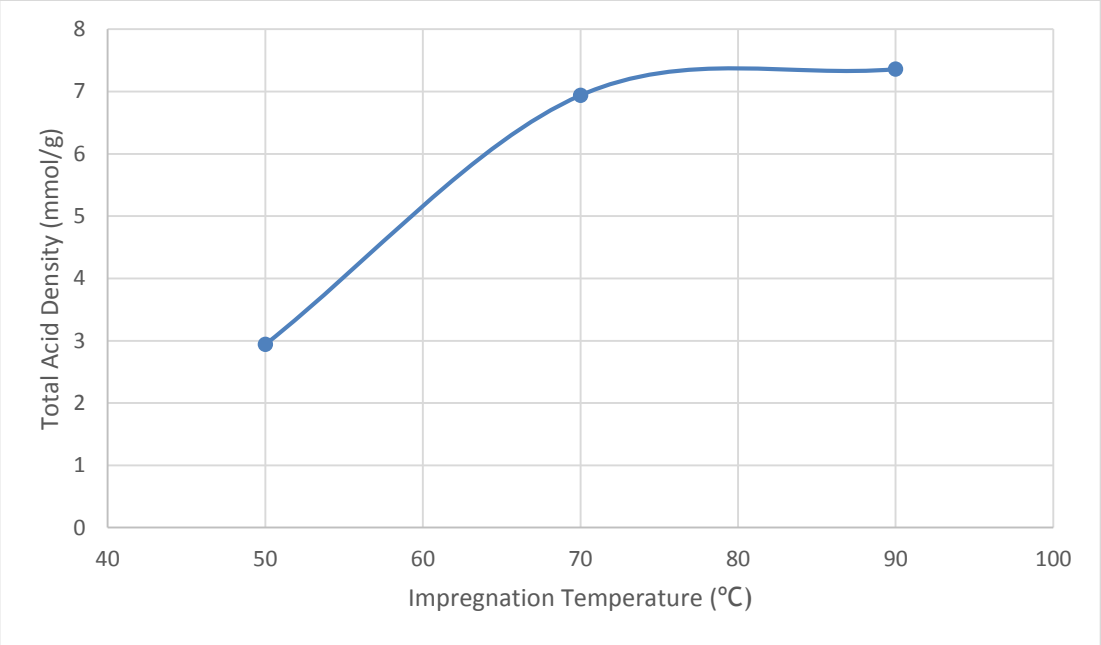


Figure 4.10: Total Acid Density of Catalyst Synthesised at Different Impregnation Temperatures

## 4.3 Pretreatment Parameters Studies

The catalytic performance for all synthesised catalysts was tested in esterification of feedstock PFAD with methanol in order to determine the most efficient and cost-effective method to produce carbon-based catalyst in large scale. The esterification reaction conditions were kept constant for all the experimental runs in order to focus on the effect of pretreatment parameters on biodiesel production. The effect of pretreatment parameters included carbonisation temperature, impregnation ratio and impregnation temperature.

In Section 4.3.1, the effect of pretreatment parameters on the biodiesel production was studied based on the results obtained from gas chromatography and acid value test, which were the main indicator for catalytic activity. The data obtained from the analysis mentioned could be converted into FAME yield and FAME conversion respectively. The calculation steps to obtain FAME yield and conversion could be found in Appendix F. In gas chromatography, the peaks appeared at the respective retention time was used to confirm the presence of the four

methyl ester peaks (methyl palmitate, methyl stearate, methyl oleate and methyl linoleate) while the area under the peaks was used to calculate the concentration of methyl esters produced. Figure 4.11 shows a chromatogram including the four primary methyl esters peaks produced in the esterification reaction. For acid value test, the difference in the fatty acid value between feedstock PFAD and FAME produced represents the percentage of free fatty acid being converted to the desired methyl esters.

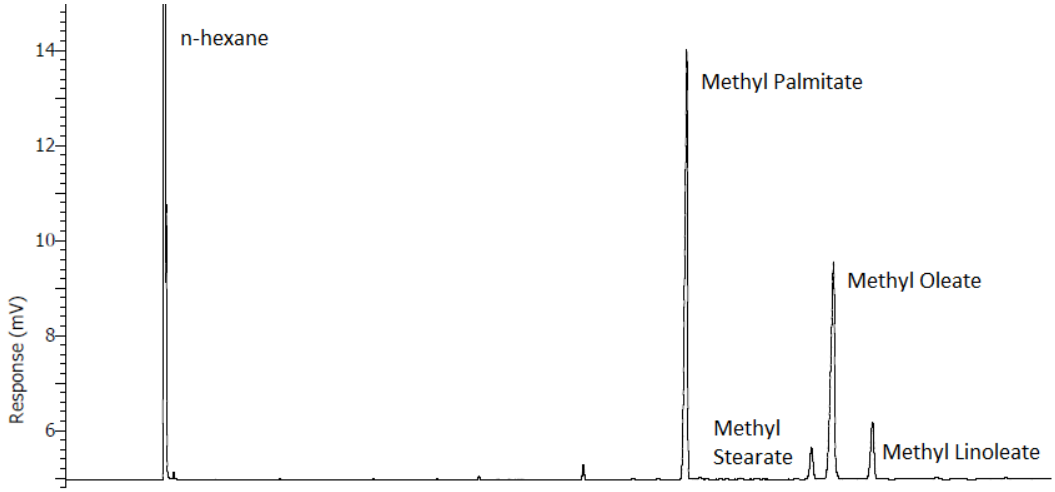


Figure 4.11: Gas Chromatogram of FAME Produced

### 4.3.1 Effect of Carbonisation Temperature

Looking into the pattern of conversion and yield curve plotted in Figure 4.12, FAME yield and conversion reached the peak value of 49.54% and 90.73%, respectively when catalyst was carbonised at 600℃. These findings were conformed to the micrograph from SEM analysis which showed that a more ordered-structure was likely to be developed in Cat_0.5 as compared to the others. It is further confirmed in the FT-IR spectrum which showed Cat_0.5 carbonised at 600℃ has the highest $SO_3H$ and O=S=O peaks intensities compared to others. Other than that, similar trend was also proven by the outcomes of acid density test. It was observed that the FAME yield and conversion was not remarkable when temperature was at 400℃ and 800℃. These results were also supported by the TGA weight loss profile which demonstrated that the weight loss of catalyst from 500 ℃ to 700 ℃ were more significant compared to the other temperature range.

Carbonisation process was meant to remove volatile and organic matters, leaving rigid carbon framework and developed highly porous structure under elevated temperature. Although all activated carbon produced consisted of pores and channels, however, the size of pores formed was crucial as it affected the surface area and adsorption of acid functional group on the carbon surface. Most importantly, the size of pores and the hydrophilicity of catalyst decided whether the reactant molecules could enter the catalyst bulk and access to the active sites during chemical reaction.

When carbonisation temperature was too low, incomplete carbonisation happened where the carbon structure was not destructed sufficiently. The irregular small pores created did not favour larger reactant molecules such as PFAD to participate in the reaction and ultimately resulted in low and unsatisfied biodiesel yield and conversion. The FAME produced solidified at room temperature once methanol was evaporated, showing that there was still a portion of PFAD unreacted. The pour point of the biodiesel produced did not compliant with the commercial biodiesel ASTM standard. On the other hand, although Cat_800 was carbonised at extremely high temperature, the FAME conversion was still low. The low conversion was mainly due to the aggressive gasification of oxidising gas which resulted in more compact pores that inhibited the attachment of sulfonic group.

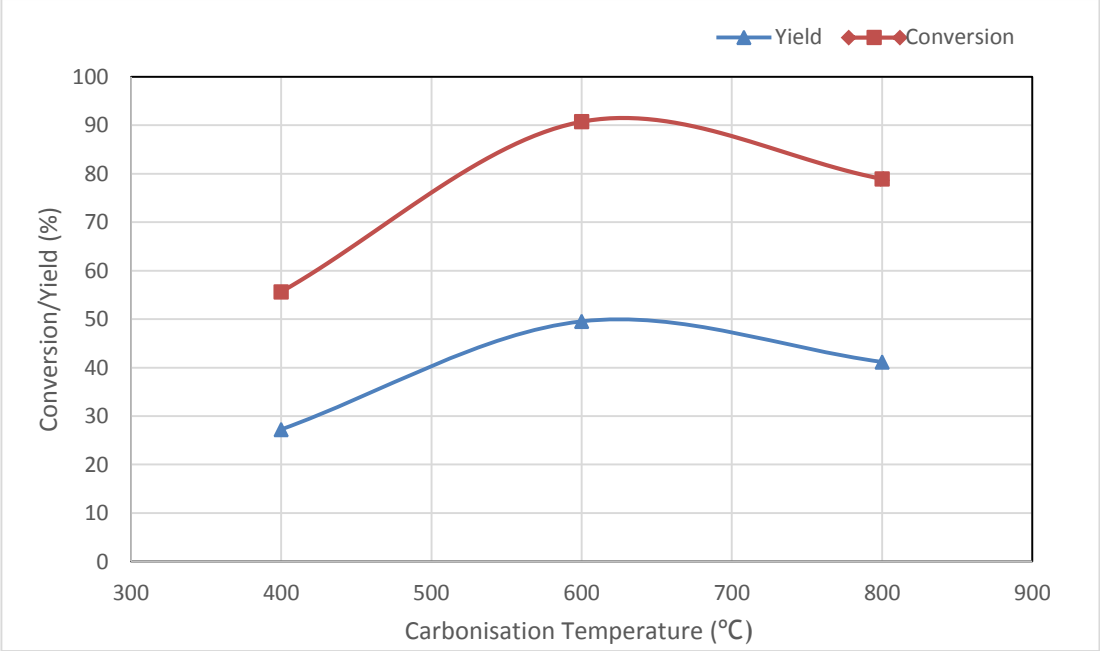


Figure 4.12: FAME Yield and Conversion using Catalyst Synthesised at Different Carbonisation Temperatures

### 4.3.2 Effect of Impregnation Ratio

Impregnation ratio is one of the essential factors in the chemical activation of biomass precursors since it had a direct effect on the porosity development of catalyst. This section is devoted to study the effect of impregnation ratio by varying the precursor to activating agent ratio from 1:0.1 to 1:1. Figure 4.13 shows that initially, the increase in impregnation ratio from 1:0.1 to 1:0.5 yielded remarkable results, which was 82.71% and 93.54% for FAME yield and FAME conversion respectively. However, a downward trend in FAME yield and conversion was noticed when the impregnation ratio was increased to 1:1.

During the impregnation process, NaOH solution destructed the lignin structure and partially dissolved hemicellulose materials, allowing better contact of the interior of biomass with NaOH to create micropores (Kumar and Jena, 2016). In general, it was found that higher chemical dose was favourable for activation since it accelerated the rate of degradation of cellulosic structure. This explained why impregnation ratio of 1:0.5 found to be better compared to 1:0.1.

After achieving the maximum yield at ratio of 1:0.5, a downward trend was observed due to the fact that excessive attack of NaOH deteriorated the wall between microporous structure, leading to the widening of micropores. Beyond a certain impregnation ratio, the pore size distribution was altered as reported by Mopoung, et al. (2015) who claimed that an increase in impregnation ratio modified the initial microporosity of carbon. At high NaOH concentration, there was a competition between the mechanisms of new pores formation and existing pores widening in which mesopores or macropores dominated eventually due to collapse of pore walls. Another drawback of high NaOH concentration was that the excess NaOH molecules formed a thin coating on the biomass surface, therefore inhibited the degradation of cellulose in the interior of biomass, causing the surface structure to retain.

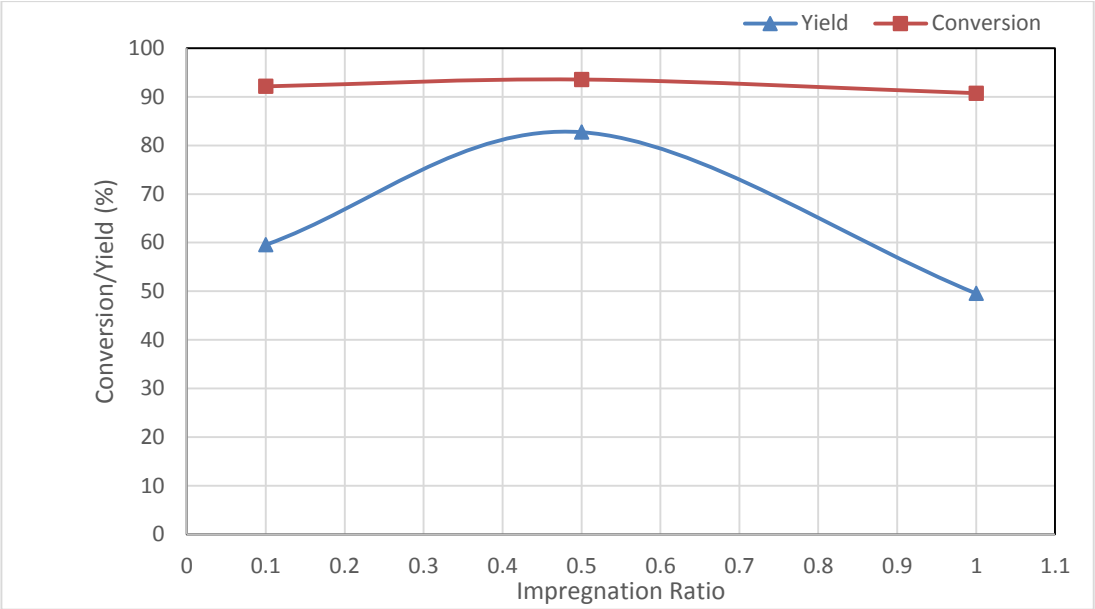


Figure 4.13: FAME Yield and Conversion Using Catalyst Synthesised at Different Impregnation Ratios

### 4.3.3 Effect of Impregnation Temperature

The effect of impregnation temperature on biodiesel production was different from the effect of carbonisation temperature. As shown in Figure 4.14, the FAME yield and conversion increased proportionally with the impregnation temperature from 52.52% to 82.71% when the temperature increased from 50℃ to 90℃. Similar trend was observed from the FAME conversion curve whereby Cat_90 attained the highest conversion of 93.54% was found to be the most promising catalyst.

The result obtained followed the trend of the total acid density of the catalyst. Since increasing the impregnation temperature was able to increase the collision between NaOH molecules and the carbon support, which in turn increased the rate of reaction between NaOH and carbon surface. The higher destruction rate of lignin and cellulose structure resulted in more micropores content available for binding sites. Therefore, the optimum FAME yield and conversion was obtained by using Cat_90 synthesised at 600℃ carbonisation temperature and 1: 0.5 biomass to NaOH weight ratio.

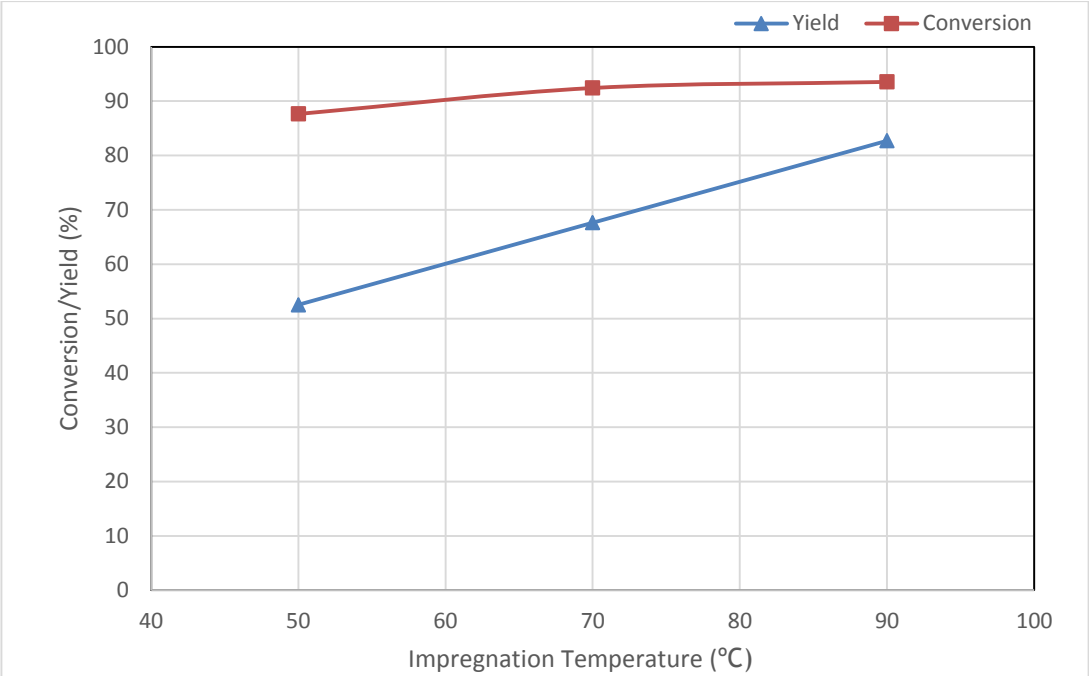


Figure 4.14: FAME Yield and Conversion Using Catalyst Synthesised at Different Impregnation Temperatures

## 4.4 Effects of Sulfonation Method on Biodiesel Production

Recently, it has been established that sulfonated carbon was found to outperform homogeneous acid catalyst owing to its high $–SO_3H$ density grafted on carbon surface, which made sulfonated carbon became the most promising heterogeneous catalyst used in biodiesel production. In this section, the active sites were grafted onto the activated carbon surface through different sulfonation methods such as direct sulfonation, arylation of 4-benzenediazonium sulfonate (4-BDS) and sulfonation by thermal decomposition of ammonium persulfate in order to investigate the effect of sulfonation methods employed on the performance of catalyst activity. The sulfonated catalyst prepared from these methods were subjected to esterification to test the catalytic performance of catalyst using low-value feedstock, PFAD. The effectiveness of various sulfonation method was credited to the $–SO_3H$ group attachment, which was consistent with the results of total acid density, FAME yield and FAME conversion.

According to the results summarised in Table 4.7, it was found that catalyst sulfonated via direct sulfonation method gave the highest FAME yield of 82.71%. On the contrary, catalyst sulfonated via 4-BDS and thermal decomposition of ammonium persulfate exhibited very low and unsatisfied FAME yield of 16.99% and

2.21%, respectively. The low FAME conversion explained the solidification of FAME produced at room temperature. Besides, the total acid density value was directly proportional to the FAME yield and conversion. Among the sulfonation methods, direct sulfonation method using concentrated sulfuric acid yielded the highest $–SO_3H$ sites of 7.36mmol/g, which implied that catalyst sulfonated by $H_2SO_4$ had high feasibility and stability as compared to other methods. However, this finding was not in agreement with Konwar, et al. (2015) who claimed that $–SO_3H$ group functionalised by 4-BDS method was higher than that of direct sulfonation and this method. This might due to the fact that the aryl radical produced during reduction of 4-BDS was less strongly bonded to the amorphous structure of palm frond derived activated carbon. In the case of sulfonation using ammonium persulfate, the low acid density might due to the poor attachment of the sulfate group on the solid structure. Besides, it also exhibited the possibility of decomposition of the acid sites during esterification process conducted at 100℃, which is very near to the decomposition temperature of ammonium persulfate at 120℃.

Table 4.7: Results for Various Sulfonation Methods

| **Sulfonation Methods** | **Total Acid Density (mmol/g)** | **FAME Yield (%)** | **FAME Conversion (%)** |
|---|---|---|---|
| **Direct Sulfonation** | 7.36 | 82.71 | 93.54 |
| **4-BDS** | 3.94 | 16.99 | 58.15 |
| **Thermal Decomposition of Ammonium Persulfate** | 1.10 | 2.21 | 16.46 |

# CHAPTER 5

# CONCLUSION AND RECOMMENDATIONS

## 5.1 Conclusion

The present research focused on the synthesising of carbon-based acid catalyst from waste oil palm frond (OPF) for biodiesel production. The synthesised catalyst was successfully used in esterification of low-value feedstock PFAD at a reaction condition of 1:20 oil to methanol molar ratio, 5 wt% catalyst loading, reaction temperature of 100℃ and reaction duration of 4 hours. The biodiesel produced using the best-performed catalyst (Cat_0.5) yielded a remarkable FAME yield of 82.71% and FAME conversion of 93.54%. The optimum catalyst showed a steady performance and promising catalytic efficiency in esterifying feedstock with high FFA value using only a small amount of catalyst which was considered cost-effective in large-scale biodiesel production.

Several characterisation techniques such as SEM-EDX, FTIR, TGA, TPR and XRD were conducted for the analysis of synthesised catalysts. SEM micrographs showed that the catalysts produced had well-developed pores arranged in a honeycomb manner which allowed sulfonic groups to form covalent bond on the carbon surface. EDX analysis showed a distinct S peak on the spectra of sulfonated activated carbon confirmed the successful incorporation of $–SO_3H$ groups on the catalyst support. This finding was further proven by the FT-IR analysis in which the O=S=O stretching and $–SO_3H$ symmetric vibration band found on the spectrum showed the present of the active functional group on the catalyst.

On the other hand, TGA result showed that the catalyst undergone three stages of weight loss under nitrogen flow where first mass loss step was due to the evaporation of moisture that adsorbed within the activated carbon, second weight loss stage was due to the decomposition of $SO_3H$ functional group anchored on the carbon support and the third weight loss was associated with the thermal decomposition of cellulose and lignin material within the temperature range of 500℃-700℃. The main finding of this analysis showed that palm frond derived catalyst exhibited excellent thermal stability up to 225℃. From the TPR analysis, the TPR plot showed that the reduction of carbon catalyst was the highest at 890 ℃. The

high reduction temperature of the catalyst allowed it to be used in other application with low level of reduction such as hydrogenation.

Catalytic performance of catalyst prepared at different pretreatment parameters was also tested through esterification of PFAD to determine the most efficient and cost-effective condition to produce carbon-based catalyst in large scale. First and foremost, catalyst carbonised at varied temperature showed that Cat_600 gave the highest biodiesel yield and conversion as compared to other catalysts. These findings were confirmed to the SEM micrograph which showed a more ordered-structure was likely to be developed in Cat_0.5. It was further confirmed in the FT-IR spectrum which showed Cat_0.5 had the highest $–SO_3H$ and O=S=O peaks intensities compared to others. Other than that, similar trend was also proven by the outcomes of acid density test. These results were also supported by the TGA weight loss profile which demonstrated that the weight loss of catalyst from 500℃ to 700℃ were more significant compared to the other temperature range.

Next, the biomass activated at different impregnation ratio and impregnation temperature were also tested through esterification of PFAD. The result showed that Cat_0.5 was the optimum catalyst as a too high concentration of activating agent resulted in excessive destruction of carbon structure. Cat_90 also reported having the highest biodiesel yield which is 82.71% since at high temperature, activating agent gains sufficient energy and collide more often with the carbon surface which accelerate the rate of destruction. In overall, the acidic carbon catalyst synthesised at a condition of carbonisation temperature of 600℃, impregnation ratio of 1:0.5 and impregnation temperature of 90 ℃ exhibited the highest total acid density and biodiesel yield. Overall, all the planned objectives were fulfilled. The presented results were remarkable but there is always room for improvement. Further research is still needed to improve and optimise the biodiesel yield in the future.

## 5.2 Recommendations for Future Research

Despite the experimental work was conducted accordingly to the scope of study, however there was still some fluctuations in results that need to be further confirmed by performing more repetition works. The discrepancies in the results might due to material and equipment limitations, time constraint and most importantly the inconsistency in each batch samples collected. Therefore, several suggestions were made to improve the accuracy and reliability of the results. Listed below are the

recommendations which may be useful for future research.

i. To ensure the catalysts produced are consistent, mass production of sample in single batch is more favourable. This is to ensure that the samples produced carry the same structural properties since production in separate batch will result in deviation of sample properties although the same condition was applied.

ii. Ensure that the equipment used in every repetitive reaction set is consistent to maintain the uniformity of condition such as heating rate of hot plate.

iii. Besides pretreatment parameter study, more parameter studies on sulfonation and esterification process can be conducted in the next research.

iv. More experimental run is needed for the same parameter study to get a more accurate and reliable result especially in determining the optimum condition.

v. A wider experimental range in parameter study is required to obtain the absolute optimum conditions in synthesising the best-performed catalyst.

vi. Characterisation of catalyst should be conducted as soon as the catalysts were produced to avoid degradation or contamination of samples.

vii. Conduct GC test by using internal standard to reduce deviations in results caused by the instable equipment response and errors arise during sample handling.

viii. Use of thermocouple during the sulfonation and esterification process is required to ensure that the reaction temperature is kept constant throughout the reaction.

# REFERENCES

Abbaszaadeh, A., Ghobadian, B., Omidkhah, M. and Najafi, G., 2012. Current biodiesel production technologies: A comparative review. *Energy Conversion and Management*, 63, pp.138-148.

Aransiola, E., Ojumu, T., Oyekola, O., Madzimbamuto, T. and Ikhu-Omoregbe, D., 2014. A review of current technology for biodiesel production: State of the art. *Biomass and Bioenergy*, 61, pp.276-297.

Balat, M., 2008. Diesel-Like Fuel Obtained by Catalytic Pyrolysis of Waste Engine Oil. *Energy Exploration & Exploitation*, 26(3), pp.197-208.

Baroutian, S., Aroua, M., Raman, A. and Sulaiman, N., 2010. Potassium hydroxide catalyst supported on palm shell activated carbon for transesterification of palm oil. *Fuel Processing Technology*, 91(11), pp.1378-1385.

Bobbili, S. and Mosali, R., 2011. *Biodiesel Magazine - Homogenous Catalyst and Effects on Multifeedstock Processing*. [online] Biodieselmagazine.com. Available at: <http://www.biodieselmagazine.com/articles/7793/homogenous-catalyst-and-effects-on-multifeedstock-processing> [Accessed 29 Jun. 2018].

Buasri, A., Chaiyut, N., Loryuenyong, V., Rodklum, C., Chaikwan, T., Kumphan, N., Jadee, K., Klinklom, P. and Wittayarounayut, W., 2012. Transesterification of waste frying oil for synthesizing biodiesel by KOH supported on coconut shell activated carbon in packed bed reactor. *ScienceAsia*, 38(3), p.283.

Buasri, A., Chaiyut, N., Loryuenyong, V., Rodklum, C., Chaikwan, T. and Kumphan, N., 2012. Continuous Process for Biodiesel Production in Packed Bed Reactor from Waste Frying Oil Using Potassium Hydroxide Supported on Jatropha curcas Fruit Shell as Solid Catalyst. *Applied Sciences*, 2(3), pp.641-653.

Budi, E., Umiatin, Nasbey, H., Bintoro, R., Wulandari, F. and Erlina, 2016. Activated coconut shell charcoal carbon using chemical-physical activation.

Cheenmatchaya, A. and Kungwankunakorn, S., 2014. Preparation of Activated Carbon Derived from Rice Husk by Simple Carbonization and Chemical Activation for Using as Gasoline Adsorbent. *International Journal of Environmental Science and Development*, pp.171-175.

Dalai, A. and Baroi, C., 2012. *Catalysis for Alternative Energy Generation*. New York: Springer, pp.237-304.

Dhawane, S., Kumar, T. and Halder, G., 2016. Biodiesel synthesis from Hevea brasiliensis oil employing carbon supported heterogeneous catalyst: Optimization by Taguchi method. *Renewable Energy*, 89, pp.506-514.

Department of Statistics, Malaysia, 2017. *Current Population Estimates, Malaysia, 2016-2017*. [online] Available at: <https://www.dosm.gov.my/v1/index.php?r=column/pdfPrev&id=a1d1UTFZazd5ajJiRWFHNDduOXFFQT09> [Accessed 29 Jun. 2018].

Eia.gov, 2018. *EIA - International Energy Outlook 2017*. [online] Available at: <https://www.eia.gov/outlooks/ieo/> [Accessed 29 Jun. 2018].

Ezebor, F., Khairuddean, M., Abdullah, A. and Boey, P., 2014. Esterification of oily-FFA and transesterification of high FFA waste oils using novel palm trunk and bagasse-derived catalysts. *Energy Conversion and Management*, 88, pp.1143-1150.

Gui, M., Lee, K. and Bhatia, S., 2008. Feasibility of edible oil vs. non-edible oil vs. waste edible oil as biodiesel feedstock. *Energy*, 33(11), pp.1646-1653.

Hadiyanto, H., Afianti, A., Navi'a, U., Adetya, N., Widayat, W. and Sutanto, H., 2017. The development of heterogeneous catalyst C/CaO/NaOH from waste of green mussel shell ( Perna varidis ) for biodiesel synthesis. *Journal of Environmental Chemical Engineering*, 5(5), pp.4559-4563.

Hassan, M. and Kalam, M., 2013. An Overview of Biofuel as a Renewable Energy Source: Development and Challenges. *Procedia Engineering*, 56, pp.39-53.

Hayashi, J., Kazehaya, A., Muroyama, K. and Watkinson, A., 2000. Preparation of activated carbon from lignin by chemical activation. *Carbon*, 38(13), pp.1873-1878.

Iea.org, 2018. *WEO 2017 : Key Findings*. [online] Available at: <http://www.iea.org/weo2017/> [Accessed 29 Jun. 2018].

IOANNIDOU, O. and ZABANIOTOU, A., 2007. Agricultural residues as precursors for activated carbon production—A review. *Renewable and Sustainable Energy Reviews*, 11(9), pp.1966-2005.

Islam, M., Rouf, M., Fujimoto, S. and Minowa, T., 2018. Preparation and characterisation of activated carbon from bio-diesel by-products (Jatropha seedcake) by steam activation. *Fuel*, 187, pp180-188.

Ismail, N., Taha, M. and Ramli, A., 2016. Preparation and characterisation activated carbon from rice husk and oil palm empty fruit bunches for removal of Zn2+ in aqueous solution. *Journal of Environmental Chemical Engineering*, 5(5), pp.3679-3897.

Kalderis, D., Bethanis, S., Paraskeva, P. and Diamadopoulos, E., 2008. Production of activated carbon from bagasse and rice husk by a single-stage chemical activation method at low retention times. *Bioresource Technology*, 99(15), pp.6809-6816.

Kiss, F., Jovanović, M. and Bošković, G., 2010. Economic and ecological aspects of biodiesel production over homogeneous and heterogeneous catalysts. *Fuel Processing Technology*, 91(10), pp.1316-1320.

Konwar, L., Mäki-Arvela, P., Salminen, E., Kumar, N., Thakur, A., Mikkola, J. and Deka, D., 2015. Towards carbon efficient biorefining: Multifunctional mesoporous solid acids obtained from biodiesel production wastes for biomass conversion. *Applied Catalysis B: Environmental*, 176-177, pp.20-35.

Kumar, A. and Jena, H., 2016. Preparation and characterization of high surface area activated carbon from Fox nut (Euryale ferox) shell by chemical activation with H3PO4. *Results in Physics*.

Lai, L. and Idris, A., 2013. Disruption of Oil Palm Trunks and Fronds by Microwave-Alkali Pretreatment. *BioResources*, 8(2).

Li, W., Yang, K., Peng, J., Zhang, L., Guo, S. and Xia, H., 2008. Effects of carbonisation temperatures on characteristics of porosity in coconut shell chars and activated carbons derived from carbonised coconut shell chars. *Industrial Crops and Products*, 28(2), pp.190-198.

Liou, T. and Wu, S., 2009. Characteristics of microporous/mesoporous carbons prepared from rice husk under base- and acid-treated conditions. *Journal of Hazardous Materials*, 171(1-3), pp.693-703.

Ma, F. and Hanna, M., 1999. Biodiesel production: a review1Journal Series #12109, Agricultural Research Division, Institute of Agriculture and Natural Resources, University of Nebraska–Lincoln.1. *Bioresource Technology*, 70(1), pp.1-15.

Md Arshad, S., Ngadi, N., Aziz, A., Amin, N., Jusoh, M. and Wong, S., 2016. Preparation of activated carbon from empty fruit bunch for hydrogen storage. *Journal of Energy Storage*, 8, pp.257-261.

Meih.st.gov.my., 2018. *Statistics - Malaysia Energy Information Hub*. [online] Available at: <http://meih.st.gov.my/statistics> [Accessed 29 Jun. 2018].

Mopoung, S., Moonsri, P., Palas, W. and Khumpai, S., 2015. Characterization and Properties of Activated Carbon Prepared from Tamarind Seeds by KOH Activation for Fe(III) Adsorption from Aqueous Solution. *The Scientific World Journal*, 2015, pp.1-9.

Muniandy, L., Adam, F., Mohamed, A. and Ng, E., 2014. The synthesis and characterisation of high purity mixed microporous/mesoporous activated carbon from rice husk using chemical activation with NaOH and KOH. *Microporous and Mesoporous Materials*, 197, pp.316-323.

Prahas, D., Kartika, Y., Indraswati, N. and Ismadji, S., 2008. Activated carbon from jackfruit peel waste by $H_3PO$ chemical activation: Pore structure and surface chemistry characterisation. *Chemical Engineering Journal*, 140(1-3), pp.32-42.

Pua, F., Fang, Z., Zakaria, S., Guo, F. and Chia, C., 2011. Direct production of biodiesel from high-acid value Jatropha oil with solid acid catalyst derived from lignin. *Biotechnology for Biofuels*, 4(1), p.56.

Raymundo-Piñero, E., Azaïs, P., Cacciaguerra, T., Cazorla-Amorós, D., Linares-Solano, A. and Béguin, F., 2005. KOH and NaOH activation mechanisms of multiwalled carbon nanotubes with different structural organisation. *Carbon*, 43(4), pp.786-795.

Refaat, A., 2009. Different techniques for the production of biodiesel from waste vegetable oil. *International Journal of Environmental Science & Technology*, 7(1), pp.183-213.

Renewable Energy Market Analysis: Southeast Asia., 2018. [ebook] Abu Dhabi.: IRENA. Available at: <https://irena.org/-/media/Files/IRENA/Agency/Publication/2018/Jan/IRENA_Market_Southeast_Asia_2018.pdf >[Accessed 29 Jun. 2018].

Rincón, L., Jaramillo, J. and Cardona, C., 2014. Comparison of feedstocks and technologies for biodiesel production: An environmental and techno-economic evaluation. *Renewable Energy*, 69, pp.479-487.

Salman, J., 2014. Optimization of preparation conditions for activated carbon from palm oil fronds using response surface methodology on removal of pesticides from aqueous solution. *Arabian Journal of Chemistry*, 7(1), pp.101-108.

Salman, J. and Hameed, B., 2010. Effect of preparation conditions of oil palm fronds activated carbon on adsorption of bentazon from aqueous solutions. *Journal of Hazardous Materials*, 175(1-3), pp.133-137.

Shuit, S. and Tan, S., 2014. Feasibility study of various sulphonation methods for transforming carbon nanotubes into catalysts for the esterification of palm fatty acid distillate. *Energy Conversion and Management*, 88, pp.1283-1289.

Subramonia Pillai, N., Kannan, P., Vettivel, S. and Suresh, S., 2017. Optimization of transesterification of biodiesel using green catalyst derived from Albizia Lebbeck Pods by mixture design. *Renewable Energy*, 104, pp.185-196.

Sumathi, S., Chai, S. and Mohamed, A., 2008. Utilization of oil palm as a source of renewable energy in Malaysia. *Renewable and Sustainable Energy Reviews*, 12(9), pp.2404-2421.

Thanh, L., Okitsu, K., Boi, L. and Maeda, Y., 2012. Catalytic Technologies for Biodiesel Fuel Production and Utilization of Glycerol: A Review. *Catalysts*, 2(1), pp.191-222.

The Edge Markets., 2018. *Bank Negara: Malaysia 2017 GDP growth at 5.9%*. [online] Available at: <http://www.theedgemarkets.com/article/bank-negara-malaysia-2017-gdp-growth-59> [Accessed 29 Jun. 2018].

Wang, S., Yuan, H., Wang, Y. and Shan, R., 2017. Transesterification of vegetable oil on low cost and efficient meat and bone meal biochar catalysts. *Energy Conversion and Management*, 150, pp.214-221.

Worldcat.org, 2018. *BP statistical review of world energy*. [online] Available at: <http://www.worldcat.org/title/bp-statistical-review-of-world-energy/oclc/8530077%3Fpage%3Dcitation> [Accessed 29 Jun. 2018].

Yahya, M., Al-Qodah, Z. and Ngah, C., 2015. Agricultural bio-waste materials as potential sustainable precursors used for activated carbon production: A review. *Renewable and Sustainable Energy Reviews*, 46, pp.218-235.

Zhao, C., Lv, P., Yang, L., Xing, S., Luo, W. and Wang, Z., 2018. Biodiesel synthesis over biochar-based catalyst from biomass waste pomelo peel. *Energy Conversion and Management*, 160, pp.477-485.

# APPENDICES

## APPENDIX A: EDX Reports

| Element | Wt% | At% |
|---|---|---|
| CK | 56.06 | 63.11 |
| OK | 43.16 | 36.47 |
| NaK | 00.56 | 00.33 |
| SK | 00.22 | 00.09 |
| Matrix | Correction | ZAF |

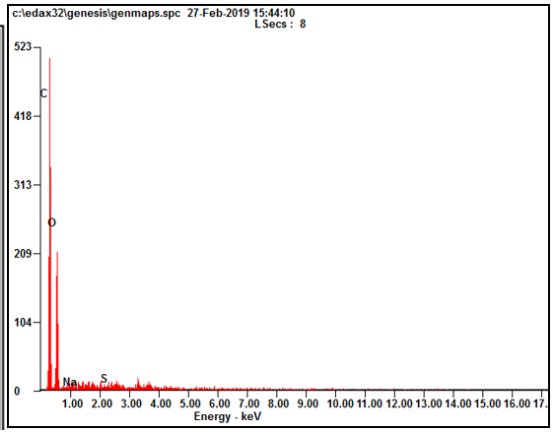


Figure A-1:EDX Analysis of Raw Palm Frond

| Element | Wt% | At% |
|---|---|---|
| CK | 58.00 | 64.93 |
| OK | 41.22 | 34.64 |
| NaK | 00.59 | 00.35 |
| SK | 00.19 | 00.08 |
| Matrix | Correction | ZAF |

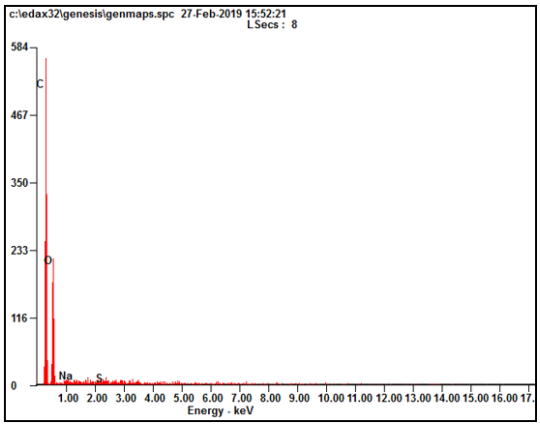


Figure A-2:EDX Analysis of Chemically Activated Palm Frond

| Element | Wt% | At% |
|---|---|---|
| CK | 87.69 | 90.60 |
| OK | 11.69 | 09.06 |
| NaK | 00.62 | 00.34 |
| SK | 00.00 | 00.00 |
| Matrix | Correction | ZAF |

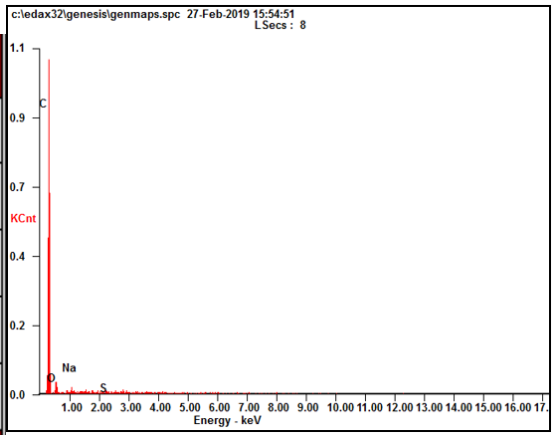


Figure A-3: EDX Analysis of Activated Carbon

| Element | Wt% | At% |
|---|---|---|
| CK | 64.82 | 74.13 |
| OK | 25.01 | 21.48 |
| NaK | 00.20 | 00.12 |
| SK | 09.97 | 04.27 |
| Matrix | Correction | ZAF |

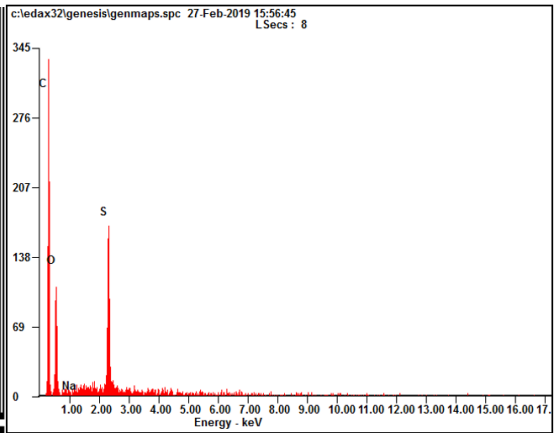


Figure A-4: EDX Analysis of Sulfonated Activated Carbon

# APPENDIX B: FT-IR Reports

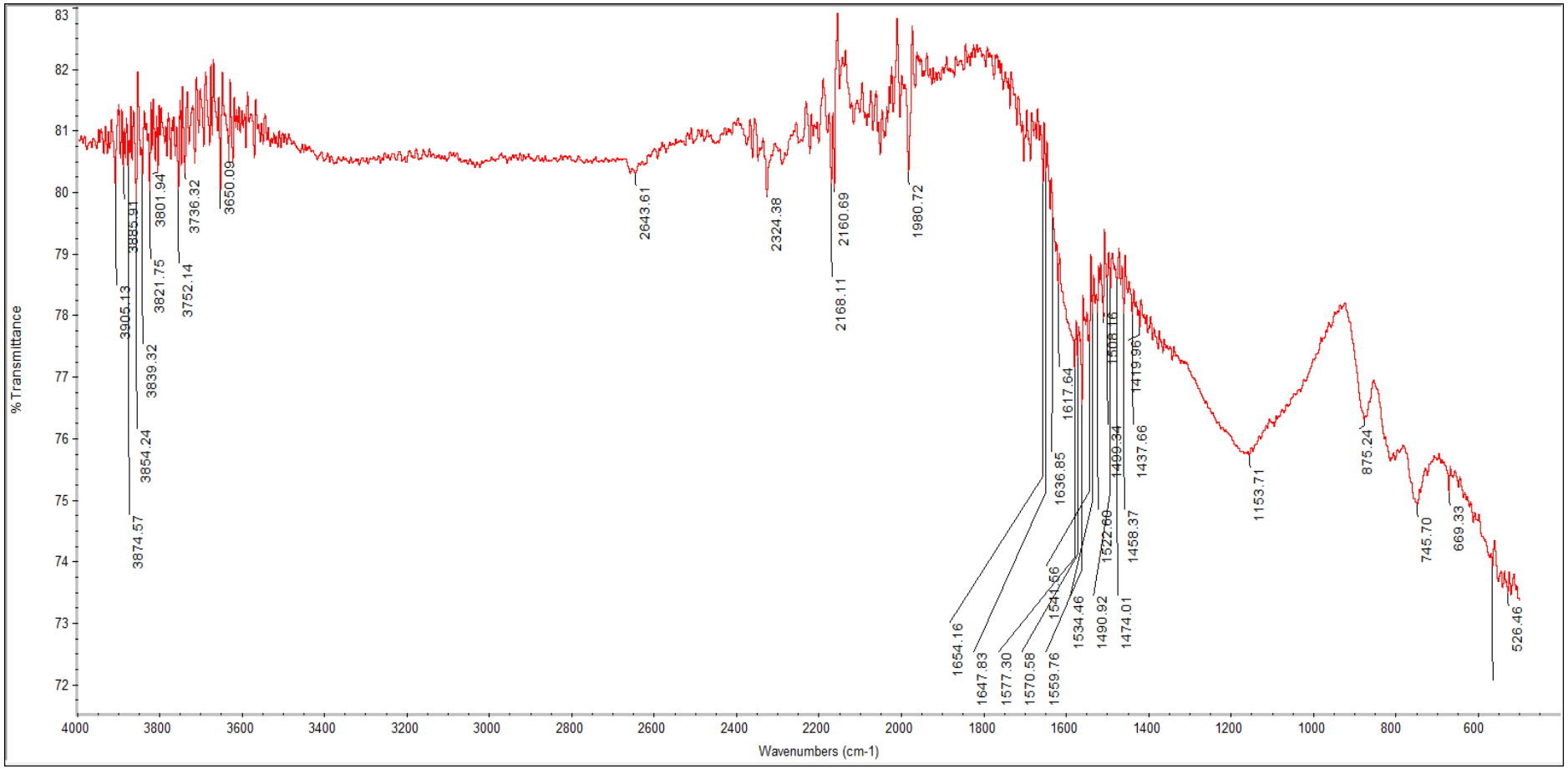


Figure B-1: FTIR Spectrum of Activated Carbon Carbonised at 600$^{o}$C

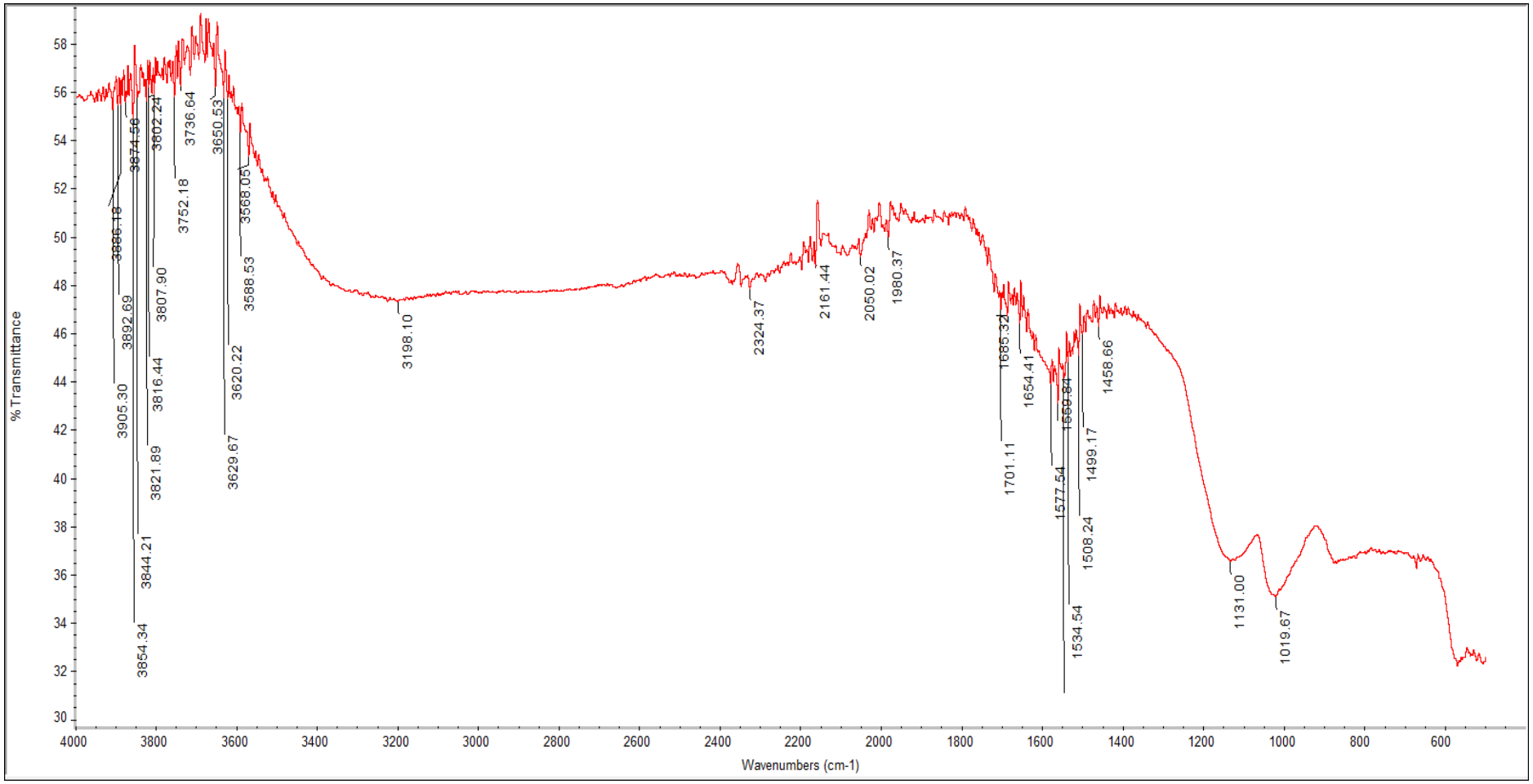


Figure B-2: FTIR Spectrum of Cat_600

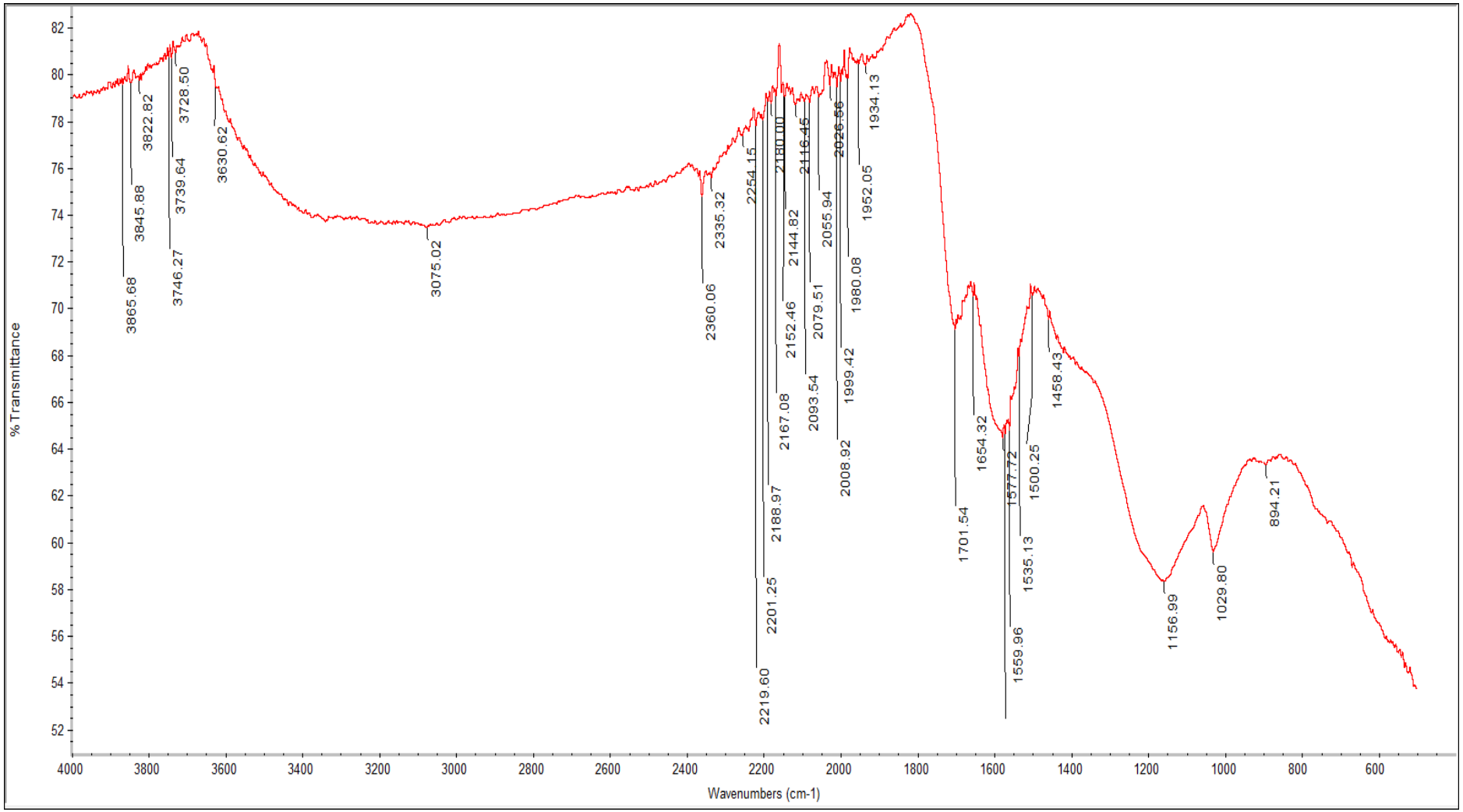


Figure B-3: FTIR Spectrum of Cat_400

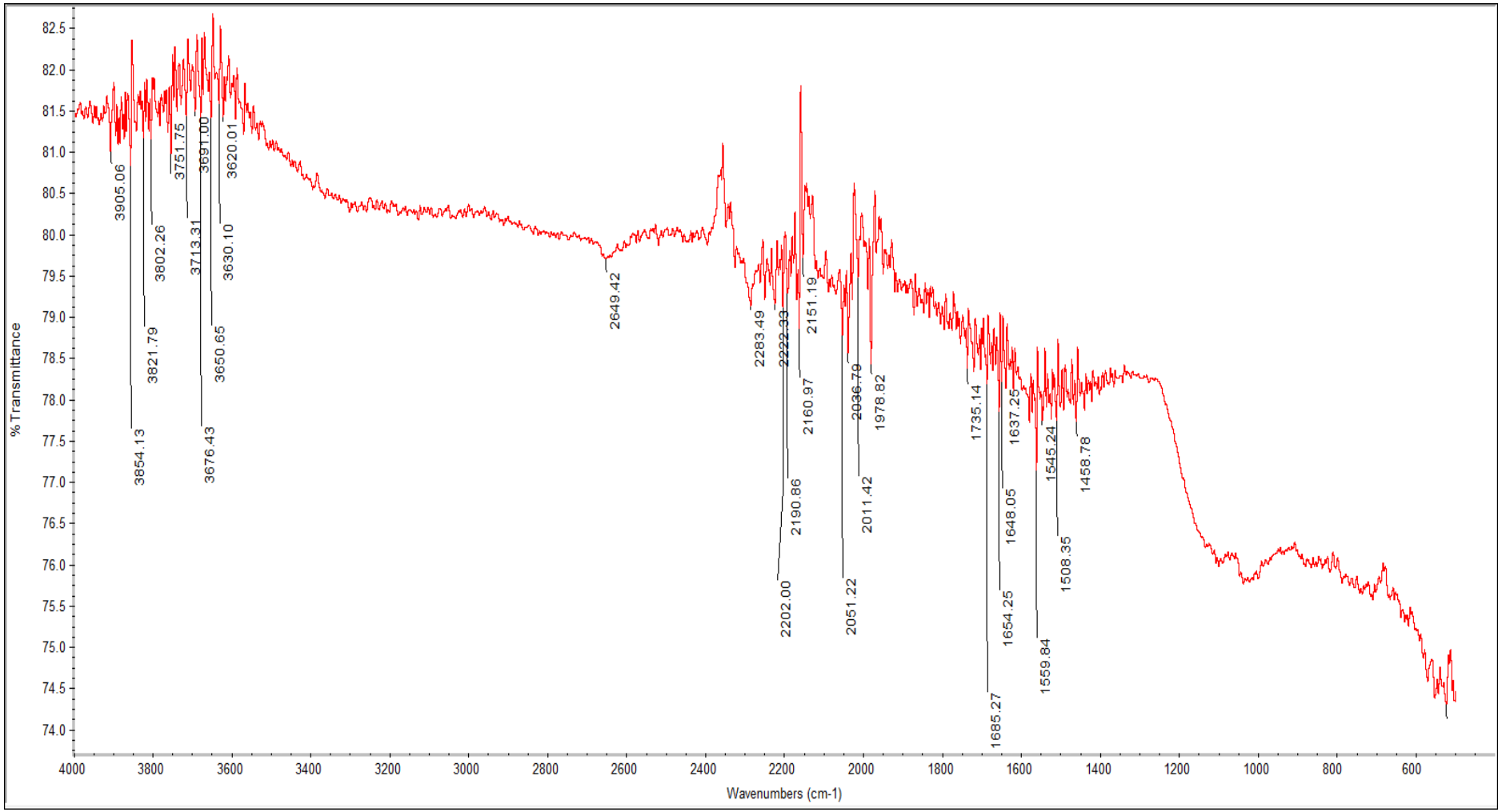


Figure B-4: FTIR Spectrum of Cat_800

# APPENDIX C: GC Reports

DEFAULT REPORT

| Peak # | Time [min] | Area [µV·s] | Height [µV] | Area [%] | Norm. Area [%] | BL | Area/Height [s] |
|---|---|---|---|---|---|---|---|
| 1 | 1.921 | 1321244.57 | 984746.41 | 96.67 | 96.67 | BE | 1.3417 |
| 2 | 1.968 | 4745.86 | 4468.53 | 0.35 | 0.35 | EV | 1.0621 |
| 3 | 2.111 | 377.43 | 258.50 | 0.03 | 0.03 | VB | 1.4601 |
| 4 | 8.097 | 55.93 | 28.60 | 0.00 | 0.00 | BB | 1.9552 |
| 5 | 10.148 | 326.62 | 146.13 | 0.02 | 0.02 | BB | 2.2352 |
| 6 | 12.156 | 16077.45 | 5232.20 | 1.18 | 1.18 | BB | 3.0728 |
| 7 | 14.619 | 1449.17 | 360.57 | 0.11 | 0.11 | BB | 4.0191 |
| 8 | 15.030 | 12172.68 | 2651.66 | 0.89 | 0.89 | BB | 4.5906 |
| 9 | 15.817 | 2942.29 | 653.37 | 0.22 | 0.22 | BB | 4.5032 |
| 10 | 18.140 | 7365.99 | 771.26 | 0.54 | 0.54 | BB | 9.5506 |
| | | 1366757.99 | 999317.23 | 100.00 | 100.00 | | |

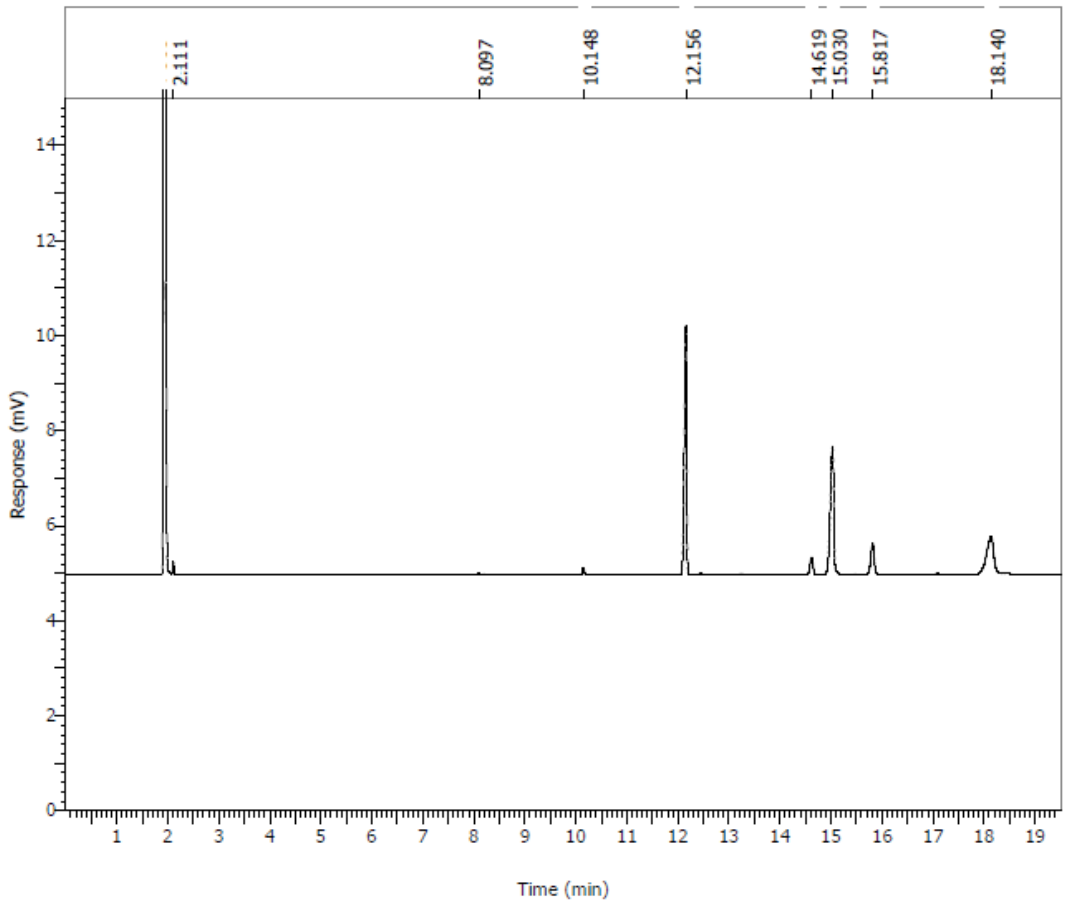


Figure C-1: Peak Report and Chromatogram of Catalyst Prepared in Preliminary Study

DEFAULT REPORT

| Peak # | Time [min] | Area [µV·s] | Height [µV] | Area [%] | Norm. Area [%] | BL | Area/Height [s] |
|---|---|---|---|---|---|---|---|
| 1 | 1.916 | 1364899.68 | 984696.45 | 98.19 | 98.19 | BV | 1.3861 |
| 2 | 2.106 | 474.61 | 309.96 | 0.03 | 0.03 | VB | 1.5312 |
| 3 | 8.100 | 42.88 | 22.72 | 0.00 | 0.00 | BB | 1.8867 |
| 4 | 10.152 | 249.73 | 112.73 | 0.02 | 0.02 | BB | 2.2152 |
| 5 | 12.150 | 11982.63 | 4185.22 | 0.86 | 0.86 | BB | 2.8631 |
| 6 | 14.618 | 1032.85 | 260.35 | 0.07 | 0.07 | BB | 3.9671 |
| 7 | 15.022 | 9088.50 | 2125.53 | 0.65 | 0.65 | BB | 4.2759 |
| 8 | 15.815 | 2236.77 | 499.04 | 0.16 | 0.16 | BB | 4.4821 |
| | | 1390007.64 | 992212.01 | 100.00 | 100.00 | | |

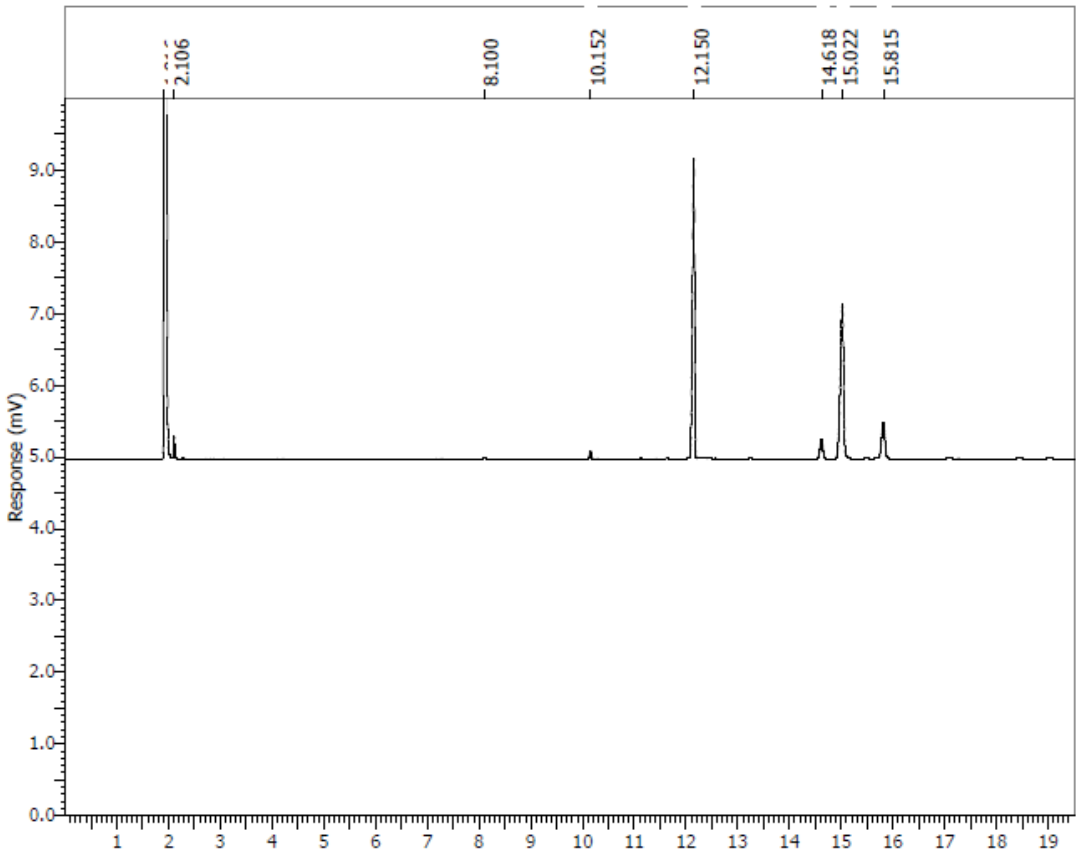


Figure C-2: Peak Report and Chromatogram of Cat_400

DEFAULT REPORT

| Peak # | Time [min] | Area [µV·s] | Height [µV] | Area [%] | Norm. Area [%] | BL | Area/Height [s] |
|---|---|---|---|---|---|---|---|
| 1 | 1.998 | 1487384.46 | 989987.13 | 97.42 | 97.42 | BB | 1.5024 |
| 2 | 8.207 | 76.43 | 37.15 | 0.01 | 0.01 | BB | 2.0570 |
| 3 | 10.263 | 412.65 | 181.29 | 0.03 | 0.03 | BB | 2.2762 |
| 4 | 12.294 | 19686.27 | 5996.60 | 1.29 | 1.29 | BB | 3.2829 |
| 5 | 14.803 | 1648.12 | 379.85 | 0.11 | 0.11 | BB | 4.3389 |
| 6 | 15.224 | 13625.12 | 2865.74 | 0.89 | 0.89 | BB | 4.7545 |
| 7 | 16.017 | 3294.16 | 707.69 | 0.22 | 0.22 | BB | 4.6548 |
| 8 | 18.206 | 544.09 | 72.86 | 0.04 | 0.04 | BB | 7.4672 |
| 9 | 18.571 | 117.01 | 27.51 | 0.01 | 0.01 | BB | 4.2529 |
| | | 1526788.31 | 1.00e+06 | 100.00 | 100.00 | | |

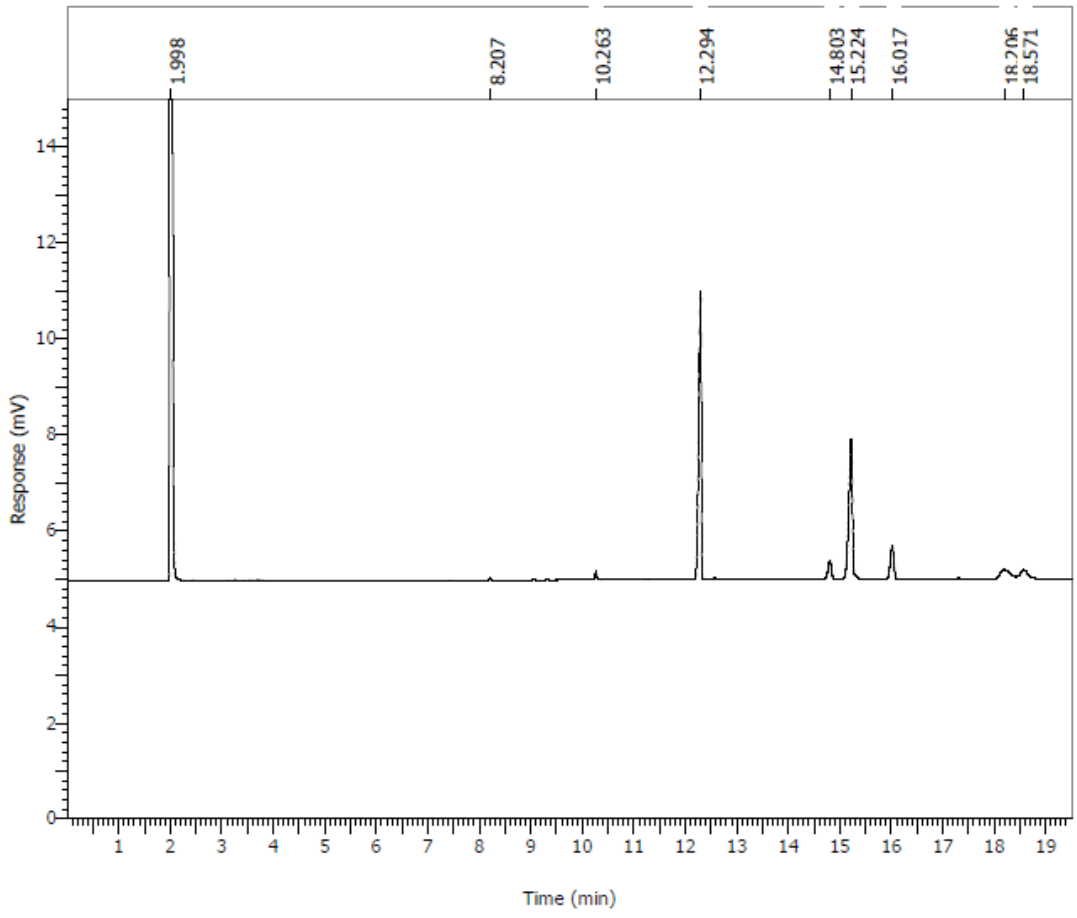


Figure C-3: Peak Report and Chromatogram of Cat_600

DEFAULT REPORT

| Peak # | Time [min] | Area [µV·s] | Height [µV] | Area [%] | Norm. Area [%] | BL | Area/Height [s] |
|---|---|---|---|---|---|---|---|
| 1 | 1.915 | 1388195.16 | 989717.57 | 97.16 | 97.16 | BE | 1.4026 |
| 2 | 1.963 | 4924.16 | 4837.42 | 0.34 | 0.34 | EB | 1.0179 |
| 3 | 8.099 | 73.75 | 36.97 | 0.01 | 0.01 | BB | 1.9952 |
| 4 | 10.153 | 348.82 | 156.16 | 0.02 | 0.02 | BB | 2.2337 |
| 5 | 12.163 | 17077.42 | 5619.56 | 1.20 | 1.20 | BB | 3.0389 |
| 6 | 14.626 | 1585.99 | 391.80 | 0.11 | 0.11 | BB | 4.0479 |
| 7 | 15.039 | 13357.97 | 2933.03 | 0.93 | 0.93 | BB | 4.5543 |
| 8 | 15.825 | 3175.98 | 707.14 | 0.22 | 0.22 | BB | 4.4913 |
| 9 | 18.073 | 52.07 | 16.30 | 0.00 | 0.00 | BB | 3.1950 |
| | | 1428791.33 | 1.00e+06 | 100.00 | 100.00 | | |

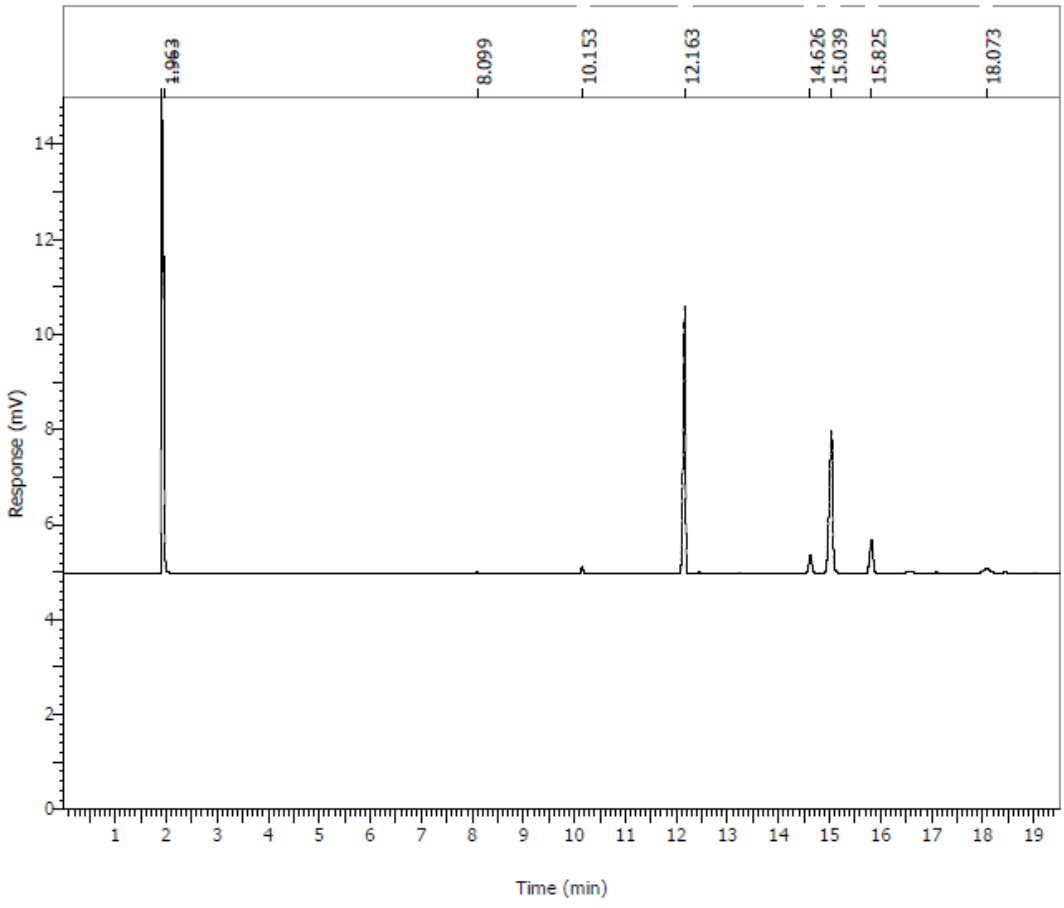


Figure C-4: Peak Report and Chromatogram of Cat_800

DEFAULT REPORT

| Peak # | Time [min] | Area [µV·s] | Height [µV] | Area [%] | Norm. Area [%] | BL | Area/Height [s] |
|---|---|---|---|---|---|---|---|
| 1 | 1.917 | 1443298.56 | 988900.43 | 96.15 | 96.15 | BE | 1.4595 |
| 2 | 1.967 | 6164.17 | 6102.02 | 0.41 | 0.41 | EB | 1.0102 |
| 3 | 2.115 | 766.59 | 550.30 | 0.05 | 0.05 | BB | 1.3931 |
| 4 | 8.196 | 72.29 | 35.88 | 0.00 | 0.00 | BB | 2.0147 |
| 5 | 10.245 | 460.21 | 204.12 | 0.03 | 0.03 | BB | 2.2546 |
| 6 | 12.264 | 23791.70 | 7040.26 | 1.58 | 1.58 | BB | 3.3794 |
| 7 | 12.539 | 93.75 | 29.72 | 0.01 | 0.01 | BB | 3.1549 |
| 8 | 14.741 | 2199.43 | 513.27 | 0.15 | 0.15 | BB | 4.2851 |
| 9 | 15.172 | 19710.95 | 3844.32 | 1.31 | 1.31 | BB | 5.1273 |
| 10 | 15.949 | 4505.23 | 959.01 | 0.30 | 0.30 | BB | 4.6978 |
| | | 1501062.89 | 1.01e+06 | 100.00 | 100.00 | | |

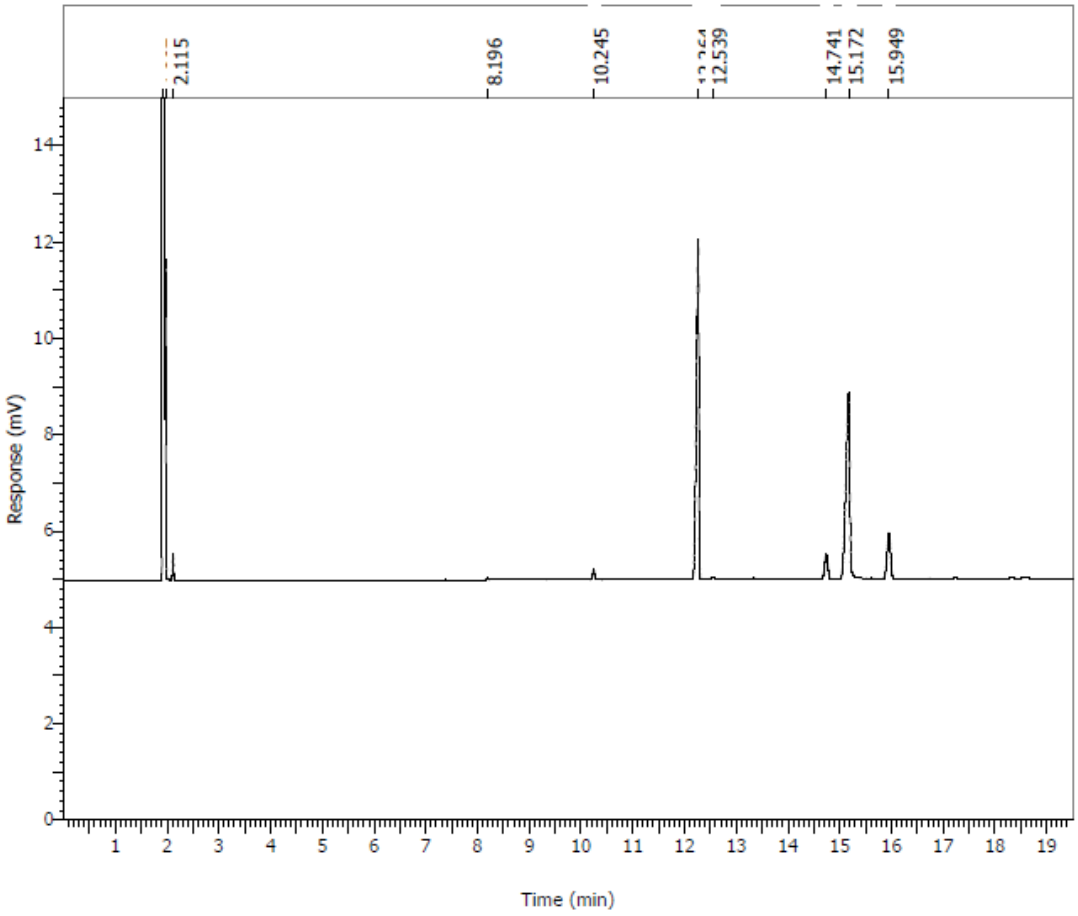


Figure C-5: Peak Report and Chromatogram of Cat_0.1

DEFAULT REPORT

| Peak # | Time [min] | Area [µV·s] | Height [µV] | Area [%] | Norm. Area [%] | BL | Area/Height [s] |
|---|---|---|---|---|---|---|---|
| 1 | 1.922 | 1261973.43 | 979130.55 | 94.66 | 94.66 | BE | 1.2889 |
| 2 | 1.970 | 4873.46 | 4847.07 | 0.37 | 0.37 | EB | 1.0054 |
| 3 | 2.113 | 198.64 | 140.95 | 0.01 | 0.01 | BB | 1.4093 |
| 4 | 8.113 | 120.87 | 58.61 | 0.01 | 0.01 | BB | 2.0623 |
| 5 | 10.165 | 676.43 | 299.48 | 0.05 | 0.05 | BB | 2.2587 |
| 6 | 12.200 | 32826.43 | 9027.40 | 2.46 | 2.46 | BB | 3.6363 |
| 7 | 12.459 | 109.58 | 40.08 | 0.01 | 0.01 | BB | 2.7344 |
| 8 | 14.652 | 2826.60 | 656.51 | 0.21 | 0.21 | BB | 4.3055 |
| 9 | 15.081 | 24009.23 | 4569.43 | 1.80 | 1.80 | BB | 5.2543 |
| 10 | 15.850 | 5603.47 | 1202.87 | 0.42 | 0.42 | BB | 4.6584 |
| | | 1333218.13 | 999972.94 | 100.00 | 100.00 | | |

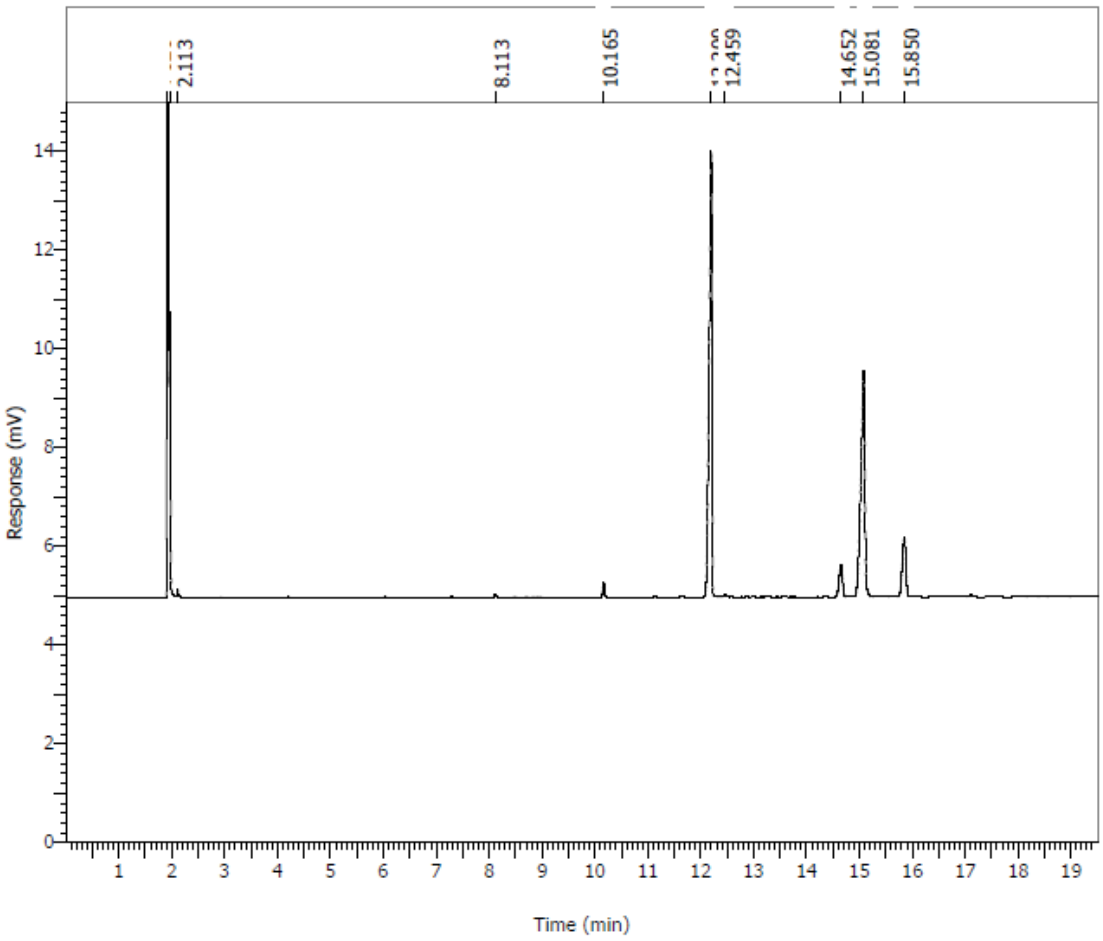


Figure C-6: Peak Report and Chromatogram of Cat_0.5

DEFAULT REPORT

| Peak # | Time [min] | Area [µV·s] | Height [µV] | Area [%] | Norm. Area [%] | BL | Area/Height [s] |
|---|---|---|---|---|---|---|---|
| 1 | 1.923 | 1467958.63 | 988902.53 | 96.02 | 96.02 | BE | 1.4844 |
| 2 | 1.972 | 5796.59 | 5762.84 | 0.38 | 0.38 | EB | 1.0059 |
| 3 | 2.120 | 974.13 | 697.91 | 0.06 | 0.06 | BB | 1.3958 |
| 4 | 8.212 | 93.46 | 46.52 | 0.01 | 0.01 | BB | 2.0090 |
| 5 | 10.261 | 532.38 | 240.40 | 0.03 | 0.03 | BB | 2.2146 |
| 6 | 12.286 | 25955.33 | 7497.29 | 1.70 | 1.70 | BB | 3.4620 |
| 7 | 12.557 | 92.21 | 31.50 | 0.01 | 0.01 | BB | 2.9275 |
| 8 | 14.767 | 2300.18 | 527.92 | 0.15 | 0.15 | BB | 4.3571 |
| 9 | 15.196 | 20435.03 | 3954.56 | 1.34 | 1.34 | BB | 5.1675 |
| 10 | 15.982 | 4744.35 | 1022.77 | 0.31 | 0.31 | BB | 4.6387 |
| | | 1528882.28 | 1.01e+06 | 100.00 | 100.00 | | |

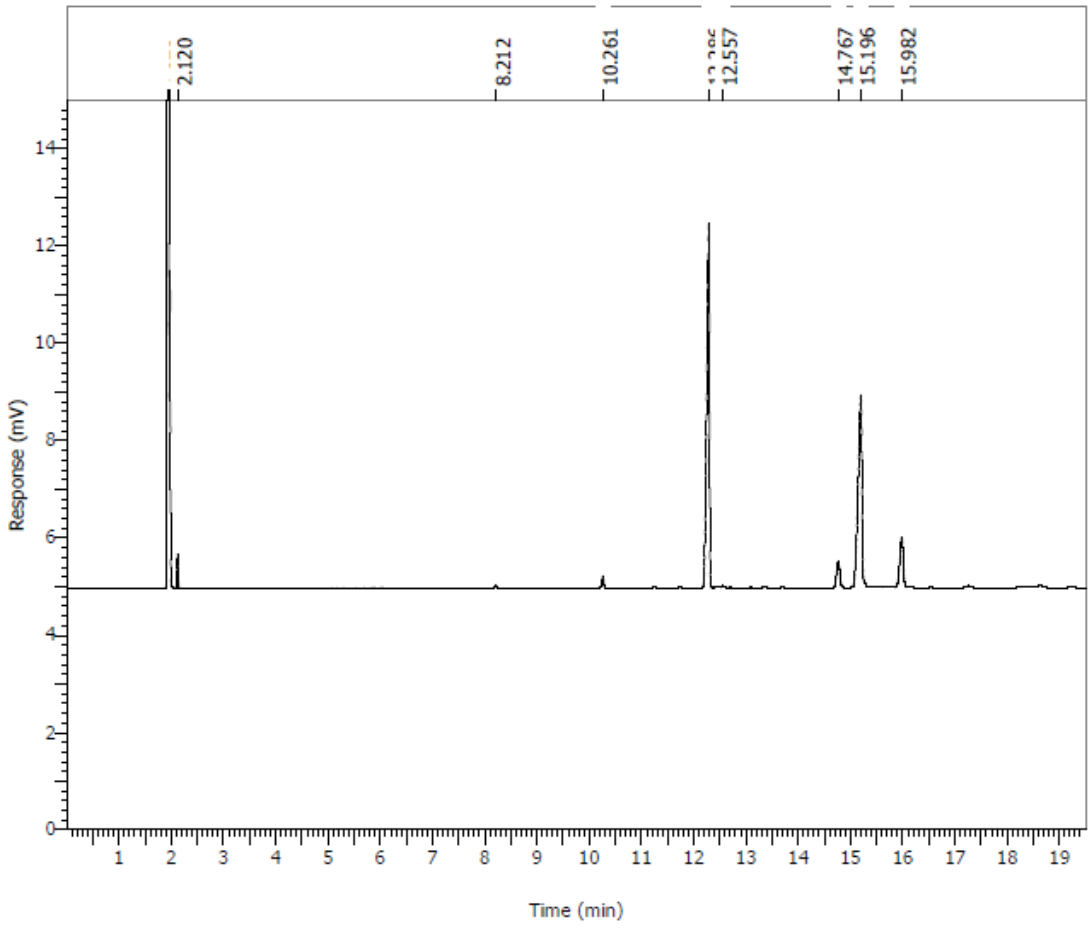


Figure C-7: Peak Report and Chromatogram of Cat_50

DEFAULT REPORT

| Peak # | Time [min] | Area [µV·s] | Height [µV] | Area [%] | Norm. Area [%] | BL | Area/Height [s] |
|---|---|---|---|---|---|---|---|
| 1 | 1.919 | 1304755.34 | 984286.67 | 96.20 | 96.20 | BE | 1.3256 |
| 2 | 1.968 | 5194.82 | 4990.99 | 0.38 | 0.38 | EB | 1.0408 |
| 3 | 2.116 | 444.94 | 317.03 | 0.03 | 0.03 | BB | 1.4034 |
| 4 | 8.205 | 74.98 | 37.52 | 0.01 | 0.01 | BB | 1.9985 |
| 5 | 10.254 | 438.82 | 197.01 | 0.03 | 0.03 | BB | 2.2274 |
| 6 | 12.273 | 21656.61 | 6600.41 | 1.60 | 1.60 | BB | 3.2811 |
| 7 | 12.549 | 75.29 | 25.77 | 0.01 | 0.01 | BB | 2.9219 |
| 8 | 14.755 | 1978.03 | 480.39 | 0.15 | 0.15 | BB | 4.1176 |
| 9 | 15.182 | 17539.27 | 3530.37 | 1.29 | 1.29 | BB | 4.9681 |
| 10 | 15.969 | 4130.80 | 895.02 | 0.30 | 0.30 | BB | 4.6153 |
| | | 1356288.90 | 1.00e+06 | 100.00 | 100.00 | | |

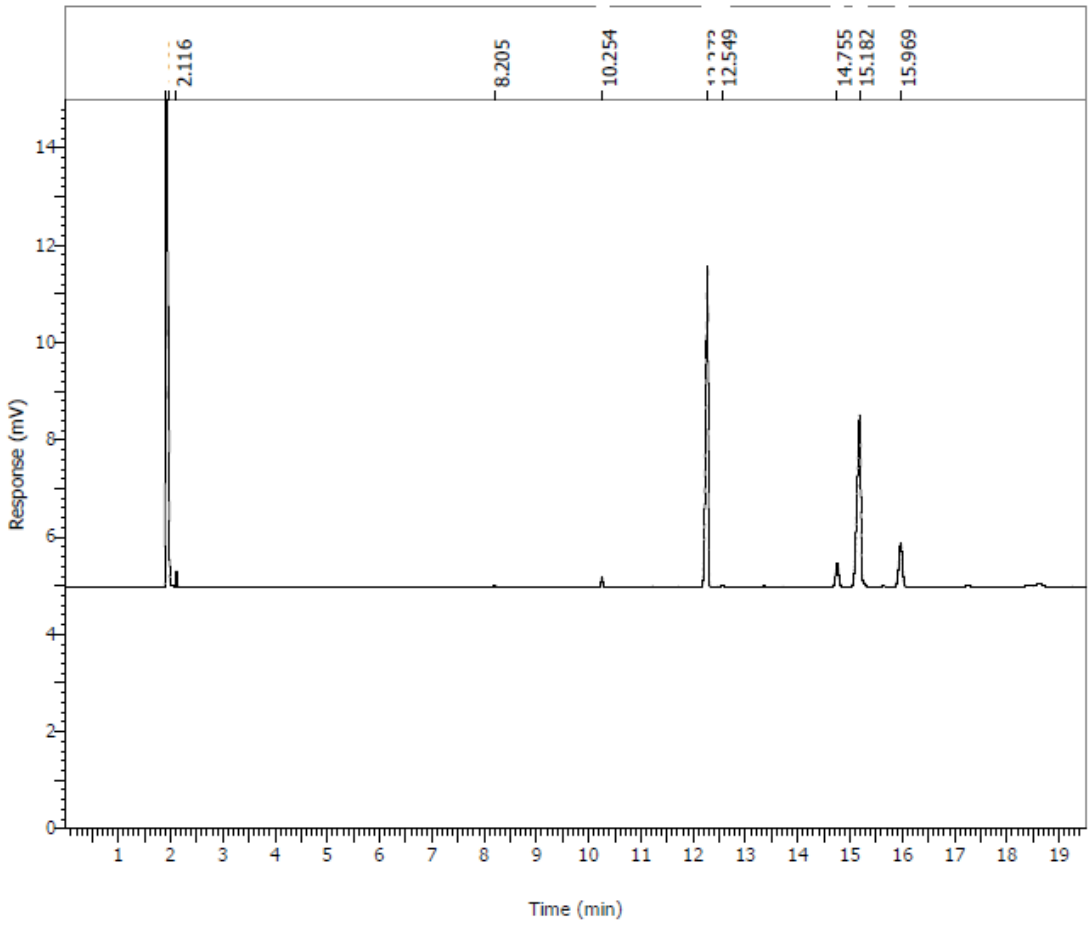


Figure C-8: Peak Report and Chromatogram of Cat_70

DEFAULT REPORT

| Peak # | Time [min] | Area [µV·s] | Height [µV] | Area [%] | Norm. Area [%] | BL | Area/Height [s] |
|---|---|---|---|---|---|---|---|
| 1 | 1.910 | 1319400.06 | 983706.98 | 97.65 | 97.65 | BV | 1.3413 |
| 2 | 2.107 | 580.83 | 399.21 | 0.04 | 0.04 | VB | 1.4549 |
| 3 | 8.686 | 164.88 | 40.62 | 0.01 | 0.01 | BB | 4.0594 |
| 4 | 10.260 | 152.93 | 69.87 | 0.01 | 0.01 | BB | 2.1888 |
| 5 | 12.243 | 7378.19 | 2687.66 | 0.55 | 0.55 | BB | 2.7452 |
| 6 | 14.751 | 568.76 | 143.43 | 0.04 | 0.04 | BB | 3.9654 |
| 7 | 15.132 | 5142.31 | 1213.94 | 0.38 | 0.38 | BB | 4.2360 |
| 8 | 15.949 | 1143.17 | 254.18 | 0.08 | 0.08 | BB | 4.4975 |
| 9 | 18.320 | 1486.74 | 222.32 | 0.11 | 0.11 | BV | 6.6874 |
| 10 | 18.588 | 15177.78 | 1580.84 | 1.12 | 1.12 | VB | 9.6011 |
| | | 1351195.65 | 990319.05 | 100.00 | 100.00 | | |

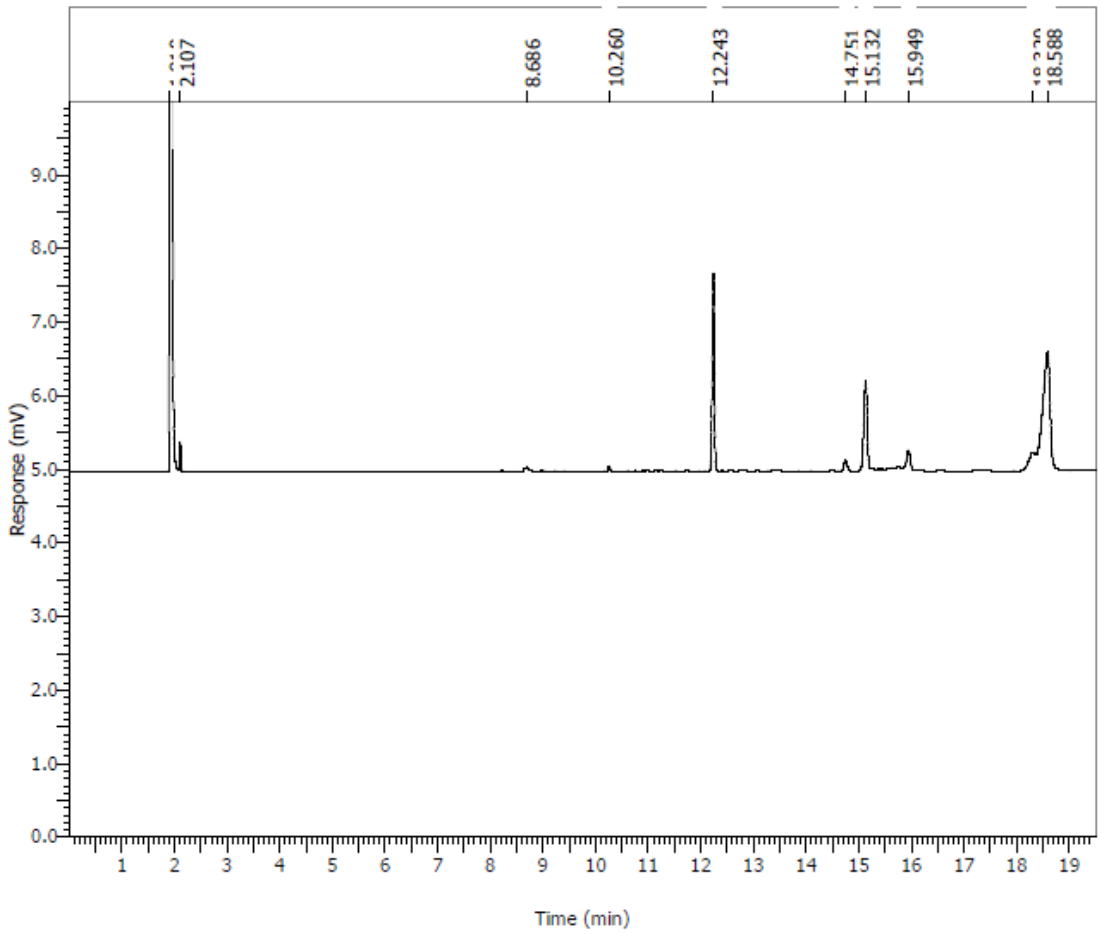


Figure C-9: Peak Report and Chromatogram of Catalyst Prepared by 4-BDS Method

DEFAULT REPORT

| Peak # | Time [min] | Area [µV·s] | Height [µV] | Area [%] | Norm. Area [%] | BL | Area/Height [s] |
|---|---|---|---|---|---|---|---|
| 1 | 1.926 | 775394.67 | 695753.10 | 85.69 | 85.69 | BE | 1.1145 |
| 2 | 1.969 | 3391.03 | 2937.25 | 0.37 | 0.37 | EB | 1.1545 |
| 3 | 2.087 | 124532.73 | 60740.00 | 13.76 | 13.76 | BB | 2.0503 |
| 4 | 12.241 | 874.61 | 334.78 | 0.10 | 0.10 | BB | 2.6125 |
| 5 | 15.142 | 734.38 | 175.23 | 0.08 | 0.08 | BB | 4.1910 |
| | | 904927.42 | 759940.35 | 100.00 | 100.00 | | |

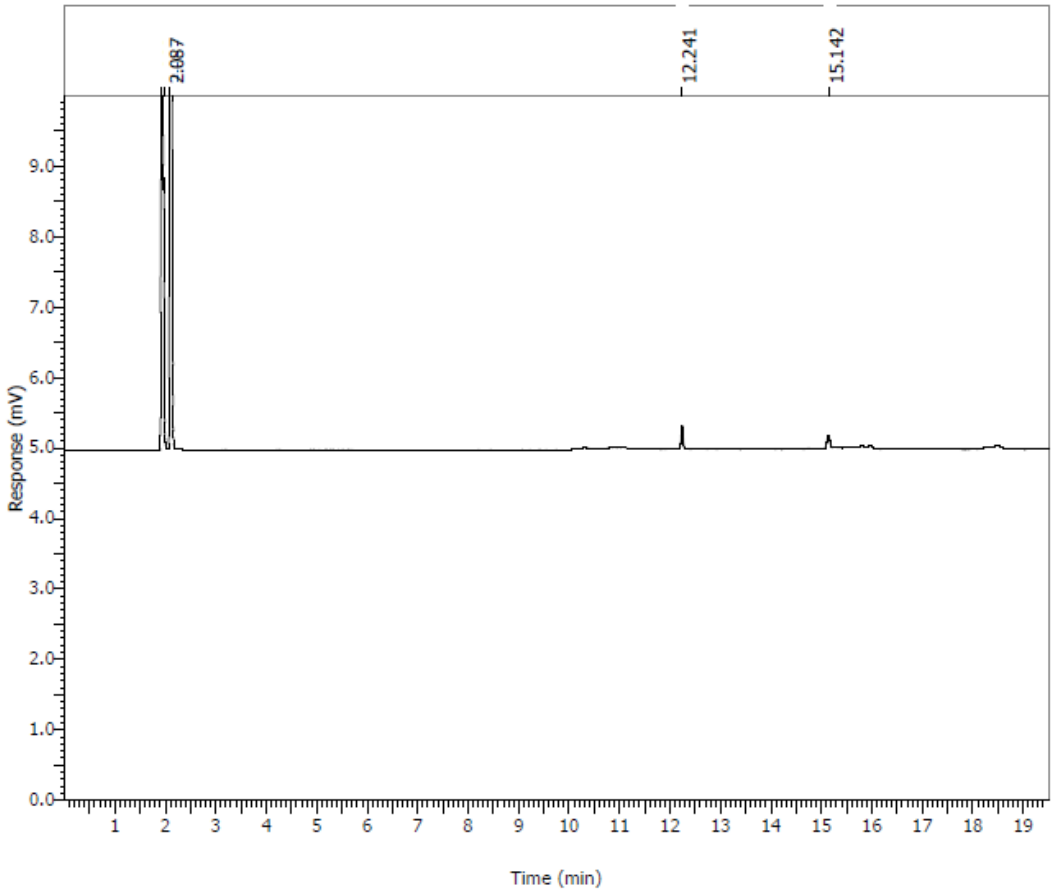


Figure C-10: Peak Report and Chromatogram of Catalyst Prepared by Thermal Decomposition of Ammonium Persulfate Method

# APPENDIX D: TPR Report

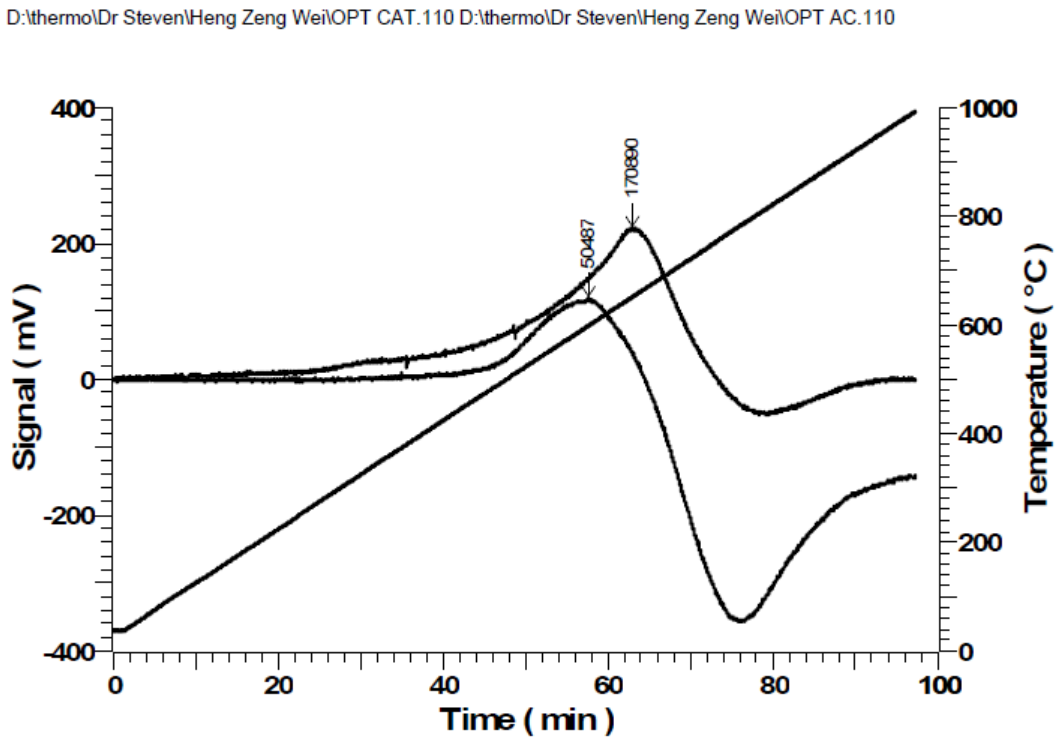


Figure D- 1: TPR Profile of Activated Carbon and Cat_0.5

# APPENDIX E: TGA Report

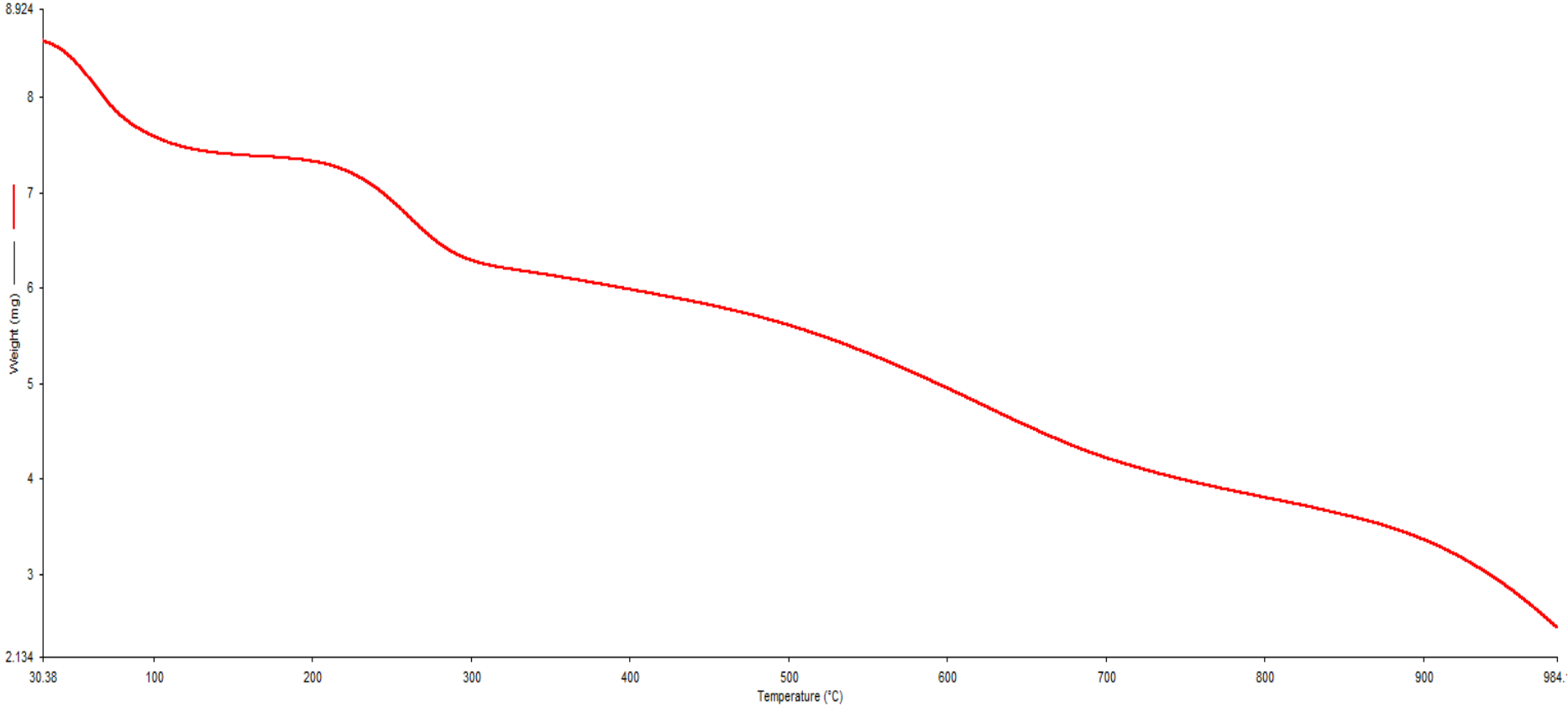


Figure E- 1: TGA Profile of Cat_0.5

# APPENDIX F: Sample Calculations

## Acid Density Calculation

Table F- 1: Acid Density of Catalyst Sample

| Catalyst | Volume of HCl used (ml) | Acid Density (mmol/g) |
|---|---|---|
| **Cat_400** | 48.5 | 2.3 |
| **Cat_600** | 37.7 | 4.46 |
| **Cat_800** | 43.7 | 3.26 |
| **Cat_0.1** | 28.2 | 6.36 |
| **Cat_0.5** | 23.2 | 7.36 |
| **Cat_50** | 45.3 | 2.94 |
| **Cat_70** | 25.3 | 6.94 |

For Cat_600:

$$Mole\ of\ HCl\ used = Mole\ of NaOH$$

$$Mole\ of\ HCl\ used\ (mol)$$
$$= Volume\ of\ HCl\ used(mL) \times \frac{1L}{1000mL} \times 0.02\,\frac{mol}{L}$$
$$= 37.7 \times \frac{1L}{1000mL} \times 0.02\,\frac{mol}{L}$$
$$= 0.00075mol$$

$$Total\ Acid\ Density\ \left(\frac{mmol}{g} NaOH\right)$$
$$= \frac{Mole\ of\ NaOH\ used\ to\ neutralize\ acid\ sites\ on\ catalyst}{0.1g}$$
$$= \frac{0.0012 - 0.00075}{0.1g} \times \frac{1000mmol}{mol}$$
$$= 4.46\ \text{mmol/g}$$

Acid Value Calculation

Table F- 2: FAME Conversion of Catalyst Sample

| Catalyst | Volume of KOH used (ml) | FAME Conversion |
|---|---|---|
| **Cat_400** | 15.8 | 55.62 |
| **Cat_600** | 3.3 | 90.73 |
| **Cat_800** | 7.5 | 78.93 |
| **Cat_0.1** | 2.8 | 92.13 |
| **Cat_0.5** | 2.3 | 93.54 |
| **Cat_50** | 4.4 | 87.64 |
| **Cat_70** | 2.7 | 92.42 |

For Cat_600,

$$Acid\ Value, AV\ \left(\frac{mgKOH}{g}\right)$$
$$= \frac{V \times N \times MW}{W_S}$$
$$= \frac{3.3 \times 0.1N \times 56.11g/mol}{1g} \times \frac{1000mg}{g}$$
$$= 18516.3\ mg\ KOH/g$$

$$Acid\ Value\ Conversion\ (\%)$$
$$= \frac{a_i - a_f}{a_i} \times 100$$
$$= \frac{199751.6 - 18516.3}{199751.6} \times 100\%$$
$$= 90.73\%$$

FAME Yield Calculation

Table F- 3: Concentration of Methyl Esters in Cat_600

| Methyl Ester | Calibration Equation | Peak Area | Concentration (g/L) |
|---|---|---|---|
| **Methyl Palmitate** | y=1388.1x | 19686.27 | 14.18 |
| **Methyl Stearate** | y=1298.1x | 1648.12 | 1.27 |
| **Methyl Oleate** | y=1439.5x | 13625.12 | 9.47 |
| **Methyl Linoleate** | y=1278.6x | 3294.16 | 2.58 |
| Total Concentration | | | 27.49 |

Methyl Palmitate Concentration:

$$y = 1388.1x$$
$$x = \frac{y}{1388.1}$$
$$= \frac{19686.27}{1388.1}$$
$$= 14.18 g/L$$

Methyl Stearate Concentration:

$$y = 1298.1x$$
$$x = \frac{y}{1298.1}$$
$$= \frac{1648.12}{1298.1}$$
$$= 1.27 g/L$$

Methyl Oleate Concentration:

$$y = 1439.5x$$
$$x = \frac{y}{1439.5}$$
$$= \frac{13625.12}{1439.5}$$
$$= 9.47 g/L$$

Methyl Linoleate Concentration:

$$y = 1278.6x$$
$$x = \frac{y}{1278.6}$$
$$= \frac{3249.16}{1278.6}$$
$$= 2.58 g/L$$

Concentration of FAME = $27.49\frac{g}{L} \times 0.02\frac{L\ sample}{g}$

$= 0.55\ gFAME/gsample$

$$\text{Yield (\%)} = \frac{\sum(\text{concentration of methyl esters})\times\text{mass of product produced}}{10\text{g PFAD}}$$

$$= \frac{0.55\ (9.01)}{10\text{g PFAD}}$$

$$= 49.54\%$$

Table F- 4: FAME Yield Results of Catalyst Samples

| Catalyst | Concentration (g FAME/g sample) | Weight (g) | FAME Yield |
|---|---|---|---|
| **Cat_400** | 0.349827 | 7.79 | 27.25 |
| **Cat_600** | 0.549875 | 9.01 | 49.54 |
| **Cat_800** | 0.505769 | 8.14 | 41.17 |
| **Cat_0.1** | 0.721023 | 8.26 | 59.56 |
| **Cat_0.5** | 0.937761 | 8.82 | 82.71 |
| **Cat_50** | 0.650818 | 8.07 | 52.52 |
| **Cat_70** | 0.76755 | 8.81 | 67.62 |